

Abstract

As experimental collider physics is able to access higher and higher energies, testable predictions are needed to guide the searches for new Beyond-the-Standard-Model theories. Most models predict new coloured particles, and these may form QCD bound states with Standard Model quarks and gluons. In particular, if the coloured particles are from the octet, decuplet, 27-plet, 28-plet or 35-plet representation of $SU(3)$, these colour-singlet bound states may occur just with Standard Model background (gluons and virtual quarks) without any valence quarks. Such states are referred to as gluelumps, and they are the focus of this work. Gluelumps arising from colour-octet particles have been studied previously, both in some analytic approximations as well as directly with lattice quantum chromodynamics, but not to the depth and completeness presented here. Treatments of gluelumps containing larger colour-multiplet particles are novel to this work and represent pioneering research. Group-theoretic foundations are laid for the study of all five of these colour representations on the lattice. A full spectrum is presented for octet-rep gluelumps with a detailed discussion of errors. The hierarchy of states agrees well with previous studies, but is much more complete and precise. The spectrum of decuplet gluelumps is also given, as well as preliminary results for the 27-plet and 35-plet. The results found here are published in Ref. [1] and predict clear experimental signatures and can be easily adapted to numerous different theoretic models of Beyond-the-Standard-Model physics.

Spectrum of Gluelumps Containing Various QCD Colour-Multiplet Particles

by

Kristen Alanna Marsh
B.Sc., McMaster University, 2005
M.Sc., University of Victoria, 2007

A Dissertation Submitted to
the Faculty of Graduate Studies
in Partial Fulfillment of the
Requirements for the Degree of
DOCTOR OF PHILOSOPHY

Graduate Program in Physics and Astronomy
York University
Toronto, Ontario

October 2013

© Kristen Alanna Marsh, 2013

Abstract

As experimental collider physics is able to access higher and higher energies, testable predictions are needed to guide the searches for new Beyond-the-Standard-Model theories. Most models predict new coloured particles, and these may form QCD bound states with Standard Model quarks and gluons. In particular, if the coloured particles are from the octet, decuplet, 27-plet, 28-plet or 35-plet representation of $SU(3)$, these colour-singlet bound states may occur just with Standard Model background (gluons and virtual quarks) without any valence quarks. Such states are referred to as gluelumps, and they are the focus of this work. Gluelumps arising from colour-octet particles have been studied previously, both in some analytic approximations as well as directly with lattice quantum chromodynamics, but not to the depth and completeness presented here. Treatments of gluelumps containing larger colour-multiplet particles are novel to this work and represent pioneering research. Group theory foundations are laid for the study of all five of these colour representations on the lattice. A full spectrum is presented for octet-rep gluelumps with a detailed discussion of errors. The hierarchy of states agrees well with previous studies, but is much more complete and precise. The spectrum of decuplet gluelumps is also given, as well as preliminary results for the 27-plet and 35-plet. The results found here are published in Ref. [1] and predict clear experimental signatures and can be easily adapted to numerous different theoretic models of Beyond-the-Standard-Model physics.

Dedication

To my darling daughter. You have been both the inspiration to finish my degree, and the distraction preventing me from doing it! Thank you for your patience, and for sharing your Mommy with this project for the first year and a half of your life.

Acknowledgments

First and foremost, I would like to thank my supervisor, Dr. Randy Lewis, for his endless support and guidance throughout my degree and also for his patience and understanding in accommodating my family obligations. I am also grateful for the valuable input offered to me by the rest of my supervisory committee, and for the help of the support staff at the Departments of Physics at both York University and the University of Regina, where I started my degree. I am very lucky to have had funding from a variety of sources while working on this degree, including an NSERC CGS-D scholarship, the Queen Elizabeth II scholarship, and teaching and research assistantships at the University of Regina and York University. I would like to acknowledge the use of Compute Canada resources, specifically the SHARCNET clusters, without which it would not have been possible to run my simulations. I would also like to acknowledge the use of ensembles of lattice configurations prepared by the CP-PACS and JLQCD Collaborations, as well as data analysis code by Numerical Recipes used under the free Intermediate Licence.

Table of Contents

Abstract	ii
Dedication	iii
Acknowledgments	iv
Table of Contents	v
List of Tables	ix
List of Figures	xi
1 Introduction	1
1.1 Overview	2
1.2 Gluelumps	6
1.3 Theoretical Motivation	7
1.4 Previous Gluelump Studies	10
1.4.1 Lattice Studies	10
1.4.2 Bag Model Studies	11
1.4.3 Other Analytic and Computational Gluelump Studies	14
2 A Brief Overview of Lattice QCD	16

2.1	Introduction	17
2.2	Configurations	17
2.3	Operators	22
2.4	Propagators	25
2.5	Correlators	26
3	Colour Representations	28
3.1	Young Tableaux	29
3.2	Casimir Operators	33
3.3	Tensors	37
3.3.1	Octet	38
3.3.2	Decuplet	42
3.3.3	27-plet	44
3.3.4	28-plet	49
3.3.5	35-plet	51
4	The Octet System	57
4.1	Operators	57
4.2	Propagator	73
4.3	Correlator	74
5	The Decuplet System	76
5.1	Operators	76
5.2	Propagator	82
5.3	Correlator	82
6	The 27-Plet System	83
6.1	Operators	83

6.2	Propagator	86
6.3	Correlator	86
7	The 28-Plet System	87
7.1	Operators	87
7.2	Propagator	89
7.3	Correlator	90
8	The 35-Plet System	91
8.1	Operators	91
8.2	Propagator	93
8.3	Correlator	94
9	Simulations	95
9.1	Smearing	95
9.2	Overview of Lattice Calculations	102
9.3	Signal Extraction	104
9.4	Errors	110
9.5	Simultaneous Fits	115
10	Results	117
10.1	Spectrum	117
10.2	Masses	129
11	Conclusion	144
	Bibliography	146
	Appendices	149

A Abbreviations and Symbols	150
B Results of Fitting	151

List of Tables

1.1	Properties of lattice ensembles used in previous gluelump studies . . .	11
1.2	Previous lattice gluelump energy spectrum	12
1.3	Gluelump energy spectrum from various model calculations	15
2.1	Properties of lattice ensembles used in current gluelump studies . . .	22
2.2	Projection of continuum spin J onto octahedral group irreps	24
3.1	Examples of several SU(3) Young tableaux.	31
3.2	SU(3) representations that couple to pure gauge fields.	34
3.3	Gluelump multiplet colour factors	37
9.1	Lattice calculation run-times.	103
9.2	A one-exponential fit to the T_1^{+-} octet correlator	106
10.1	Octet gluelump spectrum	133
10.2	Decuplet gluelump spectrum	134
10.3	27-plet gluelump spectrum	135
10.4	Summary of octet mass splittings in previous studies	138
10.5	Re-analysis of previous lattice octet gluelump spectrum	142
A.1	List of abbreviations and symbols	150
B.1	Raw results: 1×1 plaquette-based octet at $a = 0.0982$ fm	152

B.2	Raw results: 2×2 plaquette-based Octet at $a = 0.0982$ fm	154
B.3	Raw results: chair-based octet at $a = 0.0982$ fm	156
B.4	Raw results: chair-based octet at $a = 0.0685$ fm	159
B.5	Raw results: chair-based decuplet at $a = 0.0982$ fm	163
B.6	Raw results: chair-based 27-plet at $a = 0.0982$ fm	164
B.7	Raw results: chair-based 35-plet at $a = 0.0982$ fm	166

List of Figures

4.1	Example of a chair on the lattice.	59
4.2	A C_2 rotation of a cube.	62
4.3	The octet chairs.	65
5.1	An example of a decuplet “chair” building block.	77
5.2	The decuplet chairs.	79
5.3	Operator-propagator-operator flow in the decuplet case.	81
9.1	The effects of smearing on the octet gluelump states.	98
9.2	Choosing smearing parameters.	101
9.3	Signal extraction.	108
10.1	The octet correlators based on 1×1 plaquettes.	119
10.2	The octet correlators based on 2×2 plaquettes.	120
10.3	The complete set of octet correlators.	121
10.4	The complete set of octet correlators on a finer lattice.	122
10.5	The decuplet correlators.	123
10.6	The decuplet correlators on a finer lattice.	124
10.7	The 27-plet correlators.	125
10.8	The 35-plet correlators.	126
10.9	The full spectrum of octet effective energies.	127

10.10	The full spectrum of octet effective energies on a finer lattice.	128
10.11	Octet gluelump spectrum	137
10.12	Comparison of octet mass splittings	139

Chapter 1

Introduction

The Standard Model (SM) of particle physics is remarkably successful and equally well studied. It is, however, not a final theory of particle physics as there are several problems it cannot explain, such as for example the unknown identity of Dark Matter. Huge international experiments (notably the ATLAS and CMS projects at the Large Hadron Collider) were built in order to look for signs of Beyond-the-Standard-Model (BSM) physics. In order to guide experimentalists' searches and to help explain the spectrum of particles that is observed, it is important for theorists to provide detailed predictions. It is to this end that this work attempts to discover the properties of some bound states involving heavy colour-multiplet BSM particles. In this chapter, the motivation for studying these heavy coloured particles will be discussed from a particle physics point of view. In the first section, an overview of the scope of this work will be presented, and the layout of this thesis will be explained. The results of this thesis have also recently been reported in a more condensed form in Ref. [1].

1.1 Overview

Beyond-the-Standard-Model (BSM) theories include the possibility of new coloured objects. If they are from an appropriate colour representation, they may form colour-singlet bound states called gluelumps with Standard Model gluons and virtual quarks. The BSM coloured particles would have masses larger than the QCD (quantum chromodynamics) scale of about $\Lambda_{\text{QCD}} \sim \mathcal{O}(100 \text{ MeV})$. There are scenarios where these particles may also be stable or at least long-lived, such as the case of a gluino LSP (lightest Supersymmetric particle). Even though many forms of supersymmetry seem to be excluded by recent searches at CERN (see for example recent ATLAS limits on gluino and squark masses in Ref. [2]), the search for physics beyond the Standard Model continues, motivated by concerns such as fine tuning, hierarchy problems, and the identity of Dark Matter. These will be discussed in Section 1.3.

The known elementary particles of QCD are quarks which belong to the triplet representation of colour, and gluons which belong to an octet. Supersymmetry introduces new colour-triplet particles (the squarks) and new colour-octet particles (the gluinos). The fermionic gluinos are candidates for forming gluelumps, but they are not the only proposed particles that could form gluelumps. There has been some recent attention in the literature to possible massive vector bosons which are also in the colour-octet representation of $SU(3)$. Such states appear in many BSM theories as discussed for example in Ref. [3] (and especially references 1-14 within) as well as Ref. [4] (and especially references 3-24 within). These include *colourons* from various models which extend the QCD gauge group to $SU(3)_1 \times SU(3)_2$. When the third generation of quarks is assigned to one of these $SU(3)$ groups and the lighter quarks to the other, this gives rise to the *topgluons* of topcolour models. In chiral colour model variations, the gauge groups have explicit chirality, $SU(3)_L \times SU(3)_R$, and this results in the prediction of *axigluons*. All of these various versions of colourons are bosons

belonging to the octet representation of $SU(3)$. In Kaluza-Klein models, towers of excited gluonic states also present previously unseen colour-octet states, relying on the presence of extra spatial dimensions. String theory, various technicolour models, and other theories which propose new strong dynamics also predict new coloured particles in the octet representation, and even allow for particles of colour representations beyond the octet. For example, if new elementary particles akin to techniquarks carry QCD colour charge, then they can bind into composite states such as technihadrons which are technicolour singlets but can carry QCD colour. Vector mesons like technirhos are in the octet representation of $SU(3)$ colour, and in general the composite particles can occur as octets, decuplets, or other colour-multiplets of $SU(3)$. A technibaryon (like a techniproton) could occur as an octet or a decuplet. The technicolour equivalent of a di-meson (with two techniquarks and two anti-techniquarks) can occur in $SU(3)$ 27-plets, decuplets (or anti-decuplets) or octets, as can a techni-pentaquark, which could additionally be in a 35-plet $SU(3)$ representation. For recent discussion of these various BSM models (and the colour representations they predict) in the context of physics at the LHC, see for example Refs. [5–11].

Beyond the colour-octet, larger colour representations have also been examined from a more theoretical point of view, for example by studying the conformal windows for such states. Ref. [12] and references therein provide a good general review of this, and Refs. [13–15] focus on larger colour representations in general $SU(N)$ theories. Larger colour representations of $SU(3)$ have also been studied in other contexts, and some group theory inspiration was drawn from these previous works, which include a 27-plet of dibaryons [16] and a study of finite transformations of triplet, octet and decuplet systems in $SU(3)$ [17].

Experimentally, the Large Hadron Collider (LHC) collides protons with protons at high energy. At the particle level it is the coloured constituents - the quarks and gluons - that are interacting. Because of the coloured nature of these interactions,

the rate for production of new coloured resonances is very high. Ref. [3] estimates possible cross-sections for detecting some new coloured states in different scenarios in the dijet spectrum at the LHC.

In Chapter 3, it is shown that the lowest-order representations which contain coloured particles that can form bound states with Standard Model gluons and sea quarks without requiring any valence quarks are the octet, decuplet, 27-plet, 28-plet and 35-plet. All five of these systems are studied here. The heavy colour-multiplet particles from these various representations of $SU(3)$ will hereafter be referred to simply as the “colour-multiplet particles.” It is assumed that they cannot decay strongly, so they are stable in QCD. Although colour bound states involving colour-multiplet particles from the *octet* representation have been studied previously [18–21], there are no previous lattice calculations involving the larger representations. In the late 1990’s, Foster and Michael addressed QCD bound states involving a gluino-like particle (a heavy coloured particle in the octet representation of $SU(3)$), and used the term “gluelump” for such states [18]. This term will henceforth be applied to all bound states of a heavy colour-multiplet particle with Standard Model background, regardless of which $SU(3)$ representation the colour-multiplet particle is from.

In this study of larger colour-multiplet gluelumps, techniques from lattice quantum chromodynamics are employed. In the coming chapters, the underlying group theory required to put exotic colour-multiplet particles on the lattice is developed, and the spectrum is presented for gluelumps containing various colour-multiplet particles. This study revisits the gluelump work of Foster and Michael [18], and extends the search for gluelumps to include colour-multiplet objects from representations beyond the octet. Gluelump systems involve only a heavy coloured object and gauge (gluonic) fields, and as such are inherently noisy, but careful analysis resulted in exceptionally good results especially in the octet sector. Detailed data analysis was possible, as was a thorough exploration of errors, both statistical and systematic. In addition

to the octet gluelump spectrum, results are presented for gluelumps involving larger colour-multiplet particles. These serve as a good first examination of these previously unstudied sectors, but further work may be required to refine and improve upon the quality of the results.

This dissertation is laid out as follows. In Chapter 1, the theoretical motivation for the work is presented, and previous work on the subject is reviewed. Chapter 2 is devoted to a brief overview of lattice quantum chromodynamics in order to familiarize the reader both with the terminology and procedures used in this field, as well as the obstacles and hurdles that are involved. Chapter 3 is devoted primarily to a study of the group theory considerations involved in formulating the various $SU(3)$ representations for the lattice.

Chapters 4 through 8 present the theoretical underpinning needed in each of the specific colour-multiplet representations, namely the octet, decuplet, 27-plet, 28-plet and 35-plet in that order. The algebraic basis is laid out explicitly and all the details of the physics behind the lattice calculations are given. Details of the computational aspects of the calculations are reserved for the following chapter. Chapter 9 discusses some of the computational techniques used and explains the analysis that was done on the data.

Chapter 10 summarizes the results of this work, and presents the spectrum of states in the various representations that were studied. Final comparisons with the previous work of Foster and Michael are also provided. Brief conclusions are given in Chapter 11, and the importance of the continued study of gluelump systems is emphasized.

A table of the abbreviations and symbols used in this text is provided in Appendix A, and tables of fitted data are presented in Appendix B.

1.2 Gluelumps

In 1999, Foster and Michael published a paper in which they examined the spectrum of QCD bound states involving a gluino-like BSM particle [18]. This particle was not restricted to being the supersymmetric gluino, it merely had to be a heavy coloured particle in the octet representation of $SU(3)$. They had previously examined the two lightest such states in an $SU(2)$ model [19] and later in an $SU(3)$ model [20], as well as examining the static force involved in such states in $SU(3)$ [21]. The problem has not been revisited on the lattice since then. In the 1999 paper, they studied the spectrum of gluelumps (a term referring to the bound state $g\tilde{g}$ of a heavy gluino and gluons) and adjoint mesons (bound states $\tilde{g}q\bar{q}$ of a heavy gluino and two quarks, with the study limited to light quarks), and mentioned the possibility of studying adjoint baryons ($\tilde{g}qqq$), though this was beyond the scope of their work. They did not consider particles from any $SU(3)$ colour representations beyond the octet.

With significantly more computing power than was available 15 years ago when Foster and Michael first studied this problem, a modern re-calculation of their results is warranted. At the very least, the inherent 10% systematic error introduced by using quenched lattices¹ can be eliminated. Foster and Michael acknowledge this source of error in their results. Today, it is not a concern as a whole network of pre-prepared dynamical (unquenched) lattices is available to be used in calculations.

In addition to the systematic error introduced by using quenched lattices, there were other limitations to Foster and Michael's work. Because of the way they chose to construct their gluelump operators (more on this in Section 4.1), they were only able to access half of the possible Λ^{PC} octahedral group representations on the lattice. They may have missed key states that couple to continuum states with J^{PC} quantum numbers this way. Foster and Michael also restricted their study to exotic particles

¹See more about quenched lattices in Section 2.2.

that belong to a colour octet, such as the gluino. It is possible, however, that some Beyond-the-Standard-Model schemes may involve colour-multiplet particles that belong to a different representation of $SU(3)$.

1.3 Theoretical Motivation

Although the Standard Model is a remarkably successful theory, it has many limitations, and there are several issues in physics that it does not address. For example, fermion masses do not appear naturally and it does not offer an explanation of the gravitational force, nor does it provide a Dark Matter candidate. For these reasons, it is important to search for new physics beyond the Standard Model. Supersymmetry (SUSY) and other Beyond-the-Standard-Model (BSM) theories in general predict a whole host of other heavy particles which have not yet been observed. Experiments at CERN are poised to search for BSM particles and distinguish between the proposed theories. Most BSM physics is motivated by three primary theoretical considerations [22]. First and foremost is to stabilize the Higgs mass, which otherwise gets radiative corrections from loop diagrams (involving mostly the top quark) that make the Higgs mass diverge quadratically. This is a fine-tuning problem known as the weak scale hierarchy problem, and supersymmetry is able to offer a “natural” solution to this problem by the introduction of a symmetry between fermions and bosons. Secondly, the “grand unification” of the gauge couplings of the strong, weak, and electromagnetic forces is another strong theoretical motivation for looking for new physics at around the electroweak scale of several hundreds of GeV. This is another fine-tuning problems of physics - the different forces of nature have very different strengths. The weak force is more than 10^{30} times stronger than the gravitational force. SUSY provides a mechanism through which to unify the gauge couplings at high energy. It also contains in its algebra the generator for space-time translations,

which is a necessary component of quantum gravity. As such, supersymmetry is required for string theory, M-theory and other such quantum gravity models. The third important motivation for BSM physics is to address the cosmological problem of Dark Matter.

One of the unsolved mysteries of physics today is to explain what the universe is made of. It is known that only about 24% of the energy density of the present universe comes from matter [23], and the rest is from an entity called Dark Energy, about which very little is known. Perhaps even more shocking, however, is the fact that all the stars and gas and matter that is observed in the universe only make up about 4% of the energy density required for closure [23]. From the WMAP survey, it is now known that the universe is indeed flat, implying that most of this 24% matter is unaccounted for. As such, this unaccounted matter is generically known as Dark Matter.

Unlike for Dark Energy, there are possible solutions on the horizon for identifying the source of Dark Matter. It is generally agreed today that Dark Matter must be “cold,” meaning that the particles that account for it must be nonrelativistic and probably heavy. Dark Matter interacts only through the weak and gravitational forces, since any strong or electromagnetic interactions would have led to observation.

One of the attractive features of supersymmetry is that it naturally supplies a Dark Matter candidate if R-parity is conserved. R-parity is a discrete symmetry that assigns $R = -1$ to all SUSY particles, and $R = +1$ to all Standard Model particles. It is a multiplicative quantum number, meaning that a SUSY particle must decay into an odd number of SUSY particles (plus some number of Standard Model particles). If R-parity holds, then that means that the lightest SUSY particle must be stable, since there is nothing it can decay into in an energy conserving process. This lightest SUSY particle (LSP) is therefore a Dark Matter candidate. The fact that supersymmetry naturally provides a possible solution to the Dark Matter problem is an attractive

feature of the theory, and one of its prime motivations.

Supersymmetry is a so-called “broken” symmetry. If it was a perfect symmetry, the masses of the sparticles (the SUSY partners to the SM particles) would be degenerate with the masses of their Standard Model partners, but it is known that no such particles exist at energies comparable to the Standard Model particles. Preliminary results from ATLAS indicate that the threshold for gluinos is above about 860 GeV, and squarks are excluded with masses less than about 1320 GeV [2]. The SUSY particles are expected to have masses around the TeV-scale, and searches at the Large Hadron Collider (LHC) at CERN are underway in an attempt to detect these particles. Currently there is no experimental evidence for SUSY, and it is not known which form supersymmetry will take if it is indeed a correct theory of nature. It is hoped that detector searches at the LHC will soon resolve this question.

The above considerations are compelling motivation for some sort of new physics at the TeV-scale. It is natural therefore to expect a whole spectrum of new heavy particles at that scale, including the possibility of new coloured particles. If these are meta-stable, they may form gluelump colour-singlet bound states with Standard Model quarks and gluons. As new coloured particles may be produced at the LHC, knowing the spectrum of these bound states is of great interest. Gluelump binding is in the non-perturbative regime of strong force coupling, and the only known method for studying such states rigorously is with the computational tool of lattice QCD. Since the coloured particles are assumed to be heavy, they will act as stationary sources on the lattice, propagating only in the time direction. Their spin statistics may be ignored. As such, heavy octet particles studied on the lattice may belong to any theory, and do not rely on a supersymmetric framework. Bound gluelump states involving coloured particles from representations beyond the octet have not previously been considered. The gluelump spectrum is indeed an important addition to the understanding of Beyond-the-Standard-Model physics, and it warrants further

study. This study improves upon previous gluelump calculations, and extends the search to previously unstudied larger colour representations.

1.4 Previous Gluelump Studies

1.4.1 Lattice Studies

Although they did not first propose the idea of gluino bound states (work was done previously especially in the case of light gluinos [24, 25]), Foster and Michael brought the topic to the fore in their comprehensive lattice study in the late 1990's. They built operators from square plaquettes on the lattice. Using these building blocks, they were only able to access ten out of the twenty possible Λ^{PC} quantum states on the lattice.² They claimed that these were likely to be the lowest energy states, but there are many continuum quantum numbers that their operators cannot access, such as for example $J^{PC} = 0^{+-}, 0^{-+}, 0^{--}, 1^{++}$, etc. Foster and Michael also restricted their study to octet-representation gluelumps. The examination of larger colour representations is novel to this current work.

Foster and Michael carried out their calculations on various sizes of lattices. The characteristics of these configurations are listed in Table 1.1, and may be compared to the parameters in Table 2.1 used in this work. A discussion of what these parameters mean can be found in Section 2.2. By measuring the spectrum at several lattice spacings, they were able to extrapolate to a spacing of $a = 0$ and estimate continuum mass splittings for their gluelump spectrum for some of their lightest states.

Foster and Michael employed a smearing (or “fuzzing”) algorithm to improve their signal. They then used the variational technique on a matrix of correlations built using results from different amounts of smearing and using different sized operators.

²More detail can be found about lattice quantum numbers and symmetries in Section 2.3.

Table 1.1: Properties of ensembles of lattice configurations used by Foster and Michael in previous gluelump studies.

β	Size	Number of Lattices	Lattice spacing, a (fm)
5.7	$12^3 \times 24$	99	0.1701
6.0	$16^3 \times 48$	202	0.09484
6.2	$24^3 \times 48$	60	0.06832

This allowed them to improve their ground state signal and in some cases also detect excited states. Their final mass fitting method was slightly less rigorous than the one used here, and involved pairwise fits to the data as described in Section 10.2.

A comparison of the results obtained by Foster and Michael and the current results can be found in Figure 10.12. It is worth noting that Foster and Michael only had operators that coupled to ten of the twenty possible octet gluelump states. While they performed fits at several different lattice spacings for all these states, their final summary and analysis was only for the lightest five mass splittings. By contrast, this current work applies a full detailed analysis on all twenty possible states, and includes an in-depth treatment of errors, both statistical and systematic, which was also not present in previous work.

The final reported mass splittings (energies above the 1^{+-} ground state) as found by Foster and Michael are shown in Table 1.2.

1.4.2 Bag Model Studies

Although a full treatment of the gluelump system cannot be done in perturbative QCD, other more antiquated models are still able to make a rough analytic approximation without lattice calculations. The Bag Model is a very intuitive albeit old-fashioned model. It is simple to understand and gives good first order mass estimates for most bound hadrons. It can even deal with scattering and fission/fusion processes.

Table 1.2: Gluelump energy spectrum mass splittings from the lattice calculations of Ref. [18] with statistical errors only.

J^{PC}	Relative Energy (GeV)
1^{+-}	–
1^{--}	0.368(7)
2^{--}	0.567(10) ^a
3^{+-}	0.972(24)
2^{+-}	0.973(36)
0^{++}	1.092(28)

^a This entry repairs a simple typo in column 4 of Table III in Ref. [18], as can be seen by comparing with column 3 of that same table and with Fig. 3 in Ref. [18].

The Bag Model was first developed in the late 1960’s at a time when the quark model was established, but the mechanism for both long-distance confinement and short-range asymptotic freedom was not well described by any predictive theory. In the Bag Model, hadrons are described as 3-dimensional “bags” with all the constituent quarks and gluons inside the bag, and no QCD fields outside the bag. Inside the bag, the particles are essentially non-interacting (subject only to weak forces), and act as free particles. The vacuum energy outside the bag is lower, and the surface of the bag itself has a certain tension. “Pulling” a quark out of the bag requires more energy than quark-antiquark pair production, so if one of the bound quarks inside the bag is bumped with enough energy, a jet of mesons can be produced just as is found in collider physics. The Bag Model was quite successful, predicting nucleon masses to within about 30% of the experimental values as well as resolving excited states, the axial vector current, and other important quantities. For an introduction to Bag Models, see for example Chapter 8 of Ref. [26] or Ref. [27].

Solving for states in the Bag Model involves confining particles in a cavity (often spherical) of a given radius and solving the resulting Lagrangians to match boundary conditions on the surface of the bag. Among other things, this demands that the

quark vector current normal to the surface vanishes. Physically, this imposes quark confinement by ensuring that quark fields are restricted to the inside of the bag. Solutions to basic bag configurations are Dirac equations.

Gluelump states are quite easily studied (at least to first order) in the Bag Model, and there were several early discussions of these systems with supersymmetric gluinos as the colour-multiplet particle [25,28]. In particular, it was found that gluino masses greater than about 1 GeV always resulted in charged shadrons that are stable against strong interactions.

After the lattice study by Foster and Michael, Karl and Paton utilized the Bag Model to confirm the hierarchy of states found on the lattice [28]. They started by considering a heavy gluino (a colour-octet particle) bound with just one gluon in a bag. To lowest order, the energies of the states they found related to the energy of the gluon mode. These were calculated based on the known dynamics of a confined massless vector field, analogously to an electromagnetic field in a box. Colour-electric and colour-magnetic fields were defined. They were required to have certain behaviour on the bag boundary (no electric component parallel to the surface, and no magnetic component perpendicular to it). Solving for the components of the electric and magnetic fields gave initial energy estimates for the gluon modes. There were also smaller contributions to the gluelump mass from Coulomb interactions between the gluon and gluino, and these were estimated with some uncertainty due to choice of model parameters. All of these 1-gluon states have negative charge conjugation. Karl and Paton also approximated a 2-gluon solution, but were not able to predict the splittings between the resulting $J^{PC} = 0^{++}$, 1^{++} or 2^{++} states and so assumed that the 0^{++} was the lightest. It is therefore the only positive charge conjugation state for which they estimate an energy. The final energy spectrum suggested by their Bag Model study is reproduced below in Table 1.3. This will be compared to the lattice spectrum in later chapters, but it is worth noting that the hierarchy of the first few

states is in good (though not perfect) agreement with the lattice predictions.

1.4.3 Other Analytic and Computational Gluelump Studies

After Foster and Michael's 1999 paper with initial lattice predictions for the gluelump spectrum, there was a flurry of interest in the topic. One noteworthy gluelump study is the analytic calculation done in Coulomb gauge QCD via the variational approach [29]. In that study, the colour-octet particle is not represented by a gluino-type object, but rather by a quark-antiquark pair in the octet representation. The gluelump is a bound state of this pair with a single gluon. This model is interchangeable in many aspects with the more conventional gluino-based gluelump since all the quantum numbers are the same if the quarks are both placed at the origin with zero separation. The system is rotationally symmetric as well as invariant under parity and charge conjugation. The hierarchy of states that was found agreed with that found on the lattice by Foster and Michael. The authors also give a detailed description of phenomenological reasons for the spin states to occur in the order that they do, which at first may not be intuitive. For example, the two lightest states are the 1^{+-} followed by the 1^{--} , however if the bound state is interpreted as a single gluon bound to the heavy octet particle, then the lighter state is in a p -wave configuration and the heavier one is in an s -wave. Normally one would expect the s -wave to be the lighter state, however Ref. [29] finds that 3-body interactions drive the mass of that state higher than the p -wave. In this system, 3-body interactions involve simultaneous interactions between the gluon in the bound gluelump state with both of the quarks in the quark-antiquark octet pair.

The gluelump spectrum from the Coulomb gauge study [29] is presented in Table 1.3 along with Bag Model results [28] and results from a QCD string model [30], as well as a transverse gluon model (choosing $r_0 = 0.5$ fm to display their results) [31].

Table 1.3: Estimate of the gluelump energy spectrum from various model calculations.

J^{PC}	Energy (GeV)			
	bag model [28]	Coulomb gauge [29]	string [30]	transverse gluons [31]
1^{+-}	1.43	0.88	1.87	0.89
1^{--}	1.98	1.27	2.34	1.26
2^{--}	1.97	1.47	2.36	1.46
3^{+-}	2.44	2.00	2.71	1.85
2^{+-}	2.64	1.59	2.70	1.83
0^{++}	2.6		2.78	
4^{--}		2.49		2.18
3^{--}				2.23

On the lattice, three gluelump states were also calculated using an abelian projection in both quenched and $N_f = 2$ full QCD, however this was done in a proof-of-concept manner that was intended to probe the method of abelian projection more than to discover gluelump properties [32]. Abelian projections are used when one wants to probe the possibility of magnetic monopoles in a theory.

The fact these models independently confirm the basic ordering of the gluelump spectrum is excellent reassurance, but they are all still approximations in one way or another. In order to study full QCD and rigorously examine these SU(3) bound states, one *must* use the lattice, and the study done by Foster and Michael in the 1990's remained the most current such examination until now. This work will modernize the lattice results, fill in the missing states that were not accessible to Foster and Michael, and explore new territory beyond the octet representation gluelumps. Errors both statistical and systematic will be rigorously considered (such a discussion was missing in earlier studies), and the fully dynamical spectrum will be presented.

Chapter 2

A Brief Overview of Lattice QCD

Quantum Chromodynamics (QCD) is the theory of the strong interactions that occur between quarks, gluons and other particles carrying colour charge. In the high-energy limit, it describes asymptotically free elementary coloured particles. In the low-energy limit it describes bound states such as hadrons as well as low energy scattering. Unlike Quantum Electrodynamics (QED), QCD cannot in general be solved analytically except in the high energy (short distance) regime where perturbation theory may be applied. In order to understand even the basic properties of hadrons, however, a regularization scheme is needed to deal with divergent integrals that occur. Lattice Quantum Chromodynamics is such a scheme, and in fact it is the only rigorous method for performing calculations where the strong force is *strong*. It works by discretizing continuous space and time into small steps and approximating infinite spacetime in a finite volume hypercube. Lattice QCD is well formulated for computer calculations and has proven to be both useful and extremely accurate. As computing power has increased, the field has enjoyed huge advances to the point where it is now a useful theoretical tool for explaining or even predicting the properties of various systems.

2.1 Introduction

Lattice Quantum Chromodynamics or Lattice QCD is a regularization scheme that allows QCD quantities to be calculated on a discretized 4-dimensional lattice in Euclidean spacetime. It is not a “model” - it is full QCD physics in the limit where the lattice spacing a goes to zero. The field originated in the 1970’s and grew into a well-established method that has been used to successfully calculate particle masses, form factors, and decay constants as well as finding use in a whole spectrum of other applications from studying Higgs models to answering questions about possible Beyond-the-Standard-Model scenarios. For a full working description of lattice methods, see for example Refs. [33–37]. In this chapter, the various terminology and techniques that are used in this thesis will be described.

Lattice QCD simulates quark and gluon fields on a finite 4-dimensional grid with three spatial directions and a time direction. The time direction is measured in Euclidean units of $\tau = it$, where t is standard time. Quark fields are evaluated on the sites of the lattice and gluons appear as gauge fields on the links or bonds between the sites.

In order to calculate the mass of an object on the lattice, one needs several components which are described briefly below.

2.2 Configurations

Configurations represent the background fields of a theory such as SU(3). In the so-called “quenched” approximation, this just involves gluons by means of gauge fields. “Dynamical” configurations also have sea-quark fields built into them. For SU(3) theories, a configuration is a collection of statistically independent complex SU(3) matrices. At each lattice site, there are four such matrices, one pointing in each of

the four space-time directions, to pictorially create the “links” between lattice sites. Just like in experimental particle physics where many events need to be observed to properly detect the properties of a particle, so too any one lattice calculation requires runs on a whole ensemble of hundreds of independent uncorrelated configurations in order to get statistically significant results. Configuration generation can be computationally time-consuming, but there are several resources for acquiring ensembles that have already been prepared by other researchers. For example, the International Lattice Data Grid (ILDG) along with its various regional branches facilitate the sharing of lattice gauge configurations, making ensembles available to other researchers to use.

In order to generate an SU(3) lattice configuration, one could start with a random SU(3) matrix $U_\mu(\vec{x}, \tau)$ at each lattice space-time point, (\vec{x}, τ) and pointing in each of the four directions, μ . These can be visualized as the “links” on the lattice. This is a configuration, however in order to represent real physics, it should be “thermalized” so that an observable is stable against fluctuations of this background. *Importance sampling* dictates that the probability of arriving at a particular configuration of links, C , is

$$P(C) = \frac{e^{-S(C)}}{\sum_{C'} e^{-S(C')}} \quad (2.1)$$

where $S(C)$ is the action of configuration C . For example, the SU(3) Wilson gauge action (which does not involve quark fields) is

$$S_{G,Wil}[U] = \frac{\beta}{2} \sum_{x,\mu,\nu} \left(1 - \frac{1}{3} \text{ReTr} P_{\mu\nu}(x)\right). \quad (2.2)$$

This involves the lattice parameter β which will be discussed below and the real part of the trace of the plaquette $P_{\mu\nu}(x)$. This plaquette is the product of four links tracing out a square on the lattice starting and ending at space-time point x . It is in the $\mu\nu$

plane, where μ and ν are any two of the four space-time directions. All values of x , μ and ν are averaged over.

In order to thermalize a configuration, one can modify individual links to create a new configuration, then modify links in the new configuration to create another updated version and so on. This sequence is called a Markov chain. A Markov chain has the correct importance sampling if the probability of arriving at configuration C' from configuration C is,

$$P(C \rightarrow C') = \frac{e^{-S(C')}}{e^{-S(C)}} P(C' \rightarrow C). \quad (2.3)$$

In practice, this can be accomplished for example by the Metropolis algorithm starting with a random configuration C and measuring its action. Then an updated configuration is proposed by replacing an individual link with a different SU(3) matrix. The action of new configuration, C' , is calculated. If it is less than the action of the original configuration, that is if $S(C') < S(C)$, then the configuration C is discarded and replaced by configuration C' . If $S(C') > S(C)$ then it is necessary to generate a random number r between 0 and 1. If $r \leq \frac{e^{-S(C')}}{e^{-S(C)}}$, then the configuration C is discarded and replaced by configuration C' . Otherwise C' is abandoned and C is retained. The retained configuration is updated and the process is repeated. In general, all the links of a lattice are updated numerous times. If one individual link is updated repeatedly before moving on to the next link, then this is called a multi-hit (or in the limit of completely thermalizing a link to its surroundings before moving on, a *heat bath*) Metropolis. A configuration is thermalized when, for example, the value of some observable like the average trace of all plaquettes $P_{\mu\nu}(x)$ does not change with subsequent configuration updates. It can then be saved. The next configuration in an ensemble can be generated the same way, or it can start with the previous configuration as a starting point as long as there are sufficient updates between the

two configurations so that they are not statistically correlated.

Lattice QCD contains two fundamental parameters (although many more exist, as seen below in Table 2.1). The first is the gauge coupling constant, g , or equivalently $\beta = 6/g^2$. This is related to the fine-structure constant, $\alpha_S = g^2/4\pi$. The continuum limit is when $g = 0$, or $\beta \rightarrow \infty$. A larger β corresponds to a finer lattice spacing. The continuum limit takes the spacing to zero to recover continuous physics from the discrete lattice.

It is desirable to do lattice calculations at large β so as to better approach the continuum, but a finer and finer spacing means that the overall physical volume of the lattice shrinks unless more and more lattice sites are included which begins to be very computationally expensive. For example, at $\beta \rightarrow \infty$, a lattice with 20 lattice sites in each space-time direction might be too small to physically “fit” any hadrons. Their Compton wavelength would be longer than the whole lattice. On the other hand, if $\beta \rightarrow 0$, the SU(3) gauge links on the lattice are effectively random and uncorrelated. At very small (but finite) values of β , the lattice spacing between individual lattice sites is very large. It could be much larger than the characteristic length-scale (such as the Compton wavelength) of the system being studied. The particles “fall between cracks” of the lattice. This scenario shows itself in hadron masses that are greater than 1 in lattice units, since masses on the lattice are measured in units of the inverse lattice spacing $1/a$. Ideally, the spacing between adjacent lattice sites should be smaller than the Compton wavelength of the states being studied, which should in turn be smaller than the overall dimension of the lattice configuration.

For dynamical (unquenched) lattices which include sea quarks, another important parameter of lattice QCD is the hopping parameter, $\kappa = \frac{1}{2(m_0 a + 4)}$, where m_0 is the bare quark mass¹ which is tuned in order to produce the correct hadron masses, based

¹Note that m_0 may in fact be negative, as in the case with the configurations listed in Table 2.1.

on a well-known particle such as the pion. For non-degenerate quark flavours, there may be more than one hopping parameter.

Two ensembles of configurations were used for the calculations in this study. Both were provided by the ILDG from the CP-PACS and JLQCD collaborations and they are dynamical, with two light quark flavours and a heavier strange quark [38–40]. The pedagogical discussion above of the Metropolis configuration generating technique was for a quenched lattice that does not involve fermion fields. The configurations used here were generated using the polynomial hybrid Monte Carlo method. They are based on a fully $\mathcal{O}(a)$ improved action that combines the Iwasaki gluon action and the Wilson-clover quark action. The first ensemble contains 790 configurations of dimension $20 \times 20 \times 20 \times 40$ (or $20^3 \times 40$), with the longer dimension assigned to the time direction. In terms of computer disk space and the time it takes calculations to run, it is smaller than the other ensemble of $650 \times 28^3 \times 56$ configurations. For this reason, the first ensemble was used for the majority of calculations.

Simulation masses (or energies) are not physical masses. By approximating the colour-multiplet particle as infinitely heavy on the lattice, the lattice itself acquires a fundamental “self-energy” off-set value. Only mass differences are physical, but this is sufficient to establish a spectrum. Although the absolute (unphysical) simulation energies were greater than one in lattice units in both this work and in Foster and Michael’s original work, many of the mass-splittings that were found were indeed less than one. Arguably it might still be preferential for the simulation energies to also be less than one, but it was found that mass splittings as measured on the two different ensembles at different lattice spacings agreed within error. Since lattices were chosen that were fine compared to the QCD scale of $\Lambda_{QCD} \sim \mathcal{O}(100 \text{ GeV})$, the absence of lattice spacing effects indicates that it is unlikely that either set of configurations is too coarse for the physics of the gluelump system to “fit” properly.

The characteristics of both ensembles used in this work are given below. Many

of the parameters given are configuration generation parameters. They include the clover coefficient (c_{SW}), the hopping parameters for light and strange quarks (κ_{ud} and κ_s), the number of molecular dynamics steps in one trajectory ($1/\delta\tau$), the polynomial Hybrid Monte Carlo (PHMC) polynomial order (N_{poly}), and the analyzed trajectory length. Also included are the mass ratios $\frac{m_{PS}}{m_V}$ for pseudoscalar and vector mesons with their quarks in light-light (LL) and strange-strange (SS) mass combinations.

Table 2.1: Properties of ensembles of 2+1 flavour full QCD lattice configurations used in this current gluelump study [38–40].

parameter	1 st ensemble	2 nd ensemble
β	1.90	2.05
lattice dimensions	$20^3 \times 40$	$28^3 \times 56$
lattice spacing based on K -input, a (fm)	0.0982(19)	0.0685(26)
lattice spacing based on ϕ -input, a (fm)	0.0983(19)	0.0687(25)
number of lattices	790	650
clover coefficient, c_{SW}	1.7150	1.6280
κ_s hopping parameter	0.13640	0.13540
κ_{ud} hopping parameter	0.13700	0.13560
$\delta\tau$	1/180	1/250
N_{poly} PHMC polynomial order	140	250
analyzed trajectory length	7900	6500
m_{PS}/m_V (LL) light sea quarks	0.6243(28)	0.6361(47)
m_{PS}/m_V (SS) strange sea quarks	0.7102(20)	0.6852(46)

2.3 Operators

Operators are gauge-invariant objects on the lattice that have the proper group symmetry. For this work they are constructed by taking the product of links around a path drawn between sites on the lattice. The simplest gauge-invariant object on the lattice is a plaquette. This is the product of the four links around a closed square in any plane on the lattice. It can be shown in general that any product of links in a

closed loop (or a sum of two or more such loops) is gauge-invariant. These loops do not have to stay in the same plane, but in most cases an operator is built solely out of links in the spatial directions.

Operators may be created in definite quantum states of charge or parity, but because the lattice simulates continuous space-time on an orthogonal discrete grid, some of the other symmetries of the continuum are lost. A particle with a specific angular momentum quantum number cannot directly be examined on the lattice because continuous rotation (such as angular momentum) is not a conserved quantity or a symmetry of the lattice. The group theory that describes the rotational symmetries in real continuum physics is $SO(3)$, the special orthogonal group of dimension 3, whereas rotations on the lattice belong to the octahedral group, O . This is the group of all 3-dimensional rotations of a cube that leave it invariant. This group has five irreducible representations or irreps. These irreps, Λ , are labeled A_1 , A_2 , E , T_1 and T_2 . They are connected in a known way to continuous physics, but it is not a one-to-one relationship. Each of the irreps overlaps with several angular momentum quantum numbers, and sometimes one angular momentum quantum number appears in more than one irrep. For example, a $J = 2$ state couples to both the E channel as well as the T_2 channel. The projections of the continuum $SO(3)$ irreps (the integer angular momentum quantum numbers, J) onto the irreps of O ($\Lambda \in (A_1, A_2, E, T_1, T_2)$) are shown Table 2.2 for the first several values of J . The entries in the table are the multiplicities (number of copies) of the octahedral group irrep Λ in the angular momentum irrep J of $SO(3)$. This is how lattice physics relates back to continuous physics.

Including charge and parity quantum numbers, there are twenty possible quantum states on the lattice. They will be referred to in general as Λ^{PC} and are written explicitly below, where P and C can be ± 1 .

Table 2.2: Multiplicity of octahedral irrep Λ in $SO(3)$ spin J .

$\Lambda \backslash J$	0	1	2	3	4	5	6	7	8	9	10	11	12	...
A_1	1	0	0	0	1	0	1	0	1	1	1	0	2	
A_2	0	0	0	1	0	0	1	1	0	1	1	1	1	
E	0	0	1	0	1	1	1	1	2	1	2	2	2	
T_1	0	1	0	1	1	2	1	2	2	3	2	3	3	
T_2	0	0	1	1	1	1	2	2	2	2	3	3	3	

$$A_1^{PC}, \quad A_2^{PC}, \quad E^{PC}, \quad T_1^{PC}, \quad T_2^{PC}$$

In the context of this work, operators will be built purely from QCD gauge links, and then coupled to a heavy colour-multiplet particle. It is the gauge part of the bound state that carries the Λ^{PC} quantum numbers laid out above. The colour-multiplet particle is considered to be infinitely heavy and stationary so that all of its spin statistics may be ignored without loss of generality. If the colour-multiplet particle turns out to be scalar, then the quantum numbers of the gauge component are also the quantum numbers of the bound state. Even if it is not, the resulting spectrum found in this work can still be applied. The spin assignments here relate to just the light (gauge) degrees of freedom, but the spin of the heavy colour-multiplet particle can be added to that of the light degrees of freedom using appropriate Clebsch-Gordon coefficients. For example, if the colour-octet particle is a gluino with spin 1/2, then the states listed here with $J = 1$ relate to hadrons with spins of 1/2 or 3/2. Although there may be some energy splitting between these physical states, spin is a higher-order correction in the non-relativistic expansion. They will be nearly degenerate.

Operators are used to create and destroy particles at different points on the lattice. In the case of the gluelump calculations, the colour-multiplet particle (the gluino or higher representation object) is assumed to be heavy and as such acts as a stationary source on the lattice. It only propagates in the time direction, not in

the spatial directions. Since it is static, its spin statistics may be ignored. This is a similar technique as one used to study heavy quarks on the lattice.

In order to build the gluelump operators, the colour-multiplet particle is represented by a tensor from the basis of the appropriate $SU(3)$ representation. It is placed at a specific space-time location on the lattice and connected to products of spatial gauge links that start and finish on this source site. Details of the operators are given in Chapters 4 through 8. In their 1999 paper, Foster and Michael used a square plaquette (both 1×1 and 2×2 cases were studied) as the fundamental building block for their operators. Their operators were sums of plaquettes in different spatial planes, listed explicitly in Ref. [41]. The same operators are also listed for example in Ref. [42] in an intuitive PC -symmetrized basis. Because a square still has a high degree of symmetry, they were only able to access 10 out of the 20 total possible Λ^{PC} quantum states listed above. Based on the Bag Model and other analytic approximations discussed previously, there was motivation to believe that these would couple to the lowest energy continuum states, but they could not access *all* the possible lattice quantum numbers. For that reason, a whole new set of operators based on a “bent chair” building block is developed in Chapters 4 through 8 for studying the gluelump systems more thoroughly. In this work, both plaquette- and chair-based operators were tested for octet gluelumps, and the results were consistent for the ten states accessible to both types of operator.

2.4 Propagators

A propagator describes how a particle moves through spacetime. In general, a propagator is the matrix inverse of a 2-point function. These very large sparse matrices can require a lot of computer resources in order to invert.

In the case of the gluelump systems, bound states occur between heavy stable

objects in various colour representations and Standard Model gluons and sea quarks. Because the colour-multiplet particles are so heavy, their momentum can effectively be ignored and they appear stationary on the lattice. The propagator then must just move the object forward in the time direction while it stays at the same spatial coordinates on the lattice. This simplifies the form of the propagator and it can be written as the time-directed product of lattice links, reformulated to be in the appropriate colour representation. See Chapters 4 through 8 for a detailed description of how the propagators are created and projected onto the larger colour representations in each particular case.

In approximating the colour-multiplet particles as being infinitely heavy and thus described by a static propagator, the lattice acquires fundamentally unphysical self-energy. This acts as an off-set to all the gluelump energies calculated on the lattice. Since the self-energy term is the same for all the gluelump states in any given calculation, energy differences *are* physical. So although absolute energies cannot be measured, a spectrum can be built on top of the lightest state, and this is sufficient. This is the same situation that is encountered by heavy-quark lattice calculations.

2.5 Correlators

In order to calculate the mass of a particle on the lattice, one connects a creation operator at some “source” point at time τ_i on the lattice with a propagator which travels forward some number of steps in the time direction. This is then finally terminated with a destruction operator at a “sink” point at time τ_f . The resulting quantity is called the correlator, and it is a function of the number of time steps separating the source and sink. For the n -plet SU(3) representation, this calculation contracts a $1 \times n$ creation operator, $H^{\alpha\dagger}(\tau_i)$ with an $n \times n$ matrix propagator, $G^{\alpha\beta}(\tau_i, \tau_f)$ and

then finally with the $n \times 1$ destruction operator, $H^\beta(\tau_f)$.

$$C(\tau_f - \tau_i) = H^{\alpha\dagger}(\tau_i)G^{\alpha\beta}(\tau_i, \tau_f)H^\beta(\tau_f). \quad (2.4)$$

Summation over α and β (which both run from 1 to n) is implied, and the correlator is a single number. It is calculated repeatedly for different values of $\tau = \tau_f - \tau_i$. The correlator has a time dependence of e^{-iEt} , or $e^{-E\tau}$ where $\tau = it$ is the Euclidean time which is the coordinate used on the lattice. For a static particle with no momentum, the energy E is the particle's mass, so a graph of the correlator as a function of Euclidean time will result in a decaying exponential which can be fit for the mass.

An important quality of the correlator is that it is gauge invariant. On the lattice, a local gauge transformation can be carried out by introducing a random SU(3) matrix at every lattice site.² Incoming gauge links to a site are multiplied by that matrix, and outgoing links are multiplied by its Hermitian conjugate. A gauge link goes from one lattice site to another, so a local gauge transformation will result in that link being multiplied on the left by the Hermitian conjugate of a random SU(3) matrix from the originating site, and on the right by the random SU(3) matrix that was introduced at the terminating site. It is clear that any closed loop of links on the lattice will always be gauge invariant since adjoining links cancel the sandwiched gauge term. The closed loops of the gluelump operators are coupled to tensors and gauge invariance is not trivial to see in this case. In fact, gauge invariance was an important tool in establishing exactly which basis of tensors to use for each representation.

²The parametrization suggested in Ref. [43] was used to generate random SU(3) matrices.

Chapter 3

Colour Representations

The supersymmetric gluino may form colour-singlet bound states with Standard Model quarks and gluons, leading to a whole spectrum of particles with various J^{PC} quantum numbers. Supersymmetry is not, however, the only possible theory for Beyond-the-Standard-Model physics, and one should allow for the possibility of other colour-multiplet gluino-like particles. Gluinos are fermionic manifestations of the octet representation of $SU(3)$, but it is possible that octet colour-multiplet particles exist that do not have the spin statistics of supersymmetry. Furthermore, colour-multiplet particles may originate from $SU(3)$ representations other than the octet. The gluelump systems studied here do not assume any particular theory. Spin of the colour-multiplet particles is ignored, which is justified because of the fact that they are heavy and act as stationary sources on the lattice. In this chapter, Young tableaux are employed to determine which $SU(3)$ representations might yield the kind of coloured particles that could form gluelumps. In Section 3.3 some of the group theory involved in putting these representations on the lattice is explored and the appropriate tensor basis is developed for each representation.

3.1 Young Tableaux

The goal is to study gluelump systems that involve one colour-multiplet particle coupled to Standard Model gauge fields. These bound states involve only the colour-multiplet particle and Standard Model gluons and sea quarks; systems that involve valence quarks are beyond the scope of this work. In the case where the colour-multiplet particle is a supersymmetric gluino, it belongs to the colour octet of SU(3). A colour singlet bound state can be made between this octet particle and gluons, or, more specifically, *gauge fields* on the lattice. This is because gluons also belong to an octet representation, and $8 \otimes 8$ contains the singlet 1. The octet is its own anti-representation. In fact, since

$$8 \otimes 8 = 27 \oplus 10 \oplus \bar{10} \oplus 8 \oplus 8 \oplus 1, \quad (3.1)$$

it is clear that combining two or more octet gluons will always result in more octet states (along with other states) since $8 \otimes 8$ contains more 8-reps. This is to say that combining any number of gluons (or gauge fields) from the QCD cloud will always yield an octet operator that can bind into a singlet state with the colour-octet particle. This simplifies the gluelump calculations as it means that calculating quark propagators is not necessary since bound states can form without valence quarks.

Now that it has been established that a colour-octet particle such as a gluino can form bound states with QCD gluons, the question arises as to which other SU(3) representations contain coloured particles that can also form bound singlet states with purely gluonic operators without the need for valence quarks. Clearly not all representations have this property. For example, if one considers a coloured particle from the triplet representation, there is no way to form a bound state using only gluons since combining any number of octet gluons never contains the anti-triplet

required to bind the triplet particle into a singlet state. That is, $8 \otimes 8 \otimes 8 \otimes \dots$ does not contain $\bar{3}$. The calculation of the spectrum of heavy colour-triplet particles (for example, heavy quarks) requires quark propagators, and it has been heavily studied in non-relativistic QCD (NRQCD) and heavy quark effective theory (HQET) lattice calculations.

Equation 3.1 shows that two gluons can combine to be in the 27-plet or anti-decuplet representations, so bound states are expected with coloured 27-plet or decuplet particles (the 27-plet is its own anti-rep), but the question remains as to which other representations are possible if three or more gluons are combined.

At this point it is of value to introduce Young tableaux. Young tableaux provide a pictorial way of calculating group theory relations. For $SU(N)$ theories, a Young tableau contains boxes in rows and columns with no more than N rows. In fact, the N^{th} row is redundant since any column which contains N boxes may be “cancelled” out as the identity. A row may never have more boxes than a row above it. A Young tableau is characterized by $N-1$ integers, p_i where i runs from 1 to $N-1$. The value of p_i is obtained by counting the number of boxes in row i and subtracting the number of boxes in row $i+1$. In $SU(3)$, the theory of strong-force colour interactions, Young tableaux can be written in two rows (a column with three boxes is a singlet that can be cancelled off of a larger tableau) and are characterized by (p_1, p_2) . The multiplicity, n , of a state is easily calculated from the Young tableau,

$$n = \frac{1}{2} (p_1 + 1) (p_2 + 1) (p_1 + p_2 + 2). \quad (3.2)$$

This multiplicity gives the order of the representation of the state when $p_1 \geq p_2$. When $p_1 < p_2$, the state is an *anti-rep* of order n . The anti-rep of a state (p_1, p_2) is (p_2, p_1) , so, for example, a triplet is denoted by a Young tableau with $(p_1, p_2) = (1, 0)$, while an anti-triplet is $(0, 1)$. Both have $n = 3$. A state with $p_1 = p_2$ is its own

anti-rep, such as the octet with $(p_1, p_2) = (1,1)$. As means of explanation, several SU(3) examples are listed in Table 3.1.

Table 3.1: Examples of several SU(3) Young tableaux.

Young tableau	(p_1, p_2)	representation
$\begin{array}{ c } \hline \square \\ \hline \end{array}$	(1,0)	3
$\begin{array}{ c } \hline \square \\ \square \\ \hline \end{array}$	(0,1)	$\bar{3}$
$\begin{array}{ c } \hline \square \\ \square \\ \square \\ \hline \end{array}$	(0,0)	1
$\begin{array}{ c c } \hline \square & \square \\ \square & \\ \hline \end{array}$	(1,1)	8
$\begin{array}{ c c } \hline \square & \square \\ \square & \\ \hline \end{array}$	(2,0)	6
$\begin{array}{ c c c } \hline \square & \square & \square \\ \hline \end{array}$	(3,0)	10

Young tableaux can be used to perform group operations. To find all the representations that will couple to states involving only gluons, one can calculate $8 \otimes 8 \otimes 8 \otimes \dots$ to see the representations that are contained. It will be instructive to examine the product $8 \otimes 8$ in detail. To combine two Young tableaux, start by writing letters in the boxes of the second tableau. The letters in any given row should be the same, and different from the letters used in any other row. So,

$$8 \otimes 8 = \begin{array}{|c|c|} \hline \square & \square \\ \square & \\ \hline \end{array} \otimes \begin{array}{|c|c|} \hline a & a \\ b & \\ \hline \end{array} \quad (3.3)$$

A useful property of Young tableaux is that any boxes (or indices) in the same row are symmetric indices, so in the case of the octet, the two a 's represent symmetric indices. Boxes in the same column are anti-symmetrized, so the octet is anti-symmetric in indices a and b . When performing the operation in Equation 3.3 above, all of the boxes from the second tableau are added onto the first tableau in a prescribed manner.

One begins by adding on the “ a ” boxes to produce valid tableaux (a row may never have more boxes than a row above it) in such a way that there is never more than one a in each column. This is because a ’s are symmetrized and should be kept that way. The “ b ” boxes are then added to the diagrams starting in the second row to produce valid tableaux. Recall that an $SU(3)$ tableau may have three rows, but any column with three boxes may be “cancelled” as the identity, so for example $\begin{array}{|c|c|} \hline \square & \square \\ \hline \square & \square \\ \hline \end{array} = \begin{array}{|c|} \hline \square \\ \hline \end{array}$ both represent the octet. One further requirement in the resulting tableaux is that the total number of a ’s to the right of any column is always greater than or equal to the number of b ’s to the right of the column. The operation in Equation 3.3 gives:

$$\begin{aligned}
 8 \otimes 8 &= \begin{array}{|c|c|} \hline \square & \square \\ \hline \square & \square \\ \hline \end{array} \otimes \begin{array}{|c|c|} \hline a & a \\ \hline b & \square \\ \hline \end{array} \\
 &= \begin{array}{|c|c|c|c|} \hline \square & \square & a & a \\ \hline \square & b & \square & \square \\ \hline \end{array} \oplus \begin{array}{|c|c|c|c|} \hline \square & \square & a & a \\ \hline \square & \square & \square & \square \\ \hline \square & b & \square & \square \\ \hline \end{array} \oplus \begin{array}{|c|c|c|} \hline \square & \square & a \\ \hline \square & a & b \\ \hline \square & \square & \square \\ \hline \end{array} \oplus \begin{array}{|c|c|c|} \hline \square & \square & a \\ \hline \square & a & \square \\ \hline \square & b & \square \\ \hline \end{array} \oplus \begin{array}{|c|c|c|} \hline \square & \square & a \\ \hline \square & b & \square \\ \hline \square & a & \square \\ \hline \end{array} \oplus \begin{array}{|c|c|} \hline \square & \square \\ \hline \square & a \\ \hline \square & b \\ \hline \end{array}
 \end{aligned} \tag{3.4}$$

removing a and b dummy labels and cancelling complete columns of 3 boxes leaves:

$$\begin{aligned}
 8 \otimes 8 &= \begin{array}{|c|c|c|c|} \hline \square & \square & \square & \square \\ \hline \square & \square & \square & \square \\ \hline \end{array} \oplus \begin{array}{|c|c|c|} \hline \square & \square & \square \\ \hline \square & \square & \square \\ \hline \end{array} \oplus \begin{array}{|c|c|c|} \hline \square & \square & \square \\ \hline \square & \square & \square \\ \hline \square & \square & \square \\ \hline \end{array} \oplus \begin{array}{|c|c|} \hline \square & \square \\ \hline \square & \square \\ \hline \end{array} \oplus \begin{array}{|c|c|} \hline \square & \square \\ \hline \square & \square \\ \hline \end{array} \oplus \begin{array}{|c|} \hline \square \\ \hline \square \\ \hline \square \\ \hline \end{array} \\
 &= (2, 2) \oplus (3, 0) \oplus (0, 3) \oplus (1, 1) \oplus (1, 1) \oplus (0, 0) \\
 &= 27 \oplus 10 \oplus \overline{10} \oplus 8 \oplus 8 \oplus 1.
 \end{aligned} \tag{3.5}$$

where the second line gives the (p_1, p_2) index of the Young tableaux and the final line names the representations by using the formula in Equation 3.2. Notice that the result of this calculation agrees with Equation 3.1. The above shows that combining gluons can result in operators that are in the 27-plet, decuplet, anti-decuplet, octet and singlet representations. Notice that both the octet $((p_1, p_2) = (1, 1))$ and the

27-plet $((p_1, p_2) = (2, 2))$ are their own anti-reps. Next one could calculate $8 \otimes 8 \otimes 8$, but there is a simpler way to find all the states that can be created through purely gauge fields. Notice that in the Young tableau calculation, combining an octet with another octet always meant starting with three boxes and adding three more. A third octet would add another three boxes to the diagram. Even taking into consideration the fact that complete columns of three boxes are cancelled, the resulting tableaux will always contain $3r$ boxes, for some integer r . The simplest way to find all the representations which can be built from pure glue operators is therefore to examine all the Young tableaux built of $3r$ boxes. They are shown in Table 3.2 in order of increasing representation size.

Table 3.2 shows the representations that can be built from pure gauge fields. If a colour-multiplet particle is to couple to only gauge fields without needing valence quarks, it must also belong to one of these representations (or rather the anti-rep) so that the bound state of the colour-multiplet particle with gauge fields is a singlet. Notice that for all the representations that appear in $8 \otimes 8 \otimes 8 \otimes \dots$, the corresponding anti-rep also appears (except in the cases where the representation is its own anti-rep). The colour-multiplet particle may therefore be from any of the representations listed in Table 3.2, such as the octet, decuplet, 27-plet etc.

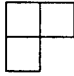
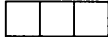
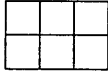
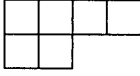
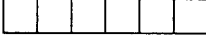
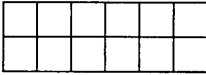
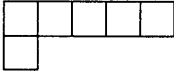
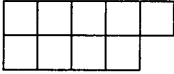

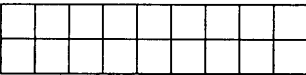
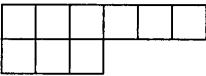
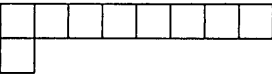



Gluelump systems will be studied for colour-multiplet particles originating from the lowest order representations that couple to pure gauge fields. These representations are the octet, decuplet, 27-plet, 28-plet and 35-plet.

3.2 Casimir Operators

Before even performing any lattice calculations, the Young tableaux may again offer insight into the characteristic mass scales of the different representations.

The colour factor or Casimir operator of a group can give an idea of the char-

Table 3.2: Representations which can be built from pure gauge operators as calculated by $8 \otimes 8 \otimes 8 \otimes \dots$ (or by examining tableaux with $3r$ boxes).

Young tableau	(p_1, p_2)	representation
	(1,1)	8
	(3,0)	10
	(0,3)	$\bar{10}$
	(2,2)	27
	(6,0)	28
	(0,6)	$\bar{28}$
	(4,1)	35
	(1,4)	$\bar{35}$
	(9,0)	55
	(0,9)	$\bar{55}$
	(3,3)	64
	(7,1)	80
	(1,7)	$\bar{80}$
	(5,2)	81
	(2,5)	$\bar{81}$
	\vdots	
	etc.	

acteristic coupling strength of that system. The Casimir scaling hypothesis [44–46] proposes that the string tension between strongly-interacting particles should be proportional to the quadratic Casimir operator. String tensions in the colour representations studied here have been tested on the lattice for Casimir scaling using Polyakov loops. See Table 2 of Ref. [47] which confirms this scaling.

In general, the Casimir factors are not trivial to calculate. The generators of the SU(3) colour group are eight matrices t_{ab}^A , where a and b are colour indices running from 1 to 3 and A runs from 1 to 8 for the eight generators of the group. These represent the eight gluons, which are in the adjoint representation of the colour group. A typical particle physics choice is $t^A = \lambda^A/2$ where λ^A are the eight Gell-Mann matrices. The generators t_{ab}^A describe how the gluons rotate quark colour in SU(3) space. They are related to the structure constants, f^{ABC} by the commutator, $[\lambda^A, \lambda^B] = if^{ABC}\lambda^C$. Technically speaking, the structure constants generate the adjoint representation of the group. Colour algebra leads to the relations,

$$\begin{aligned} \sum_{a,b} f^{abc} f^{abd} &= C_A \delta_{cd} \\ \sum_A t_{ab}^A t_{bc}^A &= C_F \delta_{ac} \\ \sum_{a,b} t_{ab}^A t_{ab}^B &= T_F \delta_{AB}. \end{aligned} \tag{3.6}$$

For a Lie group with dimension N_C (the number of colours in the theory), the colour factors or Casimir operators as defined in the above equations are,

$$\begin{aligned} C_A &= N_C \text{ is the strength of gluon self-coupling (gluon emission from gluon)} \\ C_F &= (N_C^2 - 1)/2N_C \text{ is the strength of a gluon coupling to a quark} \\ &\quad \text{(a quark emitting a gluon)} \end{aligned}$$

$T_F = 1/2$ is the strength of a gluon splitting into a quark-anti-quark pair

with subscripts A and F representing adjoint and fundamental representations respectively. For $SU(3)$, the Casimir operators take on the values,

$$\begin{aligned} C_A &= 3 \\ C_F &= 4/3 \\ T_F &= 1/2. \end{aligned} \tag{3.7}$$

This naturally defines colour factors for particles in the triplet and octet representations, since those are the fundamental and adjoint representations of $SU(3)$, but it still does not help define the Casimir operator for an arbitrary representation of $SU(3)$. This task can be approached through group theory considerations, but it is tedious. The Young tableaux provide a very quick way of calculating the colour factors for any arbitrary $SU(3)$ representation using the (p_1, p_2) indices of the corresponding tableau. The colour factor F^2 (technically the quadratic Casimir operator) for such a representation is [48],

$$F^2 = p_1 + p_2 + \frac{1}{3} (p_1^2 + p_2^2 + p_1 p_2). \tag{3.8}$$

One can easily verify that this formula yields the familiar $4/3$ for a triplet state $((p_1, p_2) = (1, 0))$. It is also easily applied to the five chosen gluelump representations. The results of applying Equation 3.8 to the various gluelump colour-multiplet particles are displayed in Table 3.3.

Colour factors relate to coupling strengths. The binding energy of a system is proportional to the colour factor of the bound state (a singlet has colour factor 0) minus the colour factors of the two constituent particles. A negative binding energy

Table 3.3: Colour factors (quadratic Casimir operator, F^2) of the chosen gluelump representations.

particle representation	(p_1, p_2)	colour factor F^2
octet	(1,1)	3
decuplet	(3,0)	6
27-plet	(2,2)	8
28-plet	(6,0)	18
35-plet	(4,1)	12

corresponds to an attractive state. The gluelump systems are all assumed to bond Standard Model gluons into colour singlet states with the colour-multiplet particle from one of the representations above. This would imply that octet systems tend to be the lightest, while the 28-plet systems (interestingly, *not* the 35-plet) are the heaviest.

3.3 Tensors

There are many representations of $SU(3)$ that could couple to Standard Model gluons and quarks. The smallest such representations that do not involve valence quarks in the bound state (that is, they can form colour-singlet bound states with just gluons and quarks or anti-quarks from the sea) are the octet, decuplet, 27-plet, 28-plet and 35-plet. In order to put any of these representations on the lattice, operators and propagators are needed to couple to the exotic colour-multiplet particle. Both the operators and the propagators require a basis of tensors that span the representation. These tensors are developed in this section. They will be denoted by T^μ where μ is an index that runs from 1 to n in the n -plet representation.

3.3.1 Octet

The octet seems to be a familiar case since it is the same representation that gives rise to the Standard Model gluons. In particle physics, a standard choice for the octet basis tensors are the Gell-Mann matrices,

$$T^\mu = \frac{\lambda^\mu}{\sqrt{2}}. \quad (3.9)$$

This is the basis used by Foster and Michael in their study of gluino (octet) gluelumps [18]. The problem with using this basis is that it does not generalize well to the higher order representations. Instead, a new set of tensors is developed from first principles. These tensors are chosen to be strictly real. The textbook by Georgi was particularly instructive in how to generate the T^μ tensors [49].

Starting with the Young tableau for the octet,

$$\begin{array}{|c|c|} \hline i & j \\ \hline k & \\ \hline \end{array}$$

one must write a set of tensors with the same symmetry, namely they must be symmetric in indices i and j , while i and k should be anti-symmetrized. This is because i and j are in the same row (symmetric), while i and k are in the same column (anti-symmetric). The Young tableau also indicates that the final tensors that generate this representation should be of rank-2, since the total number of indices (three) minus the number in the second row (one) is two. To begin, one writes an arbitrary 3-index tensor b^{ijk} and performs the necessary symmetrizations and anti-symmetrizations.

$$b^{ijk} = a^{ijk} + a^{jik} - a^{kji} - a^{jki} \quad (3.10)$$

With indices i , j , and k each running from 1 to 3 (colour indices), there are $3^3 = 27$

elements of this tensor, but many are duplicates, and there are also $3^2 = 9$ null elements which equal zero. All the elements are written explicitly below. This step will be left to the reader in the larger colour representations.

$$\begin{aligned}
b^{111} &= b^{222} = b^{333} = 0 \\
b^{121} &= b^{212} = b^{131} = b^{313} = b^{232} = b^{323} = 0 \\
b^{112} &= -b^{211} = 2a^{112} - a^{211} - a^{121} \\
b^{113} &= -b^{311} = 2a^{113} - a^{311} - a^{131} \\
b^{221} &= -b^{122} = 2a^{221} - a^{122} - a^{212} \\
b^{223} &= -b^{322} = 2a^{223} - a^{322} - a^{232} \\
b^{331} &= -b^{133} = 2a^{331} - a^{133} - a^{313} \\
b^{332} &= -b^{233} = 2a^{332} - a^{233} - a^{323} \\
b^{321} &= -b^{123} = a^{321} + a^{231} - a^{123} - a^{213} \\
b^{132} &= -b^{231} = a^{132} + a^{312} - a^{231} - a^{321} \\
b^{213} &= -b^{312} = a^{213} + a^{123} - a^{312} - a^{132}
\end{aligned}$$

There are nine non-zero elements but they are related by,

$$b^{213} + b^{321} + b^{132} = 0, \quad (3.11)$$

leaving eight linearly independent entries as one would expect for the octet. Next the anti-symmetric indices i and k are contracted using the anti-symmetric Levi-Civita symbol ϵ_{ikl} . This reduces the 3-index tensor b^{ijk} to a 2-index one, T_{jl} .

$$T_{jl} = \frac{1}{2} \epsilon_{ikl} b^{ijk}. \quad (3.12)$$

The tensor T has nine entries which can be written as the entries of a 3×3 matrix,

$$T \equiv \begin{pmatrix} T_{11} & T_{12} & T_{13} \\ T_{21} & T_{22} & T_{23} \\ T_{31} & T_{32} & T_{33} \end{pmatrix} = \begin{pmatrix} b^{213} & b^{311} & b^{112} \\ b^{223} & b^{321} & b^{122} \\ b^{233} & b^{331} & b^{132} \end{pmatrix}, \quad (3.13)$$

The matrix elements are still related by the one constraint,

$$b^{213} + b^{321} + b^{132} = T_{11} + T_{22} + T_{33} = 0, \quad (3.14)$$

which simply says the matrix T is traceless. This constraint is the singlet configuration. The remaining octet of states can be represented by different bases. In the literature, it is standard to choose the Gell-Mann matrices, $T^\mu = \lambda^\mu/\sqrt{2}$ for gluons and gluinos (this is also the choice made by Foster and Michael), however a choice of real two-index tensors proves more useful in the gluelump systems, especially in the larger colour representations. The basis chosen for the octet is,

$$\begin{aligned} T_{ij}^1 &= \delta_{i1}\delta_{j2} & T_{ij}^2 &= \delta_{i1}\delta_{j3} & T_{ij}^3 &= \delta_{i2}\delta_{j3} \\ T_{ij}^4 &= \delta_{i2}\delta_{j1} & T_{ij}^5 &= \delta_{i3}\delta_{j1} & T_{ij}^6 &= \delta_{i3}\delta_{j2} \\ T_{ij}^7 &= \frac{1}{2}(\delta_{i1}\delta_{j1} - \delta_{i2}\delta_{j2}) & T_{ij}^8 &= \frac{1}{\sqrt{6}}(\delta_{i1}\delta_{j1} + \delta_{i2}\delta_{j2} - 2\delta_{i3}\delta_{j3}) \end{aligned} \quad (3.15)$$

These tensors all obey the constraint in Equation 3.14. Much time and effort was put into thinking about what properties this basis should have. The tensors should be normalized to the number of terms in $(T^\mu)^2$, which they are. They should also be somehow *orthogonal* to one another, and to the constraint in Equation 3.14. Another important consideration was gauge invariance on the lattice. Pairs of T tensors are needed to create and destroy gluelumps on the lattice. Actual operators on the lattice will also involve the loops from the $SU(3)$ gauge terms (see Equation 4.17 which re-

visits the gauge invariance issue), but closed loops are always gauge invariant. The remaining indices in the creation-annihilation product involve only the exotic tensors, and one should examine the sum over all pairs of $T_{ij}^\alpha T_{kl}^\alpha$. For the basis above, the quantity of interest is,

$$\sum_{\alpha=1}^8 T_{ij}^\alpha T_{kl}^\alpha = \delta_{ik} \delta_{jl} - \frac{1}{3} \delta_{ij} \delta_{kl}. \quad (3.16)$$

This only involves simple delta functions and is therefore gauge invariant on the lattice. The two terms on the right side of the above equation also have a physical interpretation. The tensors in the basis (Equation 3.15) have symmetric index i and anti-symmetric index j . One can therefore think of i as a colour index and j as an anti-colour index. If one assigned colour index 1 to red, 2 to blue and 3 to green (to make discussion easier), then tensor T^1 is red anti-blue. In the $T^1 T^1$ term in Equation 3.16, red is created and destroyed, and anti-blue is created and destroyed. Visually a red line travels from source to sink, and an anti-blue line does the same (or, alternatively, a blue line travels backwards from sink to source). Tensors T^1 through T^6 all behave this way. Tensor T^7 and T^8 have additional possible couplings. T^7 is red anti-red blue anti-blue. In this case, not only can a red line travel from the source to sink, but there is also a possible self-coupling annihilation right at the source (or sink) where the red/anti-red lines could connect to themselves. These scenarios are encoded beautifully into the result in Equation 3.16. The first term $\delta_{ik} \delta_{jl}$ shows the colour line travelling from the source to the sink (i creates the colour at the source, k destroys it at the sink). The anti-colour also travels from source (j) to sink (l). The second term, $\delta_{ij} \delta_{kl}$ shows the internal coupling within the source and sink. Colour index i and anti-colour index j connect at the source, and similarly k and l at the sink. Equation 3.16 is *exactly* the relationship that is needed between the tensors. Computational tests confirm that this basis results in gauge invariant correlators.

3.3.2 Decuplet

The decuplet basis can be constructed in a similar manner as the octet one. The Young tableau for the decuplet,

$$\boxed{\begin{array}{|c|c|c|} \hline i & j & k \\ \hline \end{array}}$$

indicates that the decuplet basis will consist of ten 3-index fully symmetrized tensors. Since the tensor is to be symmetric in all three indices, it is easy to conceptualize. There are no constraints as in the octet case. The basis that will be used is,

$$\begin{aligned} T_{ijk}^1 &= \delta_{i1}\delta_{j1}\delta_{k1} \\ T_{ijk}^2 &= \delta_{i2}\delta_{j2}\delta_{k2} \\ T_{ijk}^3 &= \delta_{i3}\delta_{j3}\delta_{k3} \\ T_{ijk}^4 &= \frac{1}{\sqrt{3}}(\delta_{i1}\delta_{j1}\delta_{k2} + \delta_{i1}\delta_{j2}\delta_{k1} + \delta_{i2}\delta_{j1}\delta_{k1}) \\ T_{ijk}^5 &= \frac{1}{\sqrt{3}}(\delta_{i1}\delta_{j1}\delta_{k3} + \delta_{i1}\delta_{j3}\delta_{k1} + \delta_{i3}\delta_{j1}\delta_{k1}) \\ T_{ijk}^6 &= \frac{1}{\sqrt{3}}(\delta_{i2}\delta_{j2}\delta_{k1} + \delta_{i2}\delta_{j1}\delta_{k2} + \delta_{i1}\delta_{j2}\delta_{k2}) \\ T_{ijk}^7 &= \frac{1}{\sqrt{3}}(\delta_{i2}\delta_{j2}\delta_{k3} + \delta_{i2}\delta_{j3}\delta_{k2} + \delta_{i3}\delta_{j2}\delta_{k2}) \\ T_{ijk}^8 &= \frac{1}{\sqrt{3}}(\delta_{i3}\delta_{j3}\delta_{k1} + \delta_{i3}\delta_{j1}\delta_{k3} + \delta_{i1}\delta_{j3}\delta_{k3}) \\ T_{ijk}^9 &= \frac{1}{\sqrt{3}}(\delta_{i3}\delta_{j3}\delta_{k2} + \delta_{i3}\delta_{j2}\delta_{k3} + \delta_{i2}\delta_{j3}\delta_{k3}) \\ T_{ijk}^{10} &= \frac{1}{\sqrt{6}}(\delta_{i1}\delta_{j2}\delta_{k3} + \delta_{i1}\delta_{j3}\delta_{k2} + \delta_{i2}\delta_{j1}\delta_{k3} + \delta_{i2}\delta_{j3}\delta_{k1} + \delta_{i3}\delta_{j1}\delta_{k2} + \delta_{i3}\delta_{j2}\delta_{k1}) \end{aligned} \tag{3.17}$$

There is a lot of unnecessary notation here that will become even worse in larger colour representations. To help reduce the clutter, let l , m and n all be unequal and

define the generalized Kronecker delta functions as follows:

$$\begin{aligned}
\delta_{\{ijk\}\{lll\}} &= \delta_{il}\delta_{jl}\delta_{kl} \\
\delta_{\{ijk\}\{llm\}} &= \delta_{il}\delta_{jl}\delta_{km} + \delta_{il}\delta_{jm}\delta_{kl} + \delta_{im}\delta_{jl}\delta_{kl} \\
\delta_{\{ijk\}\{lmn\}} &= \delta_{il}\delta_{jm}\delta_{kn} + \delta_{il}\delta_{jn}\delta_{km} + \delta_{im}\delta_{jl}\delta_{kn} + \delta_{im}\delta_{jn}\delta_{kl} + \delta_{in}\delta_{jl}\delta_{km} + \delta_{in}\delta_{jm}\delta_{kl}.
\end{aligned} \tag{3.18}$$

Now the decuplet basis can be written as,

$$\begin{aligned}
T_{ijk}^1 &= \delta_{\{ijk\}\{111\}} & T_{ijk}^2 &= \delta_{\{ijk\}\{222\}} & T_{ijk}^3 &= \delta_{\{ijk\}\{333\}} \\
T_{ijk}^4 &= \frac{1}{\sqrt{3}}\delta_{\{ijk\}\{112\}} & T_{ijk}^5 &= \frac{1}{\sqrt{3}}\delta_{\{ijk\}\{113\}} & T_{ijk}^6 &= \frac{1}{\sqrt{3}}\delta_{\{ijk\}\{122\}} \\
T_{ijk}^7 &= \frac{1}{\sqrt{3}}\delta_{\{ijk\}\{223\}} & T_{ijk}^8 &= \frac{1}{\sqrt{3}}\delta_{\{ijk\}\{133\}} & T_{ijk}^9 &= \frac{1}{\sqrt{3}}\delta_{\{ijk\}\{233\}} \\
T_{ijk}^{10} &= \frac{1}{\sqrt{6}}\delta_{\{ijk\}\{123\}}
\end{aligned} \tag{3.19}$$

Notice that the normalization factors still reflect the actual number of terms in each tensor, as are written explicitly in Equation 3.19. Since all the indices are colour indices and there are no anti-colour indices, there are fewer possible interactions. A colour line cannot connect with another colour line directly at the source or sink. One would expect the sum $T_{ijk}^\alpha T_{lmn}^\alpha$ to only reflect colour lines travelling from the source to the sink. This is indeed what is seen,

$$\sum_{\alpha=1}^{10} T_{ijk}^\alpha T_{lmn}^\alpha = \frac{1}{6}\delta_{\{ijk\}\{lmn\}}. \tag{3.20}$$

Recall from the definition of the generalized Kronecker delta functions that the right side of this equation is actually six terms coupling every colour index from the source to all possibilities at the sink. This important result also proves the gauge invariance of this choice of basis, since this sum appears whenever a decuplet representation gluelump is created then destroyed on the lattice (see Equation 4.17 for a more thor-

ough motivation). The sum contains only complete delta functions so it is not affected by gauge transformations.

3.3.3 27-plet

The Young tableau for the 27-plet,

$$\begin{array}{|c|c|c|c|} \hline i & j & k & l \\ \hline m & n & & \\ \hline \end{array}$$

has four symmetrized indices in the top row and two anti-symmetric indices in the bottom row. The final 27-plet basis will consist of twenty-seven 4-index tensors with two colour degrees of freedom and two anti-colour ones. As in the octet case, the proper symmetries are obtained by starting off with an arbitrary 6-index tensor and symmetrizing all permutations of $\{i, j, k, l\}$ and separately all permutations of m and n . Finally i is antisymmetrized with m and j with n . The result is,

$$b^{ijklmn} = a^{ijklmn} - a^{mjklin} - a^{inklmj} + a^{mnkl ij} + \dots \quad (3.21)$$

There are $3^6 = 729$ elements of this tensor. Since $b^{ijklmn} = -b^{mjklin} = -b^{inklmj}$, it is clear that if $i = m$ or $j = n$, the entry is zero (though not necessarily if $i = m$ and $j = n$). In fact, the majority of the entries are either zeros or duplicates. They will not all be written out here. Next, one can proceed to contracting antisymmetric indices of the tensor. As with the octet, the antisymmetric indices (in this case i with m and j with n) are contracted using the Levi-Civita symbol. This leaves the 4-index tensor,

$$T_{klpq} = \frac{1}{4} \epsilon_{imp} \epsilon_{jnq} b^{ijklmn}. \quad (3.22)$$

With all four colour indices running from 1 to 3, there are $3^4 = 81$ possible elements.

Many elements are still the same, for example $T_{1213} = T_{2113} = T_{1231} = T_{2131}$. Let $T_{(12)(13)}$ denote any element from that set. The indices inside each set of brackets can be interchanged and the tensors will be equal, since permutation of symmetrized indices yields the same result. With this in mind, there are only 36 distinct elements, as shown below.

$$\begin{array}{cccccc}
T_{(11)(11)} & T_{(22)(11)} & T_{(11)(12)} & T_{(22)(12)} & T_{(11)(13)} & T_{(22)(13)} \\
T_{(11)(22)} & T_{(22)(22)} & T_{(11)(23)} & T_{(22)(23)} & T_{(11)(33)} & T_{(22)(33)} \\
T_{(12)(11)} & T_{(23)(11)} & T_{(12)(12)} & T_{(23)(12)} & T_{(12)(13)} & T_{(23)(13)} \\
T_{(12)(22)} & T_{(23)(22)} & T_{(12)(23)} & T_{(23)(23)} & T_{(12)(33)} & T_{(23)(33)} \\
T_{(13)(11)} & T_{(33)(11)} & T_{(13)(12)} & T_{(33)(12)} & T_{(13)(13)} & T_{(33)(13)} \\
T_{(13)(22)} & T_{(33)(22)} & T_{(13)(23)} & T_{(33)(23)} & T_{(13)(33)} & T_{(33)(33)} \quad (3.23)
\end{array}$$

There are nine constraints,

$$\begin{aligned}
T_{(11)(11)} + T_{(12)(12)} + T_{(13)(13)} &= 0, \\
T_{(22)(22)} + T_{(12)(12)} + T_{(23)(23)} &= 0, \\
T_{(33)(33)} + T_{(13)(13)} + T_{(23)(23)} &= 0, \\
T_{(11)(12)} + T_{(12)(22)} + T_{(13)(23)} &= 0, \\
T_{(12)(11)} + T_{(22)(12)} + T_{(23)(13)} &= 0, \\
T_{(11)(13)} + T_{(13)(33)} + T_{(12)(23)} &= 0, \\
T_{(23)(22)} + T_{(33)(23)} + T_{(13)(12)} &= 0, \\
T_{(22)(23)} + T_{(23)(33)} + T_{(12)(13)} &= 0, \\
T_{(33)(13)} + T_{(13)(11)} + T_{(23)(12)} &= 0, \quad (3.24)
\end{aligned}$$

leaving 27 linearly independent parameters, as one would expect. To help with notation, generalized Kronecker delta functions are again defined. Let k and l be unequal.

$$\begin{aligned}\delta_{\{ij\}\{kk\}} &= \delta_{ik}\delta_{jk} \\ \delta_{\{ij\}\{kl\}} &= \delta_{ik}\delta_{jl} + \delta_{il}\delta_{jk}.\end{aligned}\tag{3.25}$$

A real basis for the 27-plet is

$$\begin{aligned}T_{ijkl}^1 &= \delta_{\{ij\}\{11\}}\delta_{\{kl\}\{22\}} & T_{ijkl}^2 &= \delta_{\{ij\}\{11\}}\delta_{\{kl\}\{33\}} & T_{ijkl}^3 &= \delta_{\{ij\}\{22\}}\delta_{\{kl\}\{33\}} \\ T_{ijkl}^4 &= \delta_{\{ij\}\{22\}}\delta_{\{kl\}\{11\}} & T_{ijkl}^5 &= \delta_{\{ij\}\{33\}}\delta_{\{kl\}\{11\}} & T_{ijkl}^6 &= \delta_{\{ij\}\{33\}}\delta_{\{kl\}\{22\}} \\ T_{ijkl}^7 &= \frac{1}{\sqrt{2}}(\delta_{\{ij\}\{11\}}\delta_{\{kl\}\{23\}}) & T_{ijkl}^8 &= \frac{1}{\sqrt{2}}(\delta_{\{ij\}\{12\}}\delta_{\{kl\}\{33\}}) \\ T_{ijkl}^9 &= \frac{1}{\sqrt{2}}(\delta_{\{ij\}\{13\}}\delta_{\{kl\}\{22\}}) & T_{ijkl}^{10} &= \frac{1}{\sqrt{2}}(\delta_{\{ij\}\{23\}}\delta_{\{kl\}\{11\}}) \\ T_{ijkl}^{11} &= \frac{1}{\sqrt{2}}(\delta_{\{ij\}\{33\}}\delta_{\{kl\}\{12\}}) & T_{ijkl}^{12} &= \frac{1}{\sqrt{2}}(\delta_{\{ij\}\{22\}}\delta_{\{kl\}\{13\}}) \\ T_{ijkl}^{13} &= \frac{1}{2}(\delta_{\{ij\}\{11\}}\delta_{\{kl\}\{12\}} - \delta_{\{ij\}\{12\}}\delta_{\{kl\}\{22\}}) \\ T_{ijkl}^{14} &= \frac{1}{\sqrt{20}}(\delta_{\{ij\}\{11\}}\delta_{\{kl\}\{12\}} + \delta_{\{ij\}\{12\}}\delta_{\{kl\}\{22\}} - 2\delta_{\{ij\}\{13\}}\delta_{\{kl\}\{23\}}) \\ T_{ijkl}^{15} &= \frac{1}{2}(\delta_{\{ij\}\{11\}}\delta_{\{kl\}\{13\}} - \delta_{\{ij\}\{13\}}\delta_{\{kl\}\{33\}}) \\ T_{ijkl}^{16} &= \frac{1}{\sqrt{20}}(\delta_{\{ij\}\{11\}}\delta_{\{kl\}\{13\}} + \delta_{\{ij\}\{13\}}\delta_{\{kl\}\{33\}} - 2\delta_{\{ij\}\{12\}}\delta_{\{kl\}\{23\}}) \\ T_{ijkl}^{17} &= \frac{1}{2}(\delta_{\{ij\}\{12\}}\delta_{\{kl\}\{11\}} - \delta_{\{ij\}\{22\}}\delta_{\{kl\}\{12\}}) \\ T_{ijkl}^{18} &= \frac{1}{\sqrt{20}}(\delta_{\{ij\}\{12\}}\delta_{\{kl\}\{11\}} + \delta_{\{ij\}\{22\}}\delta_{\{kl\}\{12\}} - 2\delta_{\{ij\}\{23\}}\delta_{\{kl\}\{13\}}) \\ T_{ijkl}^{19} &= \frac{1}{2}(\delta_{\{ij\}\{22\}}\delta_{\{kl\}\{23\}} - \delta_{\{ij\}\{23\}}\delta_{\{kl\}\{33\}}) \\ T_{ijkl}^{20} &= \frac{1}{\sqrt{20}}(\delta_{\{ij\}\{22\}}\delta_{\{kl\}\{23\}} + \delta_{\{ij\}\{23\}}\delta_{\{kl\}\{33\}} - 2\delta_{\{ij\}\{12\}}\delta_{\{kl\}\{13\}}) \\ T_{ijkl}^{21} &= \frac{1}{2}(\delta_{\{ij\}\{13\}}\delta_{\{kl\}\{11\}} - \delta_{\{ij\}\{33\}}\delta_{\{kl\}\{13\}})\end{aligned}$$

$$\begin{aligned}
T_{ijkl}^{22} &= \frac{1}{\sqrt{20}} (\delta_{\{ij\}\{13\}} \delta_{\{kl\}\{11\}} + \delta_{\{ij\}\{33\}} \delta_{\{kl\}\{13\}} - 2\delta_{\{ij\}\{23\}} \delta_{\{kl\}\{12\}}) \\
T_{ijkl}^{23} &= \frac{1}{2} (\delta_{\{ij\}\{23\}} \delta_{\{kl\}\{22\}} - \delta_{\{ij\}\{33\}} \delta_{\{kl\}\{23\}}) \\
T_{ijkl}^{24} &= \frac{1}{\sqrt{20}} (\delta_{\{ij\}\{23\}} \delta_{\{kl\}\{22\}} + \delta_{\{ij\}\{33\}} \delta_{\{kl\}\{23\}} - 2\delta_{\{ij\}\{13\}} \delta_{\{kl\}\{12\}}) \\
T_{ijkl}^{25} &= \frac{1}{\sqrt{10}} (\delta_{\{ij\}\{11\}} \delta_{\{kl\}\{11\}} - \delta_{\{ij\}\{22\}} \delta_{\{kl\}\{22\}} \\
&\quad - \delta_{\{ij\}\{13\}} \delta_{\{kl\}\{13\}} + \delta_{\{ij\}\{23\}} \delta_{\{kl\}\{23\}}) \\
T_{ijkl}^{26} &= \frac{1}{\sqrt{30}} (\delta_{\{ij\}\{11\}} \delta_{\{kl\}\{11\}} + \delta_{\{ij\}\{22\}} \delta_{\{kl\}\{22\}} - 2\delta_{\{ij\}\{33\}} \delta_{\{kl\}\{33\}} \\
&\quad - 2\delta_{\{ij\}\{12\}} \delta_{\{kl\}\{12\}} + \delta_{\{ij\}\{13\}} \delta_{\{kl\}\{13\}} + \delta_{\{ij\}\{23\}} \delta_{\{kl\}\{23\}}) \\
T_{ijkl}^{27} &= \frac{1}{\sqrt{24}} (2\delta_{\{ij\}\{11\}} \delta_{\{kl\}\{11\}} + 2\delta_{\{ij\}\{22\}} \delta_{\{kl\}\{22\}} + 2\delta_{\{ij\}\{33\}} \delta_{\{kl\}\{33\}} \\
&\quad - \delta_{\{ij\}\{12\}} \delta_{\{kl\}\{12\}} - \delta_{\{ij\}\{13\}} \delta_{\{kl\}\{13\}} - \delta_{\{ij\}\{23\}} \delta_{\{kl\}\{23\}}) \quad (3.26)
\end{aligned}$$

Again, the normalization factors reflect the number of terms in each tensor. In the 27-plet, the symmetries encoded in the tensors mean that indices i and j are colour indices while k and l are anti-colour indices. There are many similarities between the 27-plet (with two colour and two anti-colour indices) and the octet (with one colour and one anti-colour index). The octet T^1 is red anti-blue. The 27-plet T^1 has two red indices and two anti-blue indices. In that sense, the 27-plet T^1 is like two copies of the octet T^1 . In fact, the 27-plet tensors T^1 through T^6 are all double copies of the octet T^1 through T^6 . The 27-plet tensors T^7 through T^{12} are combinations of two different octet tensors from T^1 to T^6 . For example, the 27-plet T^7 is red red anti-blue anti-green. It is like the combination of the octet T^1 and T^2 .

For the 27-plet tensors from T^1 to T^{12} , notice that there is no self-coupling at the source (or sink) location. A tensor with a red colour index does not also contain any anti-red for example. There are, however, new couplings that were not present in the octet. Each of the 27-plet tensors from T^1 to T^{12} contains two copies of at least one (sometimes two) of the colours. So for example the 27-plet T^7 has two red

charges which can connect to either one of the two red indices in a second T^7 tensor. The T^1 has even more cross-terms since it has two red charges and two blue charges, resulting in four possible ways for it to connect from source to sink.

The 27-plet tensors from T^{13} to T^{24} are combinations of one octet T^7 or T^8 (which contain self-coupling possibilities) with one octet tensor from T^1 to T^6 (which do not contain self-coupling terms). So for example, T^{13} contains the possibility of red/anti-red annihilation at the source site as well as blue/anti-blue annihilation. In this sense it is the same as the octet T^7 , however it also contains a set of colour indices (in this case red anti-blue) that are ‘‘spectators’’ to the annihilation processes. There are multiple possible cross-terms when coupling a tensor at the source to one at the sink.

Finally, 27-plet tensors T^{25} , T^{26} and T^{27} are combinations of two octet T^7 or T^8 tensors, or a T^7 with a T^8 . In this case there are no spectators and every colour index is able to annihilate with an anti-colour index at the source. All indices are also able to propagate from source to sink and couple to multiple possibilities there.

The basis was constructed in a delicate way so that all the possible couplings (there are many in this representation!) are complete in the sense that the product $T_{ijkl}^\alpha T_{mnop}^\alpha$ contains full delta functions for each possible coupling.

$$\begin{aligned}
\sum_{\alpha=1}^{27} T_{ijkl}^\alpha T_{mnop}^\alpha &= \frac{1}{4} (\delta_{im}\delta_{jn}\delta_{ko}\delta_{lp} + \delta_{im}\delta_{jn}\delta_{kp}\delta_{lo} + \delta_{in}\delta_{jm}\delta_{ko}\delta_{lp} + \delta_{in}\delta_{jm}\delta_{kp}\delta_{lo}) \\
&\quad - \frac{1}{20} (\delta_{im}\delta_{jl}\delta_{ko}\delta_{np} + \delta_{im}\delta_{jl}\delta_{kp}\delta_{no} + \delta_{in}\delta_{jl}\delta_{ko}\delta_{mp} + \delta_{in}\delta_{jl}\delta_{kp}\delta_{mo} \\
&\quad + \delta_{im}\delta_{lo}\delta_{jk}\delta_{np} + \delta_{im}\delta_{lp}\delta_{jk}\delta_{no} + \delta_{in}\delta_{lo}\delta_{jk}\delta_{mp} + \delta_{in}\delta_{lp}\delta_{jk}\delta_{mo} \\
&\quad + \delta_{il}\delta_{jm}\delta_{ko}\delta_{np} + \delta_{il}\delta_{jm}\delta_{kp}\delta_{no} + \delta_{il}\delta_{jn}\delta_{ko}\delta_{mp} + \delta_{il}\delta_{jn}\delta_{kp}\delta_{mo} \\
&\quad + \delta_{ik}\delta_{jm}\delta_{lo}\delta_{np} + \delta_{ik}\delta_{jm}\delta_{lp}\delta_{no} + \delta_{ik}\delta_{jn}\delta_{lo}\delta_{mp} + \delta_{ik}\delta_{jn}\delta_{lp}\delta_{mo}) \\
&\quad + \frac{1}{40} (\delta_{ik}\delta_{jl}\delta_{mo}\delta_{np} + \delta_{ik}\delta_{jl}\delta_{mp}\delta_{no} + \delta_{il}\delta_{jk}\delta_{mo}\delta_{np} + \delta_{il}\delta_{jk}\delta_{mp}\delta_{no})
\end{aligned} \tag{3.27}$$

This result contains all possible couplings. As is motivated in Equation 4.17, it is also the sum that one should study to confirm the gauge invariance of the system. Since it contains only delta functions, this proves the gauge invariance of this choice of basis.

3.3.4 28-plet

The 28-plet has a Young tableau with six fully symmetrized indices,

$$\boxed{i \mid j \mid k \mid l \mid m \mid n}$$

It is therefore analagous to the decuplet case, but with twice as many indices. The 28-plet basis will consist of twenty-eight 6-index fully symmetrized tensors. Generalized Kronecker delta functions are useful to reduce the amount of notation needed. With p, q and r colour indices all unequal,

$$\begin{aligned}
\delta_{\{ijklmn\}\{pppppp\}} &= \delta_{ip}\delta_{jp}\delta_{kp}\delta_{lp}\delta_{mp}\delta_{np} \quad (1 \text{ term}) \\
\delta_{\{ijklmn\}\{pppppq\}} &= \delta_{ip}\delta_{jp}\delta_{kp}\delta_{lp}\delta_{mp}\delta_{nq} + \delta_{ip}\delta_{jp}\delta_{kp}\delta_{lp}\delta_{mq}\delta_{np} \\
&\quad + \delta_{ip}\delta_{jp}\delta_{kp}\delta_{lq}\delta_{mp}\delta_{np} + \delta_{ip}\delta_{jp}\delta_{kq}\delta_{lp}\delta_{mp}\delta_{np} \\
&\quad + \delta_{ip}\delta_{jq}\delta_{kp}\delta_{lp}\delta_{mp}\delta_{np} + \delta_{iq}\delta_{jp}\delta_{kp}\delta_{lp}\delta_{mp}\delta_{np} \quad (6 \text{ terms}) \\
\delta_{\{ijklmn\}\{ppppqq\}} &= \delta_{ip}\delta_{jp}\delta_{kp}\delta_{lp}\delta_{mq}\delta_{nq} + \delta_{ip}\delta_{jp}\delta_{kp}\delta_{lq}\delta_{mp}\delta_{nq} + \dots \quad (15 \text{ terms}) \\
\delta_{\{ijklmn\}\{ppppqqq\}} &= \delta_{ip}\delta_{jp}\delta_{kp}\delta_{lq}\delta_{mq}\delta_{nq} + \delta_{ip}\delta_{jp}\delta_{kq}\delta_{lp}\delta_{mq}\delta_{nq} + \dots \quad (20 \text{ terms}) \\
\delta_{\{ijklmn\}\{ppppqqr\}} &= \delta_{ip}\delta_{jp}\delta_{kp}\delta_{lp}\delta_{mq}\delta_{nr} + \delta_{ip}\delta_{jp}\delta_{kp}\delta_{lq}\delta_{mp}\delta_{nr} + \dots \quad (30 \text{ terms}) \\
\delta_{\{ijklmn\}\{ppppqqr\}} &= \delta_{ip}\delta_{jp}\delta_{kp}\delta_{lq}\delta_{mq}\delta_{nr} + \delta_{ip}\delta_{jp}\delta_{kq}\delta_{lp}\delta_{mq}\delta_{nr} + \dots \quad (60 \text{ terms}) \\
\delta_{\{ijklmn\}\{ppppqrr\}} &= \delta_{ip}\delta_{jp}\delta_{kq}\delta_{lq}\delta_{mr}\delta_{nr} + \delta_{ip}\delta_{jq}\delta_{kp}\delta_{lq}\delta_{mr}\delta_{nr} + \dots \quad (90 \text{ terms})
\end{aligned} \tag{3.28}$$

There are no indices to anti-symmetrize or contract, and the basis is straightforward to write. Just as the 27-plet tensors could be seen as the combination of two octet tensors, the 28-plet tensors are combinations of two decuplet tensors. The real 28-plet basis for use on the lattice is as follows.

$$\begin{aligned}
T_{ijklmn}^1 &= \delta_{\{ijklmn\}\{111111\}} & T_{ijklmn}^2 &= \delta_{\{ijklmn\}\{222222\}} \\
T_{ijklmn}^3 &= \delta_{\{ijklmn\}\{333333\}} & T_{ijklmn}^4 &= \frac{1}{\sqrt{6}} \delta_{\{ijklmn\}\{111112\}} \\
T_{ijklmn}^5 &= \frac{1}{\sqrt{6}} \delta_{\{ijklmn\}\{111113\}} & T_{ijklmn}^6 &= \frac{1}{\sqrt{6}} \delta_{\{ijklmn\}\{222221\}} \\
T_{ijklmn}^7 &= \frac{1}{\sqrt{6}} \delta_{\{ijklmn\}\{222223\}} & T_{ijklmn}^8 &= \frac{1}{\sqrt{6}} \delta_{\{ijklmn\}\{333331\}} \\
T_{ijklmn}^9 &= \frac{1}{\sqrt{6}} \delta_{\{ijklmn\}\{333332\}} & T_{ijklmn}^{10} &= \frac{1}{\sqrt{15}} \delta_{\{ijklmn\}\{111122\}} \\
T_{ijklmn}^{11} &= \frac{1}{\sqrt{15}} \delta_{\{ijklmn\}\{111133\}} & T_{ijklmn}^{12} &= \frac{1}{\sqrt{15}} \delta_{\{ijklmn\}\{222211\}} \\
T_{ijklmn}^{13} &= \frac{1}{\sqrt{15}} \delta_{\{ijklmn\}\{222233\}} & T_{ijklmn}^{14} &= \frac{1}{\sqrt{15}} \delta_{\{ijklmn\}\{333311\}} \\
T_{ijklmn}^{15} &= \frac{1}{\sqrt{15}} \delta_{\{ijklmn\}\{333322\}} & T_{ijklmn}^{16} &= \frac{1}{\sqrt{20}} \delta_{\{ijklmn\}\{111222\}} \\
T_{ijklmn}^{17} &= \frac{1}{\sqrt{20}} \delta_{\{ijklmn\}\{111333\}} & T_{ijklmn}^{18} &= \frac{1}{\sqrt{20}} \delta_{\{ijklmn\}\{222333\}} \\
T_{ijklmn}^{19} &= \frac{1}{\sqrt{30}} \delta_{\{ijklmn\}\{111123\}} & T_{ijklmn}^{20} &= \frac{1}{\sqrt{30}} \delta_{\{ijklmn\}\{222213\}} \\
T_{ijklmn}^{21} &= \frac{1}{\sqrt{30}} \delta_{\{ijklmn\}\{333312\}} & T_{ijklmn}^{22} &= \frac{1}{\sqrt{60}} \delta_{\{ijklmn\}\{111223\}} \\
T_{ijklmn}^{23} &= \frac{1}{\sqrt{60}} \delta_{\{ijklmn\}\{111332\}} & T_{ijklmn}^{24} &= \frac{1}{\sqrt{60}} \delta_{\{ijklmn\}\{222113\}} \\
T_{ijklmn}^{25} &= \frac{1}{\sqrt{60}} \delta_{\{ijklmn\}\{222331\}} & T_{ijklmn}^{26} &= \frac{1}{\sqrt{60}} \delta_{\{ijklmn\}\{333112\}} \\
T_{ijklmn}^{27} &= \frac{1}{\sqrt{60}} \delta_{\{ijklmn\}\{333221\}} & T_{ijklmn}^{28} &= \frac{1}{\sqrt{90}} \delta_{\{ijklmn\}\{112233\}}
\end{aligned} \tag{3.29}$$

Although the generalized Kronecker deltas greatly simplify the notation, the normalization factors reflect the actual number of terms in each tensor, so for example T^{28} contains 90 terms. As in the decuplet case, all the indices are colour indices, so there are no possible self-couplings at the source or sink sites. The sum $T_{ijklmn}^\alpha T_{opqrst}^\alpha$ only reflects colour lines from the source travelling to the sink.

$$\sum_{\alpha=1}^{28} T_{ijklmn}^\alpha T_{opqrst}^\alpha = \frac{1}{6!} \delta_{\{ijklmn\}} \delta_{\{opqrst\}}. \quad (3.30)$$

Containing only delta functions, this is an important confirmation of the gauge invariance of this choice of basis since this sum appears whenever 28-plet representation gluelumps are created and destroyed on the lattice.

3.3.5 35-plet

The Young tableau for the 35-plet,

$$\begin{array}{|c|c|c|c|c|} \hline i & j & k & l & m \\ \hline n & & & & \\ \hline \end{array}$$

has five symmetrized indices in the top row and one anti-symmetric index in the bottom row. The final 35-plet basis will consist of thirty-five 5-index tensors with four colour degrees of freedom and one anti-colour one. The proper symmetries are obtained by starting with an arbitrary 6-index tensor and symmetrizing all permutations of $\{i, j, k, l, m\}$ and antisymmetrizing i with n . The result is,

$$b^{ijklmn} = a^{ijklmn} - a^{njklmi} + a^{jiklmn} - a^{jnklni} + \dots \quad (3.31)$$

There are $3^6 = 729$ elements of this tensor. Since it is anti-symmetric in i and n , $b^{ijklmn} = -b^{njklmi}$. When the anti-symmetric indices i and n are equal, the entry is

$$\begin{aligned}
T_{(1112)1} + T_{(1122)2} + T_{(1123)3} &= 0, & T_{(1222)1} + T_{(2222)2} + T_{(2223)3} &= 0 \\
T_{(1113)1} + T_{(1123)2} + T_{(1133)3} &= 0, & T_{(1223)1} + T_{(2223)2} + T_{(2233)3} &= 0 \\
T_{(1122)1} + T_{(1222)2} + T_{(1223)3} &= 0, & T_{(1233)1} + T_{(2233)2} + T_{(2333)3} &= 0 \\
T_{(1123)1} + T_{(1223)2} + T_{(1233)3} &= 0, & T_{(1333)1} + T_{(2333)2} + T_{(3333)3} &= 0
\end{aligned}$$

This leaves 35 linearly independent parameters. With p , q , and r unequal, define the generalized Kronecker delta functions as follows.

$$\begin{aligned}
\delta_{\{ijkl\}\{pppp\}} &= \delta_{ip}\delta_{jp}\delta_{kp}\delta_{lp} \\
\delta_{\{ijkl\}\{pppq\}} &= \delta_{ip}\delta_{jp}\delta_{kp}\delta_{lq} + \delta_{ip}\delta_{jp}\delta_{kq}\delta_{lp} + \delta_{ip}\delta_{jq}\delta_{kp}\delta_{lp} + \delta_{iq}\delta_{jp}\delta_{kp}\delta_{lp} \\
\delta_{\{ijkl\}\{ppqq\}} &= \delta_{ip}\delta_{jp}\delta_{kq}\delta_{lq} + \delta_{ip}\delta_{jq}\delta_{kp}\delta_{lq} + \delta_{iq}\delta_{jp}\delta_{kp}\delta_{lq} \\
&\quad + \delta_{ip}\delta_{jq}\delta_{kq}\delta_{lp} + \delta_{iq}\delta_{jp}\delta_{kq}\delta_{lp} + \delta_{iq}\delta_{jq}\delta_{kp}\delta_{lp} \\
\delta_{\{ijkl\}\{ppqr\}} &= \delta_{ip}\delta_{jp}\delta_{kq}\delta_{lr} + \delta_{ip}\delta_{jq}\delta_{kp}\delta_{lr} + \delta_{iq}\delta_{jp}\delta_{kp}\delta_{lr} \\
&\quad + \delta_{ip}\delta_{jq}\delta_{kr}\delta_{lp} + \delta_{iq}\delta_{jp}\delta_{kr}\delta_{lp} + \delta_{iq}\delta_{jr}\delta_{kp}\delta_{lp} \\
&\quad + \delta_{ip}\delta_{jp}\delta_{kr}\delta_{lq} + \delta_{ip}\delta_{jr}\delta_{kp}\delta_{lq} + \delta_{ir}\delta_{jp}\delta_{kp}\delta_{lq} \\
&\quad + \delta_{ip}\delta_{jr}\delta_{kq}\delta_{lp} + \delta_{ir}\delta_{jp}\delta_{kq}\delta_{lp} + \delta_{ir}\delta_{jq}\delta_{kp}\delta_{lp}
\end{aligned} \tag{3.33}$$

The real 35-plet basis that is gauge-invariant on the lattice can now be written.

$$\begin{aligned}
T_{ijklm}^1 &= \delta_{\{ijkl\}\{1111\}}\delta_{m3} & T_{ijklm}^2 &= \delta_{\{ijkl\}\{1111\}}\delta_{m2} \\
T_{ijklm}^3 &= \delta_{\{ijkl\}\{2222\}}\delta_{m3} & T_{ijklm}^4 &= \delta_{\{ijkl\}\{2222\}}\delta_{m1} \\
T_{ijklm}^5 &= \delta_{\{ijkl\}\{3333\}}\delta_{m2} & T_{ijklm}^6 &= \delta_{\{ijkl\}\{3333\}}\delta_{m1} \\
T_{ijklm}^7 &= \frac{1}{2}\delta_{\{ijkl\}\{1112\}}\delta_{m3} & T_{ijklm}^8 &= \frac{1}{2}\delta_{\{ijkl\}\{1113\}}\delta_{m2} \\
T_{ijklm}^9 &= \frac{1}{2}\delta_{\{ijkl\}\{1222\}}\delta_{m3} & T_{ijklm}^{10} &= \frac{1}{2}\delta_{\{ijkl\}\{2223\}}\delta_{m1}
\end{aligned}$$

$$\begin{aligned}
T_{ijklm}^{11} &= \frac{1}{2} \delta_{\{ijkl\}\{1333\}} \delta_{m2} & T_{ijklm}^{12} &= \frac{1}{2} \delta_{\{ijkl\}\{2333\}} \delta_{m1} \\
T_{ijklm}^{13} &= \frac{1}{\sqrt{6}} \delta_{\{ijkl\}\{1122\}} \delta_{m3} & T_{ijklm}^{14} &= \frac{1}{\sqrt{6}} \delta_{\{ijkl\}\{1133\}} \delta_{m2} \\
T_{ijklm}^{15} &= \frac{1}{\sqrt{6}} \delta_{\{ijkl\}\{2233\}} \delta_{m1} \\
T_{ijklm}^{16} &= \frac{1}{\sqrt{24}} (\delta_{\{ijkl\}\{1231\}} \delta_{m1} - \delta_{\{ijkl\}\{1232\}} \delta_{m2}) \\
T_{ijklm}^{17} &= \frac{1}{\sqrt{72}} (\delta_{\{ijkl\}\{1231\}} \delta_{m1} + \delta_{\{ijkl\}\{1232\}} \delta_{m2} - 2\delta_{\{ijkl\}\{1233\}} \delta_{m3}) \\
T_{ijklm}^{18} &= \frac{1}{\sqrt{8}} (\delta_{\{ijkl\}\{1112\}} \delta_{m2} - \delta_{\{ijkl\}\{1113\}} \delta_{m3}) \\
T_{ijklm}^{19} &= \frac{1}{\sqrt{12}} (\delta_{\{ijkl\}\{1112\}} \delta_{m2} + \delta_{\{ijkl\}\{1113\}} \delta_{m3} - 2\delta_{\{ijkl\}\{1111\}} \delta_{m1}) \\
T_{ijklm}^{20} &= \frac{1}{\sqrt{8}} (\delta_{\{ijkl\}\{2221\}} \delta_{m1} - \delta_{\{ijkl\}\{2223\}} \delta_{m3}) \\
T_{ijklm}^{21} &= \frac{1}{\sqrt{12}} (\delta_{\{ijkl\}\{2221\}} \delta_{m1} + \delta_{\{ijkl\}\{2223\}} \delta_{m3} - 2\delta_{\{ijkl\}\{2222\}} \delta_{m2}) \\
T_{ijklm}^{22} &= \frac{1}{\sqrt{8}} (\delta_{\{ijkl\}\{3331\}} \delta_{m1} - \delta_{\{ijkl\}\{3332\}} \delta_{m2}) \\
T_{ijklm}^{23} &= \frac{1}{\sqrt{12}} (\delta_{\{ijkl\}\{3331\}} \delta_{m1} + \delta_{\{ijkl\}\{3332\}} \delta_{m2} - 2\delta_{\{ijkl\}\{3333\}} \delta_{m3}) \\
T_{ijklm}^{24} &= \frac{1}{\sqrt{18}} (\delta_{\{ijkl\}\{1122\}} \delta_{m2} - \delta_{\{ijkl\}\{1123\}} \delta_{m3}) \\
T_{ijklm}^{25} &= \frac{1}{\sqrt{72}} (3\delta_{\{ijkl\}\{1121\}} \delta_{m1} - 2\delta_{\{ijkl\}\{1122\}} \delta_{m2} - 1\delta_{\{ijkl\}\{1123\}} \delta_{m3}) \\
T_{ijklm}^{26} &= \frac{1}{\sqrt{18}} (\delta_{\{ijkl\}\{1133\}} \delta_{m3} - \delta_{\{ijkl\}\{1132\}} \delta_{m2}) \\
T_{ijklm}^{27} &= \frac{1}{\sqrt{72}} (3\delta_{\{ijkl\}\{1131\}} \delta_{m1} - 2\delta_{\{ijkl\}\{1133\}} \delta_{m3} - 1\delta_{\{ijkl\}\{1132\}} \delta_{m2}) \\
T_{ijklm}^{28} &= \frac{1}{\sqrt{18}} (\delta_{\{ijkl\}\{2211\}} \delta_{m1} - \delta_{\{ijkl\}\{2213\}} \delta_{m3}) \\
T_{ijklm}^{29} &= \frac{1}{\sqrt{72}} (3\delta_{\{ijkl\}\{2212\}} \delta_{m2} - 2\delta_{\{ijkl\}\{2211\}} \delta_{m1} - 1\delta_{\{ijkl\}\{2213\}} \delta_{m3}) \\
T_{ijklm}^{30} &= \frac{1}{\sqrt{18}} (\delta_{\{ijkl\}\{2233\}} \delta_{m3} - \delta_{\{ijkl\}\{2231\}} \delta_{m1}) \\
T_{ijklm}^{31} &= \frac{1}{\sqrt{72}} (3\delta_{\{ijkl\}\{2232\}} \delta_{m2} - 2\delta_{\{ijkl\}\{2233\}} \delta_{m3} - 1\delta_{\{ijkl\}\{2231\}} \delta_{m1})
\end{aligned}$$

$$\begin{aligned}
T_{ijklm}^{32} &= \frac{1}{\sqrt{18}} (\delta_{\{ijkl\}\{3311\}}\delta_{m1} - \delta_{\{ijkl\}\{3312\}}\delta_{m2}) \\
T_{ijklm}^{33} &= \frac{1}{\sqrt{72}} (3\delta_{\{ijkl\}\{3313\}}\delta_{m3} - 2\delta_{\{ijkl\}\{3311\}}\delta_{m1} - 1\delta_{\{ijkl\}\{3312\}}\delta_{m2}) \\
T_{ijklm}^{34} &= \frac{1}{\sqrt{18}} (\delta_{\{ijkl\}\{3322\}}\delta_{m2} - \delta_{\{ijkl\}\{3321\}}\delta_{m1}) \\
T_{ijklm}^{35} &= \frac{1}{\sqrt{72}} (3\delta_{\{ijkl\}\{3323\}}\delta_{m3} - 2\delta_{\{ijkl\}\{3322\}}\delta_{m2} - 1\delta_{\{ijkl\}\{3321\}}\delta_{m1}) \quad (3.34)
\end{aligned}$$

Once again, the normalization factors reflect the number of terms in each tensor. The 35-plet tensors have four colour indices (i through l) and one anti-colour index (m). There are tensors without self-coupling (T^1 to T^{15}), and tensors with multiple possible self-coupling terms. The 35-plet is a delicate superposition of octet-type tensors with decuplet-type tensors. Coefficients were chosen carefully so as to preserve gauge invariance by ensuring that the sum $T_{ijklm}^\alpha T_{nopqr}^\alpha$ contains full delta functions for each possible coupling. This important test results in the following.

$$\begin{aligned}
\sum_{\alpha=1}^{35} T_{ijklm}^\alpha T_{nopqr}^\alpha &= \frac{1}{24} \delta_{\{ijkl\}} \delta_{\{nopq\}} \delta_{mr} \\
&\quad - \frac{1}{144} (\delta_{\{jkl\}} \delta_{\{opq\}} \delta_{im} \delta_{nr} + \delta_{\{jkl\}} \delta_{\{npq\}} \delta_{im} \delta_{or} \\
&\quad + \delta_{\{jkl\}} \delta_{\{noq\}} \delta_{im} \delta_{pr} + \delta_{\{jkl\}} \delta_{\{nop\}} \delta_{im} \delta_{qr} \\
&\quad + \delta_{\{ikl\}} \delta_{\{opq\}} \delta_{jm} \delta_{nr} + \delta_{\{ikl\}} \delta_{\{npq\}} \delta_{jm} \delta_{or} \\
&\quad + \delta_{\{ikl\}} \delta_{\{noq\}} \delta_{jm} \delta_{pr} + \delta_{\{ikl\}} \delta_{\{nop\}} \delta_{jm} \delta_{qr} \\
&\quad + \delta_{\{ijl\}} \delta_{\{opq\}} \delta_{km} \delta_{nr} + \delta_{\{ijl\}} \delta_{\{npq\}} \delta_{km} \delta_{or} \\
&\quad + \delta_{\{ijl\}} \delta_{\{noq\}} \delta_{km} \delta_{pr} + \delta_{\{ijl\}} \delta_{\{nop\}} \delta_{km} \delta_{qr} \\
&\quad + \delta_{\{ijk\}} \delta_{\{opq\}} \delta_{lm} \delta_{nr} + \delta_{\{ijk\}} \delta_{\{npq\}} \delta_{lm} \delta_{or} \\
&\quad + \delta_{\{ijk\}} \delta_{\{noq\}} \delta_{lm} \delta_{pr} + \delta_{\{ijk\}} \delta_{\{nop\}} \delta_{lm} \delta_{qr}) \quad (3.35)
\end{aligned}$$

The first term in the above is the case of no self-couplings, with four colour charges and one anti-colour charge travelling from source to sink. The other terms all reflect various self-couplings and cross-terms.

Chapter 4

The Octet System

In this chapter, operators and propagators are developed for gluelumps containing heavy particles from the octet colour representation of SU(3). Much of the foundations laid in this chapter will be applied to the larger colour representations as well, but the primary focus here is to explain all the group theory and methodology used to formulate octet gluelumps on the lattice.

4.1 Operators

Objects on the lattice obey octahedral group symmetries, and as such there are twenty possible quantum numbers, $\Lambda^{PC} \in \{A_1^{PC}, A_2^{PC}, E^{PC}, T_1^{PC}, T_2^{PC}\}$, where P and C can be ± 1 . This was discussed in detail in Section 2.3. One must construct operators in such a way that they have the same symmetries as these octahedral group irreps. For example, A_1 is a highly symmetric state - it turns into itself under any rotation. A_2 also rotates into itself, but may pick up a negative sign in some rotations. T_1 - and T_2 -type objects rotate like vectors and axial vectors respectively, and E is a 2-component object.

In their original study of gluelumps, Foster and Michael built their operators from square plaquette building blocks (either 1×1 or 2×2). By combining plaquettes in several spatial planes and orientations (all beginning and ending on one lattice site), they created operators that coupled to ten of the above quantum states. Nothing more is possible using a square building block; it has too much symmetry to couple to all the possible octahedral group states. When building operators using square plaquettes as building blocks, only 10 out of the possible 20 Λ^{PC} representations can be created. Foster and Michael claim that the lowest energy states should be described by these representations, and this is corroborated by the Bag Model as described in Chapter 1, but the Bag Model is not rigorously derived from the true theory, QCD.

This is not entirely satisfactory, so a new set of operators is generated here to couple to all states. Plaquette-based operators identical to those used by Foster and Michael were also built, however, as a test. The exact shapes of these operators was described explicitly in Ref. [41]. It is the same as the PC -symmetrized plaquette-based basis built independently by Lewis and other members of his group previously [42], but this latter formulation is much more intuitive. Calculations were performed using this basis as well as the improved basis described below. Within error, the two calculations yielded the same results for the ten possible Λ^{PC} states accessible to both sets, as described in Chapter 10.

Moving away from a plaquette-based system, one notices that a rectangle has less symmetry than a square. Using a rectangle as a building block allows for four more operators to be built in addition to the ten accessible to the square. This is still not sufficient if one wants to study the full spectrum of states. An even less symmetric building block is a 1×2 rectangle that is bent at 90° . This will be referred to as a “chair”.

A chair on the lattice has less symmetry than a square plaquette, so it would

be expected to couple to more representations than the plaquette does. A chair is formed with two orthogonal square plaquettes joined along one edge. There are two different ways to build chairs on a cubic grid. The starting point or origin of the chair could be either on the axis of bend, or at one of the corners of the chair. This origin defines the rotational centre of the chair, and is the point where two or more chairs may be joined together. There are fewest symmetries when the origin is chosen to be at one of the corners of the chair. Since less symmetry will result in more possible overlap with different Λ^{PC} representations, it is necessary to use chairs that are built starting at a corner. An example of a chair with one face in the x-y plane and one in the y-z plane (with the joining axis, or the “spine” of the “book” in the y-direction) follows the following path:

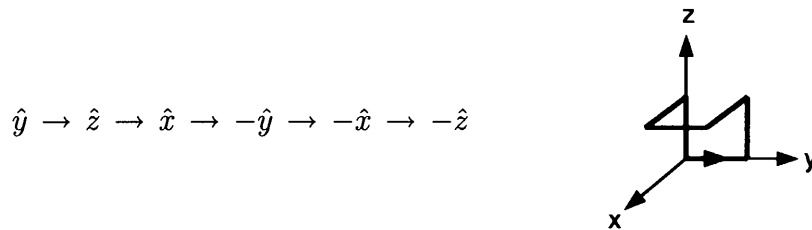


Figure 4.1: Example of a chair on the lattice which can be denoted as (y, z, x) .

This particular chair can be denoted as (y, z, x) . This is sufficient to uniquely define the particular chair of interest if it is agreed that (a, b, c) denotes the chair that follows the path $\hat{a} \rightarrow \hat{b} \rightarrow \hat{c} \rightarrow -\hat{a} \rightarrow -\hat{c} \rightarrow -\hat{b}$. Note that the fold axis will always be along the \hat{a} direction. This notation also defines the *direction* of the path along the chair, which is important.

One can define a group of chairs that spans the entire octahedral group, and use combinations of these chairs to produce operators that couple to all twenty of the Λ^{PC} representations of this group.

The octahedral group is the group of discrete 3-dimensional rotations of a cube that leave it invariant. In the continuum, 3-dimensional spatial rotations are continuous and are described by the $SO(3)$ group of 3×3 orthogonal matrices with unit determinant. The invariance of continuum QCD under such rotations leads to the conservation of angular momentum. Since the lattice is discretized, only discrete rotations are permitted. Lattice QCD is thus only invariant under such discrete rotations that leave the lattice (a cube) invariant. The group of such rotations is the octahedral group. The octahedral group is of order 24, which means that there are 24 rotations of a cube that leave it invariant. These 24 elements can be categorized into five *conjugacy classes*. A brief discussion of the octahedral group theory will be given here, but for a more detailed discussion, see for example Ref. [50] which is a discussion of glueball theory. This involves purely gauge bound states, and it deals with gluons (adjoint, or colour-octet objects) on the lattice.

Group elements g_1 and g_2 from group G are said to be conjugate if there exists an element h in G such that $g_1 = hg_2h^{-1}$. The notation used to show that group elements g_1 and g_2 are conjugate is $g_1 \sim g_2$. If $g_1 \sim g_2$ and $g_2 \sim g_3$ for $\{g_1, g_2, g_3\} \in G$, then $g_1 \sim g_3$. A conjugacy class of G is the set of all mutually conjugate elements of G . It can be shown that every element of G is a member of some conjugacy class of G , and no element of G can be a member of two different conjugacy classes. Furthermore, the identity element of G always forms a conjugacy class of its own.

There are five conjugacy classes in the octahedral group. It is conventional to denote the conjugacy class of rotations of $2\pi/m$ with a subscript m . Note that m (an integer) also denotes the number of rotations about that axis that are required to return to the identity, so C_4 would denote a conjugacy class of rotations of $2\pi/4 = \pi/2$ about a 4-fold axis. The five conjugacy classes of the octahedral group are:

- Identity* = no rotation, or rotation through 2π
- C_2 = rotations of π through an axis connecting
two diagonally opposite edges of a cube
- C_3 = rotations of $\pm 2\pi/3$ through a diagonal corner of a cube
- C_4 = rotations of $\pm \pi/2$ through a face of a cube
- C_4^2 = rotations of $\pm \pi$ through a face of a cube

These rotations could be described by 3×3 rotation matrices, but this can be very cumbersome. A more convenient technique involves the use of the *quaternion*. A quaternion is a construction,

$$q = a + ib + jc + kd, \quad (4.1)$$

where i , j , and k are generalized imaginary numbers that do not commute:

$$\begin{aligned} i^2 = j^2 = k^2 &= -1 \\ ij = k &= -ji \\ jk = i &= -kj \\ ki = j &= -ik \end{aligned} \quad (4.2)$$

The conjugate of q is q^* ,

$$q^* = a - ib - jc - kd. \quad (4.3)$$

In quaternion notation, a vector (v_x, v_y, v_z) is,

$$q_v = v_x i + v_y j + v_z k, \quad (4.4)$$

and a rotation of angle θ about an axis $\hat{n} = (n_x, n_y, n_z) = n_x i + n_y j + n_z k$ (assumed to be normalized to unit length) is,

$$q_{(\hat{n}, \theta)} = \cos(\theta/2) + \sin(\theta/2)\hat{n}. \quad (4.5)$$

So, for example, a rotation of $\pi/2$ around the z-axis would be represented by,

$$q_{(\hat{z}, \pi/2)} = \frac{1}{\sqrt{2}} + \frac{1}{\sqrt{2}}(k) = (1 + k)/\sqrt{2}. \quad (4.6)$$

To rotate a vector (represented by the quaternion q_v) by an angle θ about the \hat{n} direction (represented by the quaternion $q_{(\hat{n}, \theta)}$), one must compute the product, $q'_v = q_{(\hat{n}, \theta)} q_v q_{(\hat{n}, \theta)}^*$, and then re-interpret the resulting quaternion as a vector (the coefficient of i is the x-component, etc.)

This formalism combined with the naming convention shown in Figure 4.1 makes it easy to rotate chairs on the lattice. By way of a detailed example, consider a C_2 rotation of π through an axis (shown in red in Figure 4.2) connecting two diagonally opposite edges of a cube.

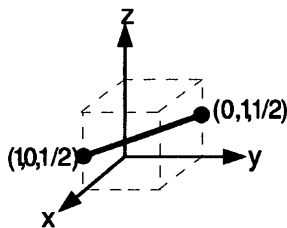


Figure 4.2: A C_2 rotation of a cube with the axis of rotation shown in red.

The coordinates of the endpoints of the axis of rotation are $(1, 0, \frac{1}{2})$ and $(0, 1, \frac{1}{2})$ as shown in the diagram. The axis of rotation is thus,

$$\begin{aligned} n &= (0, 1, \frac{1}{2}) - (1, 0, \frac{1}{2}) \\ &= (-1, 1, 0) \\ \hat{n} &= \frac{1}{\sqrt{2}}(-i + j) \end{aligned} \tag{4.7}$$

and the quaternion of the rotation is,

$$\begin{aligned} q_{(\hat{n}, \pi)} &= \cos(\pi/2) + \sin(\pi/2) \left(\frac{1}{\sqrt{2}}(-i + j) \right) \\ &= \frac{1}{\sqrt{2}}(-i + j) \end{aligned} \tag{4.8}$$

A vector in the x -direction (whose quaternion is just i) would rotate to:

$$\begin{aligned} q'_x &= q_{(\hat{n}, \pi)} i q_{(\hat{n}, \pi)}^* \\ &= \frac{1}{2}(-i + j)i(i - j) \\ &= \frac{1}{2}(1 - k)(i - j) \\ &= \frac{1}{2}(i - j - j - i) \\ &= -j \end{aligned} \tag{4.9}$$

where the identities in Equation 4.2 were used. This shows that a vector in the x direction rotates to the $-y$ direction. Similarly, one finds that y rotates to $-x$ and z to $-z$. The chair (y, z, x) shown in Figure 4.1 thus rotates to the chair $(-x, -z, -y)$ under this octahedral group rotation.

In order to create operators out of chairs, a full set of chairs is needed. There are 24 elements in the octahedral rotation group, so if one starts with an arbitrary chair

and catalogs all 24 possible rotations, this will suffice. Quaternion rotations make the process rigorous. Such a set is shown as the red chairs in Figure 4.3. The chair (y, z, x) shown earlier in Figure 4.1 is $L_6^{(8)}$. In the above example, it rotated to the chair $(-x, -z, -y)$ under a specific C_2 rotation, and this new chair is labelled $L_{22}^{(8)}$ in Figure 4.3. The (8) superscript denotes the fact that these chairs will be used to generate the octet representation, but up to this point, nothing has been said about octet colour (or any other colour), and the chairs merely adhere to octahedral group theory. Individually, the chairs do not directly relate to any of the Λ irreps, but combinations of them can be made to correspond to each of the five irreps, A_1 , A_2 , E , T_1 and T_2 .

In Figure 4.3, one may note that diagrams in the same row are related by rotations around the z-axis. Diagrams from L_1 to L_{12} in the same column are related by rotations through a diagonal axis through the cube (for example for $L_1^{(8)}$, $L_5^{(8)}$ and $L_9^{(8)}$ the axis goes from the front bottom left corner of the cube to the back top right). Diagrams from L_{13} to L_{24} which are in the same column are also related this way. The first half of the diagrams (from L_1 to L_{12}) have the “red” chair in the top hemisphere, while the second set have it in the bottom. All twenty-four possible octahedral group rotations are present. This has been confirmed by performing quaternion rotations of all the possible conjugacy class elements on the chairs.

In the continuum, QCD physics is invariant under 3-dimensional rotations but it is also invariant under parity transformations (3-dimensional spatial reflections through the origin that take (x, y, z) to $(-x, -y, -z)$) and charge conjugation. Lattice QCD should also have these properties, and the direct product of the octahedral group with parity and charge conjugation transformations leads to the 20 possible Λ^{PC} representations of interest. To deal with parity, every chair (shown in red in Figure 4.3) is partnered with its parity partner (in blue) where the transformation $(x, y, z) \rightarrow (-x, -y, -z)$ has been performed. A positive parity state is created by adding a red

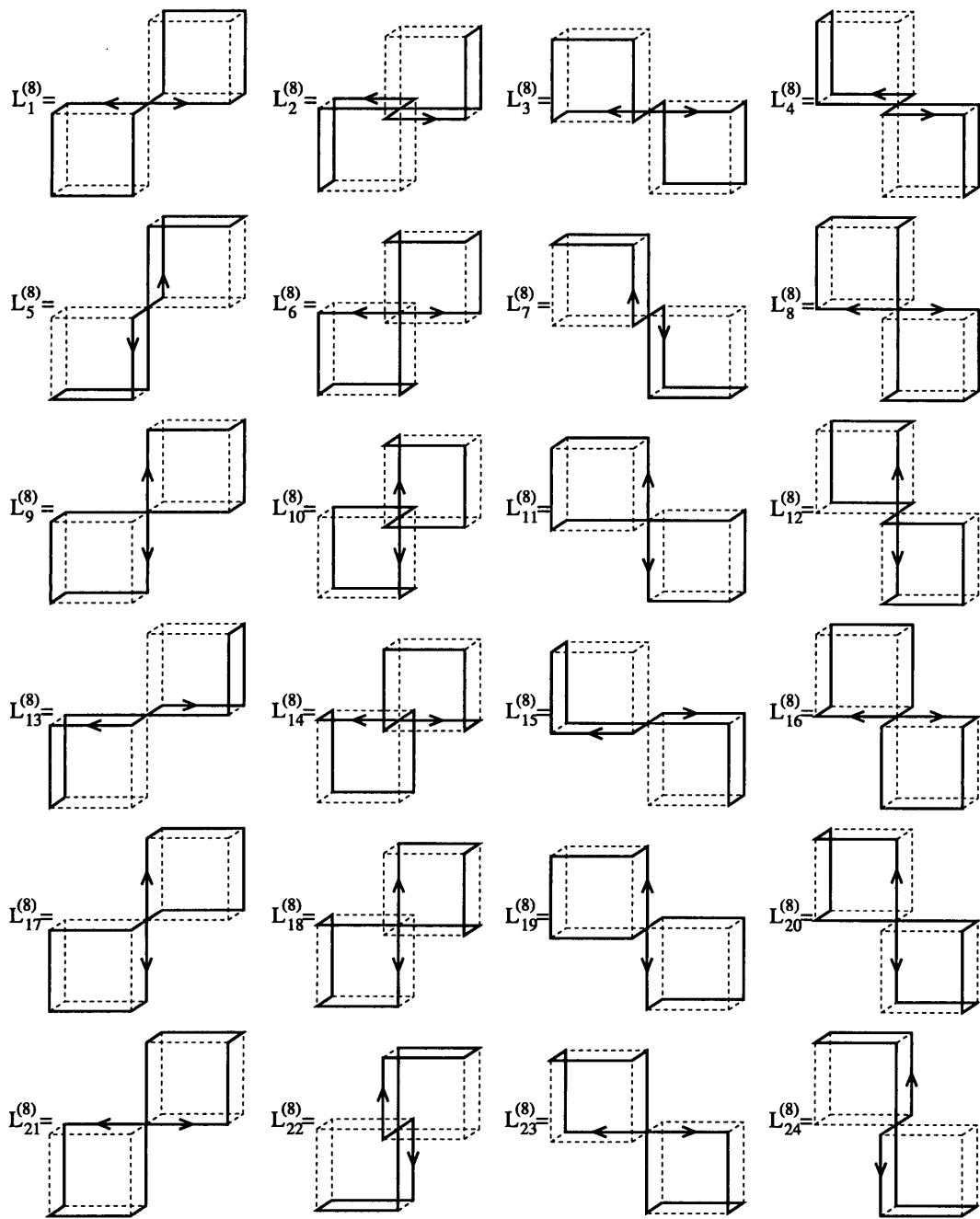


Figure 4.3: The octet chairs with arrows denoting the forward direction. In each diagram, the red and blue chairs are parity partners of one another. They should be added to obtain positive-parity states and subtracted (say always red - blue for definiteness) for negative parity.

chair and its corresponding blue parity partner. Negative parity states are created by taking red chairs and subtracting off blue chairs.

Charge conjugation transformations involve interchanging particles and anti-particles. What is meant by particles and anti-particles in these pictures of chairs? In fact, there is more information in the chairs than originally meets the eye.

Each “chair” is a product of six link variables tracing a bent chair-like path on the lattice. Perhaps a more rigorous way to think of this same chair is by starting at the origin point and identifying two different paths - each a product of three links - that start or end at the origin, and meet together at the diagonally opposite corner.

There is thus one path (a product of three links) that goes in the direction from the origin to the opposite corner of the chair. There is another path that starts at the far corner of the chair and goes in a direction towards the origin. Equivalently, this second path could be considered as the product of three *conjugate* links traveling away from the origin towards the far corner. Both paths now start at the origin and are coupled at the far corner of the chair with a delta function which is gauge invariant on the lattice. Mathematically both views are equivalent, but this second interpretation may be more enlightening as it identifies a forward path of links, and a *backward* path of conjugate links. These are the colour and anti-colour lines. This interpretation is consistent with the Young tableau diagram for the octet and resulting octet tensor which has one symmetric index (colour) and one anti-symmetric one (anti-colour).

A charge conjugation transformation interchanges colour and anti-colour. The charge conjugation partner of a chair is the same chair, but in the backwards direction. Now the colour line is a backwards (anti-colour) line, and vice versa. Note that since the links on the lattice that make up the chairs are $SU(3)$ elements, a backwards link is equal the conjugate transpose of the original link. Chairs are products of links and as such are 3×3 matrices themselves. A backwards chair is equal to the conjugate transpose of the original chair. Charge conjugation eigenstates are therefore created

by adding (or subtracting) a chair's conjugate transpose to it. Note that because of the transpose, "chair + chair[†]" is not the same as simply taking the real part of the complex chair.

Computationally, a chair is the matrix product of six SU(3) matrices around a loop. It is therefore a 3×3 matrix (rank-2 tensor) itself. It has two indices, say i and j . These both "dangle" at the source site, with index i representing a colour charge travelling around the chair, and index j representing an anti-colour charge travelling backwards around the chair. These dangling indices will be connected to the colour-multiplet particle (represented by a tensor from the appropriate representation) to form the gluelump creation or destruction operator.

Now that the chair building blocks have been created, and charge conjugation and parity are understood, it is time to build octet operators that couple to A_1 , A_2 , E , T_1 , and T_2 irreps from them. This gauge part of the gluelump bound state carries all the quantum numbers of the final state. The colour-multiplet particle itself is considered infinitely heavy, so its spin statistics can be ignored and it can be treated as a scalar, or A_1 particle. When combining this scalar state with the gauge irrep Λ_g , the result is $A_1 \otimes \Lambda_g = \Lambda_g$ for all possible irreps Λ_g . The Clebsch-Gordon coefficients for all such combinations are unity, so truly the colour-multiplet particle can be ignored, and all quantum numbers are built into the gauge components.¹ It should be noted that experimentally the colour-multiplet particle may not be a scalar, but the resulting spectrum found in this work can still be applied. The spin of the heavy particle can be added to that of the light gauge degrees of freedom as discussed in Section 2.3.

The colour-multiplet particle is connected to the gauge structures at the source site by inserting one of the tensors that generate that colour representation. This tensor contracts the indices of the gauge structure. This effectively projects the

¹See Ref. [42] for a detailed discussion of this matter.

gauge structures onto the appropriate colour representation.

Foster and Michael used gluonic operators built with square plaquettes around a single origin site. They then coupled this to the colour-octet particle by taking the trace of the matrix product of the gauge structure with one of the Gell-Mann matrices. Here, the plaquette-based gauge structures are replaced with chair-based ones, and the real octet basis of tensors shown in Section 3.3.1 is used in place of the Gell-Mann matrices.

The A_1 representation has the most symmetry. It is invariant under any octahedral group rotation. The octet A_1 operator² is an 8-component object, H^α ,

$$H^{(8)\alpha}(A_1) = \left(\sum_{a=1}^{24} L_a^{(8)} \right)_{ij} T_{ij}^\alpha, \quad (4.10)$$

where α runs from 1 to 8 in the octet and repeated Roman indices are summed over. The gauge part of the operator is created by summing together all 24 of the octet chairs. This gives it the universal A_1 symmetry. The indices of the gauge structure (index i is the colour index and index j is the anti-colour index) are contracted with one of the tensors T_{ij}^α listed in Section 3.3.1 which represents the heavy colour-octet particle. As discussed in that section, the tensors' indices can also be interpreted as colour and anti-colour.

Octahedral rotations of the A_2 representation may leave the structure invariant, or may return the negative of the structure. It can be built by

$$H^{(8)\alpha}(A_2) = \left(\sum_{a=1}^{12} (-1)^a L_a^{(8)} - \sum_{a=13}^{24} (-1)^a L_a^{(8)} \right)_{ij} T_{ij}^\alpha. \quad (4.11)$$

Pictorially, the positive terms in the sum are all the terms with red chairs in upper-

²Note that by convention, this is actually the *destruction* operator. The creation operator is the Hermitian conjugate of H^α .

back-right, upper-front-left, lower-front-right and lower-back-left quadrants in the diagrams in Figure 4.3. These are all mutually diagonal, no two of these quadrants are adjacent. The remaining terms (also in mutually diagonal quadrants) have negative signs.

The A_1 and A_2 representations are both of dimension 1. T_1 and T_2 , on the other hand, have three components and rotate like vectors or axial vectors respectively. The three components of the T_1 representation can be built as follows:

$$\begin{aligned}
H^{(8)\alpha}(T_1^x) &= \left(L_6^{(8)} + L_{20}^{(8)} + L_{21}^{(8)} + L_{11}^{(8)} - L_{18}^{(8)} - L_8^{(8)} - L_9^{(8)} - L_{23}^{(8)} \right)_{ij} T_{ij}^\alpha \\
H^{(8)\alpha}(T_1^y) &= \left(L_5^{(8)} + L_{19}^{(8)} + L_{24}^{(8)} + L_{10}^{(8)} - L_{17}^{(8)} - L_7^{(8)} - L_{12}^{(8)} - L_{22}^{(8)} \right)_{ij} T_{ij}^\alpha \\
H^{(8)\alpha}(T_1^z) &= \left(L_1^{(8)} + L_2^{(8)} + L_3^{(8)} + L_4^{(8)} - L_{13}^{(8)} - L_{14}^{(8)} - L_{15}^{(8)} - L_{16}^{(8)} \right)_{ij} T_{ij}^\alpha
\end{aligned} \tag{4.12}$$

and similarly the T_2 representation is,

$$\begin{aligned}
H^{(8)\alpha}(T_2^x) &= \left(L_6^{(8)} - L_{20}^{(8)} + L_{21}^{(8)} - L_{11}^{(8)} + L_{18}^{(8)} - L_8^{(8)} + L_9^{(8)} - L_{23}^{(8)} \right)_{ij} T_{ij}^\alpha \\
H^{(8)\alpha}(T_2^y) &= \left(L_5^{(8)} - L_{19}^{(8)} + L_{24}^{(8)} - L_{10}^{(8)} + L_{17}^{(8)} - L_7^{(8)} + L_{12}^{(8)} - L_{22}^{(8)} \right)_{ij} T_{ij}^\alpha \\
H^{(8)\alpha}(T_2^z) &= \left(L_1^{(8)} - L_2^{(8)} + L_3^{(8)} - L_4^{(8)} + L_{13}^{(8)} - L_{14}^{(8)} + L_{15}^{(8)} - L_{16}^{(8)} \right)_{ij} T_{ij}^\alpha
\end{aligned} \tag{4.13}$$

Constructed this way, any octahedral rotation of one component of T_1 (or T_2) returns itself or one of the other two components, up to a possible negative sign. Notice that all the terms in the x , y and z vector components have rotational symmetry about that axis. This is easiest to see in the z components. Chairs L_1 through L_4 are the same chair rotated around the z -axis by multiples of $\pi/4$. Using the notation introduced in Figure 4.1, these chairs are all (a, b, z) where a and b are $\pm x$ or $\pm y$. Chairs L_{13}

through L_{16} are also rotations about the z-axis, and they are all the chairs denoted by $(a, b, -z)$, again for $(a, b) \in (\pm x, \pm y)$. T_1^z is thus created with chairs (a, b, z) minus chairs $(a, b, -z)$. In the same manner, T_1^x is created with chairs (a, b, x) minus chairs $(a, b, -x)$, and similarly for T_1^y . Components of T_2 have carefully chosen alternating signs.

Finally, the E operator. While the A operators were 1-component and the T operators were 3-component, the E operator has two components. It can be built starting with three “vectors”,

$$\begin{aligned}
v^x &= L_6^{(8)} + L_{20}^{(8)} + L_{21}^{(8)} + L_{11}^{(8)} + L_{18}^{(8)} + L_8^{(8)} + L_9^{(8)} + L_{23}^{(8)} \\
v^y &= L_5^{(8)} + L_{19}^{(8)} + L_{24}^{(8)} + L_{10}^{(8)} + L_{17}^{(8)} + L_7^{(8)} + L_{12}^{(8)} + L_{22}^{(8)} \\
v^z &= L_1^{(8)} + L_2^{(8)} + L_3^{(8)} + L_4^{(8)} + L_{13}^{(8)} + L_{14}^{(8)} + L_{15}^{(8)} + L_{16}^{(8)}
\end{aligned} \tag{4.14}$$

Notice that these are similar to the components of T_1 and T_2 , but with all positive signs. The differences $v^x - v^y$, $v^y - v^z$, and $v^z - v^x$ all have the symmetries of the E representation, but they are not all linearly independent. They can be made into two independent quantities, and these are used as the two components of the E representation:

$$\begin{aligned}
H^{(8)\alpha}(E^1) &= \frac{1}{\sqrt{2}} (v^x - v^y)_{ij} T_{ij}^\alpha \\
H^{(8)\alpha}(E^2) &= -\frac{1}{\sqrt{6}} (v^x + v^y - 2v^z)_{ij} T_{ij}^\alpha
\end{aligned} \tag{4.15}$$

Note that although normalization factors are shown here, they are inconsequential and will be left out in the future. The other H^α definitions were also unnormalized in this regard. In lattice calculations, the mass of a state is extracted from the coefficient of a decaying exponential function. Taking the logarithm, one is interested in the slope. An overall multiplicative factor would show up as an added constant

and does not affect this slope.

In order to be certain that the above operators actually couple to the octet irreps that were intended, one can carry out some group-theoretic calculations. The *character* of each representation can be calculated for each of the octahedral group conjugacy classes, and then used to calculate the multiplicity of each operator type with the octahedral irreps A_1 , A_2 , E , T_1 and T_2 . Examples of such calculations are shown in Ref. [42]. The result of these calculations is that each of the operators shown here has a one-to-one correspondance with the intended octahedral group irrep.

To summarize, the octet operators³ that will be used to access all twenty Λ^{PC} irreps in the octet representation are listed below. Positive parity states are obtained by adding parity partner chairs (red and blue in Figure 4.3) and negative parity states by subtracting parity partners (red minus blue). Positive charge conjugation is obtained by adding the conjugate or “backwards” chairs, and negative charge conjugation states are the difference of forward chairs minus backwards ones.

$$\begin{aligned}
H^{(8)\alpha}(A_1) &= \left(\sum_{a=1}^{24} L_a^{(8)} \right)_{ij} T_{ij}^\alpha \\
H^{(8)\alpha}(A_2) &= \left(\sum_{a=1}^{12} (-1)^a L_a^{(8)} - \sum_{a=13}^{24} (-1)^a L_a^{(8)} \right)_{ij} T_{ij}^\alpha \\
H^{(8)\alpha}(T_1^x) &= \left(L_6^{(8)} + L_{20}^{(8)} + L_{21}^{(8)} + L_{11}^{(8)} - L_{18}^{(8)} - L_8^{(8)} - L_9^{(8)} - L_{23}^{(8)} \right)_{ij} T_{ij}^\alpha \\
H^{(8)\alpha}(T_1^y) &= \left(L_5^{(8)} + L_{19}^{(8)} + L_{24}^{(8)} + L_{10}^{(8)} - L_{17}^{(8)} - L_7^{(8)} - L_{12}^{(8)} - L_{22}^{(8)} \right)_{ij} T_{ij}^\alpha \\
H^{(8)\alpha}(T_1^z) &= \left(L_1^{(8)} + L_2^{(8)} + L_3^{(8)} + L_4^{(8)} - L_{13}^{(8)} - L_{14}^{(8)} - L_{15}^{(8)} - L_{16}^{(8)} \right)_{ij} T_{ij}^\alpha \\
H^{(8)\alpha}(T_2^x) &= \left(L_6^{(8)} - L_{20}^{(8)} + L_{21}^{(8)} - L_{11}^{(8)} + L_{18}^{(8)} - L_8^{(8)} + L_9^{(8)} - L_{23}^{(8)} \right)_{ij} T_{ij}^\alpha \\
H^{(8)\alpha}(T_2^y) &= \left(L_5^{(8)} - L_{19}^{(8)} + L_{24}^{(8)} - L_{10}^{(8)} + L_{17}^{(8)} - L_7^{(8)} + L_{12}^{(8)} - L_{22}^{(8)} \right)_{ij} T_{ij}^\alpha
\end{aligned}$$

³Recall, these are annihilation operators. The creation operators are the Hermitian conjugates of these.

$$\begin{aligned}
H^{(8)\alpha}(T_2^z) &= \left(L_1^{(8)} - L_2^{(8)} + L_3^{(8)} - L_4^{(8)} + L_{13}^{(8)} - L_{14}^{(8)} + L_{15}^{(8)} - L_{16}^{(8)} \right)_{ij} T_{ij}^\alpha \\
H^{(8)\alpha}(E^1) &= (v^x - v^y)_{ij} T_{ij}^\alpha \\
H^{(8)\alpha}(E^2) &= (v^x + v^y - 2v^z)_{ij} T_{ij}^\alpha \\
v^x &= L_6^{(8)} + L_{20}^{(8)} + L_{21}^{(8)} + L_{11}^{(8)} + L_{18}^{(8)} + L_8^{(8)} + L_9^{(8)} + L_{23}^{(8)} \\
v^y &= L_5^{(8)} + L_{19}^{(8)} + L_{24}^{(8)} + L_{10}^{(8)} + L_{17}^{(8)} + L_7^{(8)} + L_{12}^{(8)} + L_{22}^{(8)} \\
v^z &= L_1^{(8)} + L_2^{(8)} + L_3^{(8)} + L_4^{(8)} + L_{13}^{(8)} + L_{14}^{(8)} + L_{15}^{(8)} + L_{16}^{(8)}
\end{aligned} \tag{4.16}$$

Summation over i and j is implied so that H^α is a column of length $\alpha = 8$ for the octet. Each of the eight octet tensors contributes to a single (complex) entry of H^α .

As a final note about the octet operators, gauge invariance should be considered. Pains were taken in Section 3.3.1 to show that the octet tensors were gauge invariant. Without considering the propagator for a moment, to create a particle and then immediately destroy it at the same lattice space-time point, one would calculate a correlator $C = H^{\alpha\dagger} H^\alpha$, summing over $\alpha = 1 \rightarrow 8$. In the generic case, $H^\alpha = L_{ij} T_{ij}^\alpha$, so the correlator is,

$$H^{\alpha\dagger} H^\alpha = T_{ji}^\alpha L_{ji}^* L_{kl} T_{kl}^\alpha. \tag{4.17}$$

The tensors are real, so a Hermitian conjugation is just a transpose. The L factors are gauge invariant - they are closed loops which are always gauge invariant on the lattice (see Section 2.5). So the gauge invariance of this correlator comes down to the factor $T_{ji}^\alpha T_{kl}^\alpha$. This is precisely (except for the order of dummy indices) the quantity calculated in Section 3.3.1, which was found to be just the sum of delta functions and therefore invariant under gauge transformations.

4.2 Propagator

Heavy static octet-coloured particles (like for example the gluino) transform under the adjoint (or octet) representation of $SU(3)$. The gauge links on the lattice are in the fundamental (or direct) representation of $SU(3)$ and are written as $U_\mu(\vec{x}, \tau)$. Here (\vec{x}, τ) is the space-time coordinate⁴ of the starting point of the link (recall that a link goes from one lattice site to an adjacent one), and μ denotes the direction of the link. This may be $\mu = 1, 2, 3$ for the spatial directions, or $\mu = 4$ for the time direction. The gluelump propagator requires adjoint gauge links. In the octet representation, these are related to the fundamental links by,

$$\begin{aligned} U_\mu^{(8)\alpha\beta}(\vec{x}, \tau) &= \text{Tr} (U_\mu(\vec{x}, \tau) T^\beta U_\mu^\dagger(\vec{x}, \tau) T^{\alpha\dagger}) \\ &= \sum_{i,j,k,l=1}^3 [U_\mu(\vec{x}, \tau)]_{ik} T_{kl}^\beta [U_\mu^*(\vec{x}, \tau)]_{jl} T_{ij}^{\alpha*} \end{aligned} \quad (4.18)$$

Using the real basis of tensors in Section 3.3.1, $T^* = T$. With α and β both running from 1 to 8 in the octet, $U^{(8)\alpha\beta}$ is an 8×8 array. In general, for the n -plet $SU(3)$ representation, the projected gauge link is an $n \times n$ matrix. It is related to the fundamental gauge links on the lattice (U) and the n generators of the n -plet (the tensors of various rank).

The octet gluelump propagator is the product of time-directed adjoint links, $U_4^{(8)\alpha\beta}$, in incremental time steps from the creation time to the annihilation time.

$$U_4^{(8)\alpha\beta}(\vec{x}, \tau) = \sum_{i,j,k,l=1}^3 [U_4(\vec{x}, \tau)]_{ik} [U_4^*(\vec{x}, \tau)]_{jl} T_{ij}^\alpha T_{kl}^\beta \quad (4.19)$$

⁴Time is measured in Euclidean units of $\tau = it$.

For a gluelump created at time τ_i and destroyed at time τ_f , the propagator is,

$$G^{(8)\alpha\beta}(\tau_i, \tau_f) = U_4^{(8)\alpha\gamma}(\vec{x}, \tau_i) U_4^{(8)\gamma\delta}(\vec{x}, \tau_i + a) \cdots U_4^{(8)\phi\zeta}(\vec{x}, \tau_f - a) U_4^{(8)\zeta\beta}(\vec{x}, \tau_f) \quad (4.20)$$

where a is the lattice spacing between adjacent sites.

The definitions of the propagator and the adjoint links are consistent with what Foster and Michael used, although they did not explicitly show the daggers on their tensors as they used Hermitian Gell-Mann matrices. These definitions also appear in other sources, for example in the appendix of Ref. [51]. It is interesting to note that whether one uses the Gell-Mann matrices (as Foster and Michael did) or the set of real tensors developed in Section 3.3.1, the propagator is strictly real.

It has been re-iterated over and over that the octet representation involves a colour charge and an anti-colour charge. This is seen in the tensors and in the operators, and not surprisingly it is also apparent in the propagator. The adjoint links that make up the propagator involve a U_4 (the propagator for a static triplet-rep particle such as a quark) and a U_4^\dagger (the propagator for a static anti-triplet particle). Projected onto the octet representation by means of the T tensors, this shows that the propagator carries a colour charge and an anti-colour charge. Note that in Equation 4.19, the anti-symmetric indices of the T tensors (j and l) couple to the indices from the conjugate (backwards) U^\dagger link and the symmetric indices (i and k) couple to the forwards link U .

4.3 Correlator

Putting together the octet operators and propagator, one can finally write down the correlator, which is a function of the number of time steps from the creation time to annihilation. The correlator is a decaying exponential so plotting the natural

logarithm of $C(\tau_f - \tau_i)$ as a function of $\Delta\tau = \tau_f - \tau_i$ yields a linear plot whose slope is the mass of the state described by the specific operator used.⁵ The correlator for a bound state created at time τ_i and destroyed at time τ_f is,

$$C(\tau_f - \tau_i) = H^{(8)\alpha\dagger}(\tau_i)G^{(8)\alpha\beta}(\tau_i, \tau_f)H^{(8)\beta}(\tau_f). \quad (4.21)$$

Summation over α and β (which each run from 1 to 8 in the octet) results in a single number for each value of $\Delta\tau = \tau_f - \tau_i$. The lattice is large, and this correlator can be averaged over every spatial location on the lattice, as well as choosing different values of τ_i for the starting time. All twenty Λ^{PC} states can be studied for the octet representation using the formalism described above.

⁵Actually, due to the fact that the colour-multiplet particle is in the infinitely heavy approximation and the propagator is for a static particle, the lattice acquires an unphysical self-energy. So the energies gleaned from the correlator are not actually masses. They have an off-set amount. Luckily this self-energy is the same for all the states in a given calculation, so mass *differences* are physical and although absolute masses cannot be measured, a spectrum can be built on top of the lightest state.

Chapter 5

The Decuplet System

In this chapter, operators and propagators are developed gluelumps containing heavy particles from the decuplet colour representation of $SU(3)$. This builds on the methods discussed in the previous chapter, and adds to it. Some of the framework presented here will also be applied to larger colour representations (specifically the 28-plet and 35-plet), but the primary focus is to explain all the group theory and methodology used to formulate decuplet gluelumps on the lattice.

5.1 Operators

The decuplet cannot be made from the octet chairs. They have the wrong symmetries. Recall that one interpretation of the building-block chairs was that they were each made up of two paths of three links. One path (the one carrying colour charge) started at the origin and went to the diagonally opposite corner of the chair. The other (with anti-colour charge) travelled backwards, starting at the diagonally opposite corner and ending at the origin.

For the decuplet, the Young tableau has three columns, each of which consists of

just one box in the top row. This can be interpreted as three colour charges, and if the “chair” example was prudent, one might expect operators to contain three paths which all start at the origin, travelling outwards. This is precisely what is suggested. Three paths, each three links long, that lie on a “chair” shape can be used to access all the desired Λ^{PC} representations of the decuplet. These three paths will all start at the origin where they couple to the static colour through the rank-three tensor T_{ijk}^α (α runs from 1 to 10 in the decuplet) and end at the diagonally opposite corner of the chair. At this far corner, a rank-3 anti-symmetric tensor is needed to couple the three paths together. A good choice is the Levi-Civita symbol, ε_{ijk} , which is gauge invariant on the lattice.

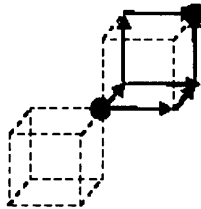


Figure 5.1: An example of a decuplet “chair” building block.

In the example in Figure 5.1, the first path follows the three red links. Let the product of these three $SU(3)$ links be $R_{i\alpha}$. The second path follows the three links drawn in blue. Let this path be $B_{j\beta}$. The third path first follows a blue link, then the green one, then the final red one. Denote this path by $G_{k\gamma}$. All the paths start at the origin and travel to the opposite corner of the chair. The chair itself should have three indices, i, j, k that will couple to the colour-multiplet particle at the source. The remaining three indices, α, β, γ are coupled at the far corner with the Levi-Civita symbol. Computationally, this means that the chair L_{ijk} is obtained by,

$$L_{ijk} = \sum_{\alpha, \beta, \gamma} R_{i\alpha} B_{j\beta} G_{k\gamma} \varepsilon_{\alpha\beta\gamma}. \quad (5.1)$$

The new set of decuplet building-block chairs looks very similar to the octet ones, but a third path appears on each chair. Also, a solid dot is added on each chair to mark the location of the antisymmetric tensor, ε_{ijk} . To reduce clutter, arrows are only shown on the first diagram, but all these chairs¹ should be interpreted as flowing from the centre outwards.

The derivations for generating the set of chairs and for combining them into operators is the same as for the octet case, except that the octet chairs ($L^{(8)}$) are replaced by decuplet chairs ($L^{(10)}$), and the octet tensors T_{ij}^α are replaced with the decuplet tensors generated in Section 3.3.2, namely T_{ijk}^α . The decuplet operators are thus,

$$\begin{aligned}
H^{(10)\alpha}(A_1) &= \left(\sum_{a=1}^{24} L_a^{(10)} \right)_{ijk} T_{ijk}^\alpha \\
H^{(10)\alpha}(A_2) &= \left(\sum_{a=1}^{12} (-1)^a L_a^{(10)} - \sum_{a=13}^{24} (-1)^a L_a^{(10)} \right)_{ijk} T_{ijk}^\alpha \\
H^{(10)\alpha}(T_1^x) &= \left(L_6^{(10)} + L_{20}^{(10)} + L_{21}^{(10)} + L_{11}^{(10)} - L_{18}^{(10)} - L_8^{(10)} - L_9^{(10)} - L_{23}^{(10)} \right)_{ijk} T_{ijk}^\alpha \\
H^{(10)\alpha}(T_1^y) &= \left(L_5^{(10)} + L_{19}^{(10)} + L_{24}^{(10)} + L_{10}^{(10)} - L_{17}^{(10)} - L_7^{(10)} - L_{12}^{(10)} - L_{22}^{(10)} \right)_{ijk} T_{ijk}^\alpha \\
H^{(10)\alpha}(T_1^z) &= \left(L_1^{(10)} + L_2^{(10)} + L_3^{(10)} + L_4^{(10)} - L_{13}^{(10)} - L_{14}^{(10)} - L_{15}^{(10)} - L_{16}^{(10)} \right)_{ijk} T_{ijk}^\alpha \\
H^{(10)\alpha}(T_2^x) &= \left(L_6^{(10)} - L_{20}^{(10)} + L_{21}^{(10)} - L_{11}^{(10)} + L_{18}^{(10)} - L_8^{(10)} + L_9^{(10)} - L_{23}^{(10)} \right)_{ijk} T_{ijk}^\alpha \\
H^{(10)\alpha}(T_2^y) &= \left(L_5^{(10)} - L_{19}^{(10)} + L_{24}^{(10)} - L_{10}^{(10)} + L_{17}^{(10)} - L_7^{(10)} + L_{12}^{(10)} - L_{22}^{(10)} \right)_{ijk} T_{ijk}^\alpha \\
H^{(10)\alpha}(T_2^z) &= \left(L_1^{(10)} - L_2^{(10)} + L_3^{(10)} - L_4^{(10)} + L_{13}^{(10)} - L_{14}^{(10)} + L_{15}^{(10)} - L_{16}^{(10)} \right)_{ijk} T_{ijk}^\alpha \\
H^{(10)\alpha}(E^1) &= (v^x - v^y)_{ijk} T_{ijk}^\alpha \\
H^{(10)\alpha}(E^2) &= (v^x + v^y - 2v^z)_{ijk} T_{ijk}^\alpha
\end{aligned}$$

¹Recall that by convention these chairs form *annihilation* operators. Creation operators are the Hermitian conjugates, and would flow from the outer corner towards the central point.

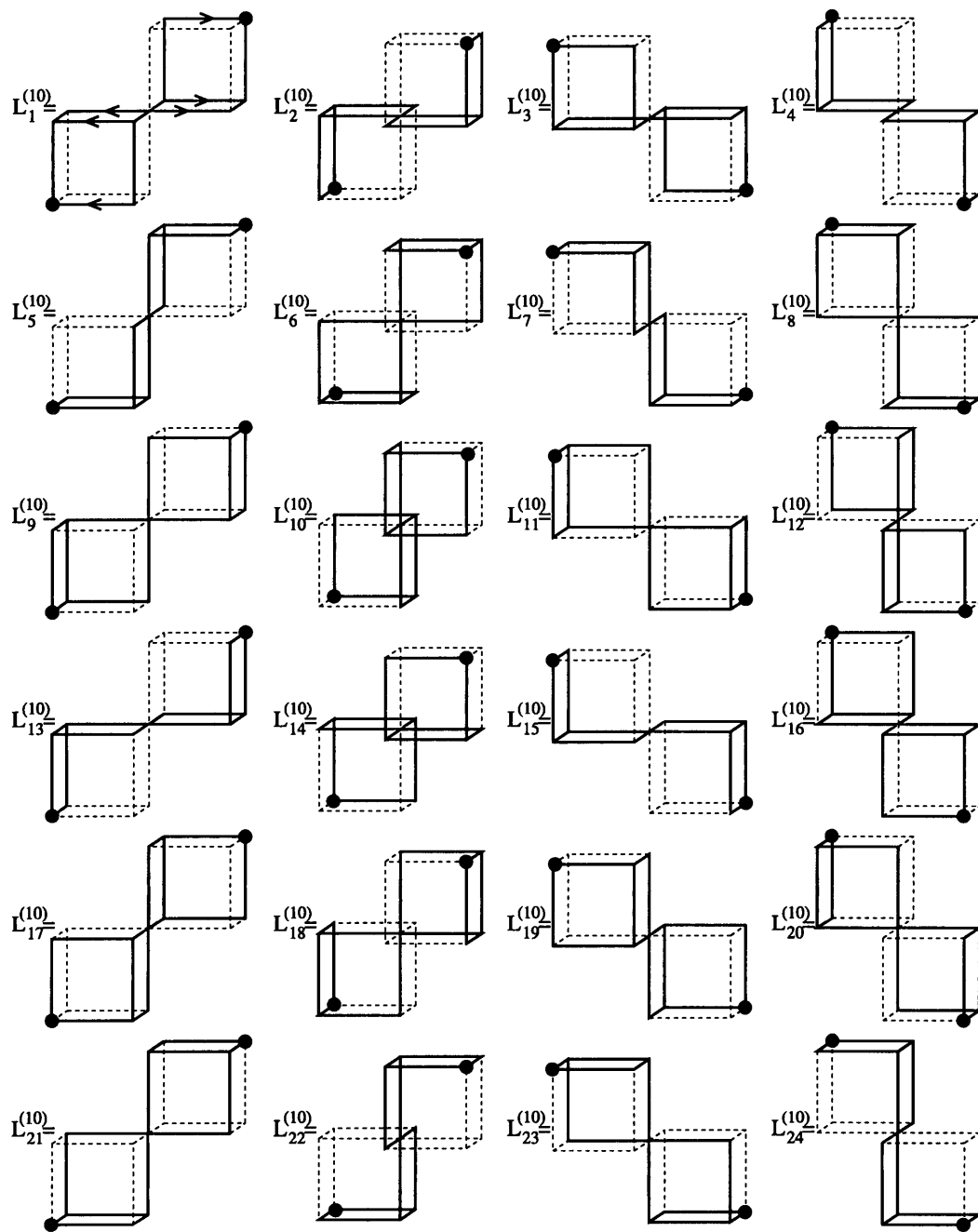


Figure 5.2: The decuplet chairs with arrows denoting the forward direction (omitted except on the first diagram). In each diagram, the red and blue chairs are parity partners of one another. They should be added to obtain positive-parity states and subtracted (say always red - blue for definiteness) for negative parity.

$$\begin{aligned}
v^x &= L_6^{(10)} + L_{20}^{(10)} + L_{21}^{(10)} + L_{11}^{(10)} + L_{18}^{(10)} + L_8^{(10)} + L_9^{(10)} + L_{23}^{(10)} \\
v^y &= L_5^{(10)} + L_{19}^{(10)} + L_{24}^{(10)} + L_{10}^{(10)} + L_{17}^{(10)} + L_7^{(10)} + L_{12}^{(10)} + L_{22}^{(10)} \\
v^z &= L_1^{(10)} + L_2^{(10)} + L_3^{(10)} + L_4^{(10)} + L_{13}^{(10)} + L_{14}^{(10)} + L_{15}^{(10)} + L_{16}^{(10)}
\end{aligned}
\tag{5.2}$$

As with the octet operators, these are actually the *annihilation* operators. The creation operators are the Hermitian conjugates of these.

One technicality arises in the decuplet case that did not appear in the octet case. The decuplet carries three colour charges. Pictorially, in the creation operators (the Hermitian conjugates of the ones shown in Figure 5.2), the lines flow from the outer corners of chairs to the central “creation” site. Then the propagator (which will be discussed in detail in the following section) carries three colour lines forward to the destruction site where they flow from the central point of the annihilation operator to the outer corners of chairs. If a “backwards” chair (a Hermitian conjugate) is placed at the destruction site with colour lines traveling from the outer corner of a chair towards the centre, these lines no longer connect with the incoming propagator at the centre. This is shown schematically in Figure 5.3. Recall that in the octet case, “backwards” chairs were needed to create charge conjugation states. Lattice calculations confirm that it is not possible to create charge conjugation eigenstates using backwards chairs in the decuplet representation.

The reason is not a coding one, nor a lattice problem. It is fundamental physics. Just like the proton which also carries three colour charges, decuplet gluelumps are not eigenstates of charge conjugation. Like the decuplet of baryons in QCD, decuplet gluelumps contain three colour charges (or three anti-colour charges) and can thus be distinguished as being in either a colour or anti-colour state. This introduces a colour “charge” to the system, and as with QCD baryons (which have electromagnetic

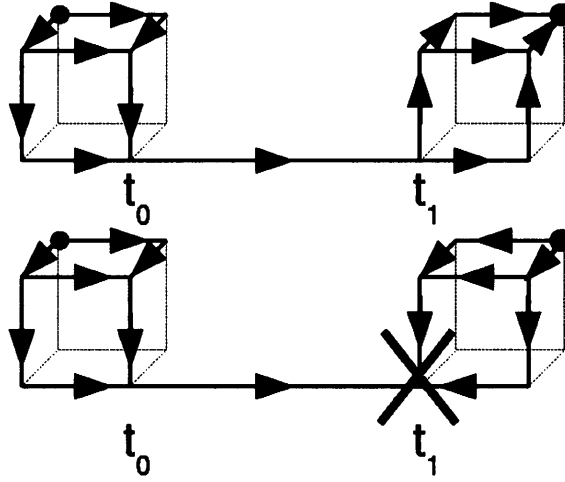


Figure 5.3: Schematic of the flow of colour charge from creation operator (at time t_0) to propagator to annihilation operator (at time t_1). In the lower diagram, a “backwards” chair was introduced at the sink location, and the flow lines no longer connect.

charge), a charged object is not an eigenstate of charge conjugation. This problem did not arise in the case of the octet, because operators there were constructed with one colour and one anti-colour index. Akin to neutral mesons, these “chargeless” states are their own anti-particles, and as such are eigenstates of C . Decuplet gluelumps do not have definite C quantum numbers. As a result, there are fundamentally only ten possible Λ^P operators for the decuplet, $\Lambda^P \in (A_1^P, A_2^P, E^P, T_1^P, T_2^P)$ for positive or negative parity. Parity states are created in the same way as in the octet - one adds or subtracts the parity partner of the chairs which are created by transforming $(x, y, z) \rightarrow (-x, -y, -z)$. These parity partners are shown as the blue chairs in Figure 5.2.

5.2 Propagator

The decuplet propagator can be constructed in an analogous way to the octet one. The result, shown in Eq. 5.4, is consistent with equations (B.2), (B.3) and (B.6) of Ref. [51]. The decuplet propagator is,

$$G^{(10)\alpha\beta}(\tau_i, \tau_f) = U_4^{(10)\alpha\gamma}(\vec{x}, \tau_i) U_4^{(10)\gamma\delta}(\vec{x}, \tau_i + a) \cdots U_4^{(10)\phi\zeta}(\vec{x}, \tau_f - a) U_4^{(10)\zeta\beta}(\vec{x}, \tau_f) \quad (5.3)$$

where,

$$U_4^{(10)\alpha\beta}(\vec{x}, \tau) = \sum_{i,j,k,l,m,n=1}^3 [U_4(\vec{x}, \tau)]_{il} [U_4(\vec{x}, \tau)]_{jm} [U_4(\vec{x}, \tau)]_{kn} T_{ijk}^\alpha T_{lmn}^\beta \quad (5.4)$$

In the decuplet representation, α and β both run from 1 to 10. The first index of each of the three U_4 links that make up $U_4^{(10)}$ is connected to the T^α tensor at the source. The second index from the three U_4 links connects to the T^β tensor at the sink. The propagator contains three U_4 terms, confirming that it carries three colour charges just like the tensors and operators for this representation.

5.3 Correlator

The decuplet correlator for a bound state created at time τ_i and destroyed at time τ_f is,

$$C(\tau_f - \tau_i) = H^{(10)\alpha\dagger}(\tau_i) G^{(10)\alpha\beta}(\tau_i, \tau_f) H^{(10)\beta}(\tau_f). \quad (5.5)$$

Summation over α and β (which each run from 1 to 10 in the decuplet) is implied. All ten Λ^P states can be studied for the decuplet representation using the methods described here. Charge conjugation is not a good quantum number in this representation, however.

Chapter 6

The 27-Plet System

In this chapter, operators and propagators are developed for gluelumps containing heavy particles from the 27-plet colour representation of $SU(3)$. This builds on the methods discussed in the previous chapters, especially the octet framework. In terms of group theory, the 27-plet acts very much like a *double* octet, as will be described below. All the required methodology used to formulate 27-plet gluelumps on the lattice is presented here.

6.1 Operators

The 27-plet has two colour indices and two anti-colour indices. Neither the octet chair building-blocks nor the decuplet ones couple to the 27-plet, but the correct symmetries can be generated if a *double* chair is defined. The 27-plet can be built based on a building block that combines two octet chairs (see Figure 4.3). Since the octet chairs each have one colour and one anti-colour index, the double chair has the required two colours and two anti-colours. Let the 27-plet building blocks be defined

as follows:

$$\begin{aligned}
\left(L_1^{(27)}\right)_{ijkl} &= \left(L_5^{(8)}\right)_{ik} \left(L_9^{(8)}\right)_{jl} & \left(L_{13}^{(27)}\right)_{ijkl} &= \left(L_{21}^{(8)}\right)_{ik} \left(L_{17}^{(8)}\right)_{jl} \\
\left(L_2^{(27)}\right)_{ijkl} &= \left(L_6^{(8)}\right)_{ik} \left(L_{10}^{(8)}\right)_{jl} & \left(L_{14}^{(27)}\right)_{ijkl} &= \left(L_{22}^{(8)}\right)_{ik} \left(L_{18}^{(8)}\right)_{jl} \\
\left(L_3^{(27)}\right)_{ijkl} &= \left(L_7^{(8)}\right)_{ik} \left(L_{11}^{(8)}\right)_{jl} & \left(L_{15}^{(27)}\right)_{ijkl} &= \left(L_{23}^{(8)}\right)_{ik} \left(L_{19}^{(8)}\right)_{jl} \\
\left(L_4^{(27)}\right)_{ijkl} &= \left(L_8^{(8)}\right)_{ik} \left(L_{12}^{(8)}\right)_{jl} & \left(L_{16}^{(27)}\right)_{ijkl} &= \left(L_{24}^{(8)}\right)_{ik} \left(L_{20}^{(8)}\right)_{jl} \\
\left(L_5^{(27)}\right)_{ijkl} &= \left(L_9^{(8)}\right)_{ik} \left(L_1^{(8)}\right)_{jl} & \left(L_{17}^{(27)}\right)_{ijkl} &= \left(L_{13}^{(8)}\right)_{ik} \left(L_{21}^{(8)}\right)_{jl} \\
\left(L_6^{(27)}\right)_{ijkl} &= \left(L_{10}^{(8)}\right)_{ik} \left(L_2^{(8)}\right)_{jl} & \left(L_{18}^{(27)}\right)_{ijkl} &= \left(L_{14}^{(8)}\right)_{ik} \left(L_{22}^{(8)}\right)_{jl} \\
\left(L_7^{(27)}\right)_{ijkl} &= \left(L_{11}^{(8)}\right)_{ik} \left(L_3^{(8)}\right)_{jl} & \left(L_{19}^{(27)}\right)_{ijkl} &= \left(L_{15}^{(8)}\right)_{ik} \left(L_{23}^{(8)}\right)_{jl} \\
\left(L_8^{(27)}\right)_{ijkl} &= \left(L_{12}^{(8)}\right)_{ik} \left(L_4^{(8)}\right)_{jl} & \left(L_{20}^{(27)}\right)_{ijkl} &= \left(L_{16}^{(8)}\right)_{ik} \left(L_{24}^{(8)}\right)_{jl} \\
\left(L_9^{(27)}\right)_{ijkl} &= \left(L_1^{(8)}\right)_{ik} \left(L_5^{(8)}\right)_{jl} & \left(L_{21}^{(27)}\right)_{ijkl} &= \left(L_{17}^{(8)}\right)_{ik} \left(L_{13}^{(8)}\right)_{jl} \\
\left(L_{10}^{(27)}\right)_{ijkl} &= \left(L_2^{(8)}\right)_{ik} \left(L_6^{(8)}\right)_{jl} & \left(L_{22}^{(27)}\right)_{ijkl} &= \left(L_{18}^{(8)}\right)_{ik} \left(L_{14}^{(8)}\right)_{jl} \\
\left(L_{11}^{(27)}\right)_{ijkl} &= \left(L_3^{(8)}\right)_{ik} \left(L_7^{(8)}\right)_{jl} & \left(L_{23}^{(27)}\right)_{ijkl} &= \left(L_{19}^{(8)}\right)_{ik} \left(L_{15}^{(8)}\right)_{jl} \\
\left(L_{12}^{(27)}\right)_{ijkl} &= \left(L_4^{(8)}\right)_{ik} \left(L_8^{(8)}\right)_{jl} & \left(L_{24}^{(27)}\right)_{ijkl} &= \left(L_{20}^{(8)}\right)_{ik} \left(L_{16}^{(8)}\right)_{jl}
\end{aligned} \tag{6.1}$$

Notice that for each $\left(L_a^{(27)}\right)_{ijkl}$ the indices i and j are symmetric (or “colour”) indices, made from the symmetric indices of two $L^{(8)}$ chairs. Indices k and l are anti-symmetric (anti-colour) indices and originate from the anti-symmetric indices of two $L^{(8)}$ chairs. It is necessary to keep track of which indices are symmetric and which are anti-symmetric because the 27-plet tensors (see Section 3.3.3) were created so that the first two indices were symmetric and the second two were anti-symmetric.

How were the constituent chairs chosen for the 27-plet building blocks? The double chairs need to be made from exactly *two* chairs as the name implies, and these two chairs should combine to have the symmetries of a different third chair. A

rotation through diagonally opposite corners of a cube has 3-fold symmetry. There are four such axes, and these rotations belong to the C_3 conjugacy class. In Figure 4.3, it is clear that $L_1^{(8)}$, $L_5^{(8)}$ and $L_9^{(8)}$ (which are all in the same column) are all related by rotations through an axis of the cube that goes from the bottom-front-left corner to the top-back-right. Chairs $L_2^{(8)}$, $L_6^{(8)}$ and $L_{10}^{(8)}$ are similarly related by C_3 rotations, as are chairs $L_{13}^{(8)}$, $L_{17}^{(8)}$ and $L_{21}^{(8)}$, etc. There are eight such groupings of three chairs, always from the same column. These groupings were used in creating the double chairs. Since there is 3-fold symmetry in these groupings that are related by C_3 rotations, one chair can be recreated from the other two in a sense. By creating $L_1^{(27)}$ out of $L_5^{(8)}$ and $L_9^{(8)}$, the proper symmetries are maintained. Pictorially, a diagram of $L_a^{(27)}$ looks just like $L_a^{(8)}$ except that the blank areas are now chairs, and the area where the chair originally was is now blank. Using the notation introduced in Figure 4.1, an (a, b, c) -type double chair is made from chairs (b, c, a) and (c, a, b) . For example, $L_1^{(8)}$ is $(y, -x, z)$, so $L_1^{(27)}$ is created with chairs $(-x, z, y)$ (which is $L_5^{(8)}$) and $(z, y, -x)$ (which is $L_9^{(8)}$).

All H^α definitions are the same as in Equation 4.16 for the octet, except that every $L_a^{(8)}$ is replaced with $L_a^{(27)}$, and every T_{ij}^α is replaced by a 27-plet tensor T_{ijkl}^α from the set developed in Section 3.3.3. By convention, these are actually the *annihilation* operators. The creation operators are the Hermitian conjugates of these.

The 27-plet operators have two colour indices and two anti-colour indices; they are their own anti-particle. A “backwards” double chair also has two colour and two anti-colour indices. Charge conjugation is a good quantum number in this representation. A positive C state is created by adding the backwards chairs to the forwards ones, and a negative C state is created by subtracting backwards chairs from the forwards ones. Computationally this is achieved by adding or subtracting Hermitian conjugates. Parity states are obtained in the same way as for the other representations - blue chairs (the parity partners) are added to or subtracted from the red ones.

6.2 Propagator

By now, the construction of propagators has become predictable. The 27-plet propagator is

$$G^{(27)\alpha\beta}(\tau_i, \tau_f) = U_4^{(27)\alpha\gamma}(\vec{x}, \tau_i) U_4^{(27)\gamma\delta}(\vec{x}, \tau_i + a) \cdots U_4^{(27)\phi\zeta}(\vec{x}, \tau_f - a) U_4^{(27)\zeta\beta}(\vec{x}, \tau_f) \quad (6.2)$$

where

$$U_4^{(27)\alpha\beta}(\vec{x}, \tau) = \sum_{i, \dots, q=1}^3 [U_4(\vec{x}, \tau)]_{im} [U_4(\vec{x}, \tau)]_{jn} [U_4^*(\vec{x}, \tau)]_{kp} [U_4^*(\vec{x}, \tau)]_{lq} T_{ijkl}^\alpha T_{mnpq}^\beta \quad (6.3)$$

As expected, each step of the propagator has two U_4 's and two U_4^* 's corresponding to two colour and two anti-colour indices. In terms of colour flow, the propagator has two forward lines, and two backward lines (the Hermition conjugate of an SU(3) U_4 link is the backwards-pointing link). Since the operators also have two backwards lines and two forwards lines, flow is maintained from source to sink.

6.3 Correlator

The 27-plet correlator for a bound state created at time τ_i and destroyed at time τ_f is

$$C(\tau_f - \tau_i) = H^{(27)\alpha\dagger}(\tau_i) G^{(27)\alpha\beta}(\tau_i, \tau_f) H^{(27)\beta}(\tau_f). \quad (6.4)$$

Summation over α and β (which each run from 1 to 27 in the 27-plet) is implied. 27-plet states are their own anti-particles, and as such are eigenstates of charge conjugation. Consequently, all twenty Λ^{PC} states can be studied for the 27-plet representation using the methods described here.

Chapter 7

The 28-Plet System

In this chapter, operators and propagators are developed for gluelumps containing heavy particles from the 28-plet colour representation of SU(3). This builds on the methods discussed in the previous chapters, especially the decuplet framework. In terms of group theory, whereas the 27-plet was a double octet, the 28-plet acts very much like a double decuplet, as will be described below. All the required methodology used to formulate 28-plet gluelumps on the lattice is presented here.

7.1 Operators

The 28-plet has six colour indices. As with the 27-plet, the building blocks for the operators are made out of double chairs, this time based on the decuplet chairs (see Figure 5.2) which each have three colour indices. The 28-plet building blocks are defined as follows:

$$\left(L_1^{(28)}\right)_{ijklmn} = \left(L_5^{(10)}\right)_{ijk} \left(L_9^{(10)}\right)_{lmn} \quad \left(L_{13}^{(28)}\right)_{ijklmn} = \left(L_{21}^{(10)}\right)_{ijk} \left(L_{17}^{(10)}\right)_{lmn}$$

$$\begin{aligned}
\left(L_2^{(28)}\right)_{ijklmn} &= \left(L_6^{(10)}\right)_{ijk} \left(L_{10}^{(10)}\right)_{lmn} & \left(L_{14}^{(28)}\right)_{ijklmn} &= \left(L_{22}^{(10)}\right)_{ijk} \left(L_{18}^{(10)}\right)_{lmn} \\
\left(L_3^{(28)}\right)_{ijklmn} &= \left(L_7^{(10)}\right)_{ijk} \left(L_{11}^{(10)}\right)_{lmn} & \left(L_{15}^{(28)}\right)_{ijklmn} &= \left(L_{23}^{(10)}\right)_{ijk} \left(L_{19}^{(10)}\right)_{lmn} \\
\left(L_4^{(28)}\right)_{ijklmn} &= \left(L_8^{(10)}\right)_{ijk} \left(L_{12}^{(10)}\right)_{lmn} & \left(L_{16}^{(28)}\right)_{ijklmn} &= \left(L_{24}^{(10)}\right)_{ijk} \left(L_{20}^{(10)}\right)_{lmn} \\
\left(L_5^{(28)}\right)_{ijklmn} &= \left(L_9^{(10)}\right)_{ijk} \left(L_1^{(10)}\right)_{lmn} & \left(L_{17}^{(28)}\right)_{ijklmn} &= \left(L_{13}^{(10)}\right)_{ijk} \left(L_{21}^{(10)}\right)_{lmn} \\
\left(L_6^{(28)}\right)_{ijklmn} &= \left(L_{10}^{(10)}\right)_{ijk} \left(L_2^{(10)}\right)_{lmn} & \left(L_{18}^{(28)}\right)_{ijklmn} &= \left(L_{14}^{(10)}\right)_{ijk} \left(L_{22}^{(10)}\right)_{lmn} \\
\left(L_7^{(28)}\right)_{ijklmn} &= \left(L_{11}^{(10)}\right)_{ijk} \left(L_3^{(10)}\right)_{lmn} & \left(L_{19}^{(28)}\right)_{ijklmn} &= \left(L_{15}^{(10)}\right)_{ijk} \left(L_{23}^{(10)}\right)_{lmn} \\
\left(L_8^{(28)}\right)_{ijklmn} &= \left(L_{12}^{(10)}\right)_{ijk} \left(L_4^{(10)}\right)_{lmn} & \left(L_{20}^{(28)}\right)_{ijklmn} &= \left(L_{16}^{(10)}\right)_{ijk} \left(L_{24}^{(10)}\right)_{lmn} \\
\left(L_9^{(28)}\right)_{ijklmn} &= \left(L_1^{(10)}\right)_{ijk} \left(L_5^{(10)}\right)_{lmn} & \left(L_{21}^{(28)}\right)_{ijklmn} &= \left(L_{17}^{(10)}\right)_{ijk} \left(L_{13}^{(10)}\right)_{lmn} \\
\left(L_{10}^{(28)}\right)_{ijklmn} &= \left(L_2^{(10)}\right)_{ijk} \left(L_6^{(10)}\right)_{lmn} & \left(L_{22}^{(28)}\right)_{ijklmn} &= \left(L_{18}^{(10)}\right)_{ijk} \left(L_{14}^{(10)}\right)_{lmn} \\
\left(L_{11}^{(28)}\right)_{ijklmn} &= \left(L_3^{(10)}\right)_{ijk} \left(L_7^{(10)}\right)_{lmn} & \left(L_{23}^{(28)}\right)_{ijklmn} &= \left(L_{19}^{(10)}\right)_{ijk} \left(L_{15}^{(10)}\right)_{lmn} \\
\left(L_{12}^{(28)}\right)_{ijklmn} &= \left(L_4^{(10)}\right)_{ijk} \left(L_8^{(10)}\right)_{lmn} & \left(L_{24}^{(28)}\right)_{ijklmn} &= \left(L_{20}^{(10)}\right)_{ijk} \left(L_{16}^{(10)}\right)_{lmn}
\end{aligned} \tag{7.1}$$

All the indices in both the $L_a^{(28)}$ and the constituent $L_a^{(10)}$ chairs are symmetric, so the order of the indices does not matter as much as it did for the 27-plet. Other than replacing octet chairs with decuplet chairs, the above basis is the same as the one created for the 27-plet. The same constituent chairs go into making the double chairs. As with the 27-plet, a diagram of $L_a^{(28)}$ looks just like $L_a^{(10)}$ except that the blank areas are now chairs, and the area where the chair originally was is now blank.

All H^α definitions are the same as in Equation 5.2 for the decuplet, except that every $L_a^{(10)}$ is replaced with $L_a^{(28)}$, and every T_{ijk}^α is replaced by a 28-plet tensor T_{ijklmn}^α from the set developed in Section 3.3.4. Again, by convention these are actually the *annihilation* operators. The creation operators are the Hermitian conjugates of these.

Since the 28-plet operators have six colour indices, they are “charged” and not

eigenstates of charge conjugation. Although states with definite charge conjugation cannot be generated, parity states are obtained in the same way as for the other representations - blue chairs (the parity partners) are added to or subtracted from the red ones.

7.2 Propagator

The 28-plet propagator is similar in form to the propagators from the other representations,

$$G^{(28)\alpha\beta}(\tau_i, \tau_f) = U_4^{(28)\alpha\gamma}(\vec{x}, \tau_i) U_4^{(28)\gamma\delta}(\vec{x}, \tau_i + a) \cdots U_4^{(28)\phi\zeta}(\vec{x}, \tau_f - a) U_4^{(28)\zeta\beta}(\vec{x}, \tau_f) \quad (7.2)$$

where

$$U_4^{(28)\alpha\beta}(\vec{x}, \tau) = \sum_{i, \dots, t=1}^3 [U_4(\vec{x}, \tau)]_{io} [U_4(\vec{x}, \tau)]_{jp} [U_4(\vec{x}, \tau)]_{kq} [U_4(\vec{x}, \tau)]_{lr} [U_4(\vec{x}, \tau)]_{ms} [U_4(\vec{x}, \tau)]_{nt} T_{ijklmn}^\alpha T_{opqrst}^\beta \quad (7.3)$$

Each step of the propagator has six U_4 links corresponding to the six colour indices. In terms of colour flow, all six lines of the propagator go in the forward direction. Colour flow is maintained from source to sink as long as the operators “point” in the right direction. See a discussion of this issue in Section 5.1 and a visual representation in Figure 5.3.

7.3 Correlator

The 28-plet correlator for a bound state created at time τ_i and destroyed at time τ_f is

$$C(\tau_f - \tau_i) = H^{(28)\alpha\dagger}(\tau_i)G^{(28)\alpha\beta}(\tau_i, \tau_f)H^{(28)\beta}(\tau_f). \quad (7.4)$$

Summation over α and β (which each run from 1 to 28 in the 28-plet) is implied. Since 28-plet states are not eigenstates of charge conjugation, only the ten Λ^P states can be studied for the 28-plet representation.

Chapter 8

The 35-Plet System

In this chapter, operators and propagators are developed for gluelumps containing heavy particles from the 35-plet colour representation of $SU(3)$. This builds on the methods discussed in the previous chapters, especially the octet and decuplet frameworks that were set out in Chapters 4 and 5. The 35-plet is a combination of these two representations, as will be described below. All the required methodology used to formulate 35-plet gluelumps on the lattice is presented here.

8.1 Operators

The 35-plet has four colour indices and one anti-colour index. As with the 27-plet and 28-plet, the building blocks for the operators are made out of double chairs, this time based on both octet chairs (see Figure 4.3) *and* decuplet chairs (see Figure 5.2). Since the octet has one symmetric and one anti-symmetric index, and the decuplet has three symmetric indices, the 35-plet has the proper symmetries. The 35-plet

building blocks are defined as follows:

$$\begin{aligned}
\left(L_1^{(35)}\right)_{ijklm} &= \left(L_5^{(8)}\right)_{im} \left(L_9^{(10)}\right)_{jkl} & \left(L_{13}^{(35)}\right)_{ijklm} &= \left(L_{21}^{(8)}\right)_{im} \left(L_{17}^{(10)}\right)_{jkl} \\
\left(L_2^{(35)}\right)_{ijklm} &= \left(L_6^{(8)}\right)_{im} \left(L_{10}^{(10)}\right)_{jkl} & \left(L_{14}^{(35)}\right)_{ijklm} &= \left(L_{22}^{(8)}\right)_{im} \left(L_{18}^{(10)}\right)_{jkl} \\
\left(L_3^{(35)}\right)_{ijklm} &= \left(L_7^{(8)}\right)_{im} \left(L_{11}^{(10)}\right)_{jkl} & \left(L_{15}^{(35)}\right)_{ijklm} &= \left(L_{23}^{(8)}\right)_{im} \left(L_{19}^{(10)}\right)_{jkl} \\
\left(L_4^{(35)}\right)_{ijklm} &= \left(L_8^{(8)}\right)_{im} \left(L_{12}^{(10)}\right)_{jkl} & \left(L_{16}^{(35)}\right)_{ijklm} &= \left(L_{24}^{(8)}\right)_{im} \left(L_{20}^{(10)}\right)_{jkl} \\
\left(L_5^{(35)}\right)_{ijklm} &= \left(L_9^{(8)}\right)_{im} \left(L_1^{(10)}\right)_{jkl} & \left(L_{17}^{(35)}\right)_{ijklm} &= \left(L_{13}^{(8)}\right)_{im} \left(L_{21}^{(10)}\right)_{jkl} \\
\left(L_6^{(35)}\right)_{ijklm} &= \left(L_{10}^{(8)}\right)_{im} \left(L_2^{(10)}\right)_{jkl} & \left(L_{18}^{(35)}\right)_{ijklm} &= \left(L_{14}^{(8)}\right)_{im} \left(L_{22}^{(10)}\right)_{jkl} \\
\left(L_7^{(35)}\right)_{ijklm} &= \left(L_{11}^{(8)}\right)_{im} \left(L_3^{(10)}\right)_{jkl} & \left(L_{19}^{(35)}\right)_{ijklm} &= \left(L_{15}^{(8)}\right)_{im} \left(L_{23}^{(10)}\right)_{jkl} \\
\left(L_8^{(35)}\right)_{ijklm} &= \left(L_{12}^{(8)}\right)_{im} \left(L_4^{(10)}\right)_{jkl} & \left(L_{20}^{(35)}\right)_{ijklm} &= \left(L_{16}^{(8)}\right)_{im} \left(L_{24}^{(10)}\right)_{jkl} \\
\left(L_9^{(35)}\right)_{ijklm} &= \left(L_1^{(8)}\right)_{im} \left(L_5^{(10)}\right)_{jkl} & \left(L_{21}^{(35)}\right)_{ijklm} &= \left(L_{17}^{(8)}\right)_{im} \left(L_{13}^{(10)}\right)_{jkl} \\
\left(L_{10}^{(35)}\right)_{ijklm} &= \left(L_2^{(8)}\right)_{im} \left(L_6^{(10)}\right)_{jkl} & \left(L_{22}^{(35)}\right)_{ijklm} &= \left(L_{18}^{(8)}\right)_{im} \left(L_{14}^{(10)}\right)_{jkl} \\
\left(L_{11}^{(35)}\right)_{ijklm} &= \left(L_3^{(8)}\right)_{im} \left(L_7^{(10)}\right)_{jkl} & \left(L_{23}^{(35)}\right)_{ijklm} &= \left(L_{19}^{(8)}\right)_{im} \left(L_{15}^{(10)}\right)_{jkl} \\
\left(L_{12}^{(35)}\right)_{ijklm} &= \left(L_4^{(8)}\right)_{im} \left(L_8^{(10)}\right)_{jkl} & \left(L_{24}^{(35)}\right)_{ijklm} &= \left(L_{20}^{(8)}\right)_{im} \left(L_{16}^{(10)}\right)_{jkl}
\end{aligned} \tag{8.1}$$

Notice that for each $\left(L_a^{(35)}\right)_{ijklm}$, indices i, j, k, l are symmetric (or “colour”) indices, made from the symmetric index of an $L^{(8)}$ octet chair and the three symmetric indices of an $L^{(10)}$ decuplet chair. Index m is anti-symmetric (anti-colour) and originates from the anti-symmetric index of the $L^{(8)}$ chair. It is necessary to keep track of which indices are symmetric and which are anti-symmetric because the 35-plet tensors (see Section 3.3.5) were created so that the first four indices were symmetric and the last one was anti-symmetric.

A diagram of $L_a^{(35)}$ looks just like $L_a^{(28)}$ except that one of the chairs is an $L^{(8)}$ and

the other is an $L^{(10)}$. The same constituent chairs go into making the double chairs for the 35-plet as went into the 27-plet and 28-plet. In the 27-plet discussion in Section 6.1, it was explained how the constituent chairs in each double chair were chosen. They were all related by a particular rotation. In the 35-plet, one must exercise care to chose which of these constituent chairs comes from the decuplet and which from the octet. It is important to use the same convention throughout the 35-plet basis. Using the notation introduced in Figure 4.1, an (a, b, c) -type 35-plet double chair is made from an *octet* (b, c, a) chair and a *decuplet* (c, a, b) chair. For example, $L_1^{(8)}$ is $(y, -x, z)$, so $L_1^{(35)}$ is created with octet chair $(-x, z, y)$ (which is $L_5^{(8)}$) and decuplet chair $(z, y, -x)$ (which is $L_9^{(10)}$). The opposite convention could also have been used, as long as the definition was consistent throughout.

All H^α definitions are the same as in Equation 5.2 for the decuplet, except that every $L_a^{(10)}$ is replaced with $L_a^{(35)}$, and every T_{ijk}^α is replaced by a 35-plet tensor T_{ijklm}^α from the set developed in Section 3.3.5. Again, by convention, these are actually the *annihilation* operators. The creation operators are the Hermition conjugates of these.

Since the 35-plet operators have more colour indices than anti-colour, they are “charged” and not eigenstates of charge conjugation. Although states with definite charge conjugation cannot be generated, parity states are obtained in the same way as for the other representations - blue chairs (the parity partners) are added to or subtracted from the red ones.

8.2 Propagator

The 35-plet propagator follows the same pattern as seen for the other representations,

$$G^{(35)\alpha\beta}(\tau_i, \tau_f) = U_4^{(35)\alpha\gamma}(\vec{x}, \tau_i) U_4^{(35)\gamma\delta}(\vec{x}, \tau_i + a) \cdots U_4^{(35)\phi\zeta}(\vec{x}, \tau_f - a) U_4^{(35)\zeta\beta}(\vec{x}, \tau_f) \quad (8.2)$$

where

$$\begin{aligned}
U_4^{(35)\alpha\beta}(\vec{x}, \tau) = & \\
& \sum_{i, \dots, r=1}^3 [U_4(\vec{x}, \tau)]_{in} [U_4(\vec{x}, \tau)]_{jo} [U_4(\vec{x}, \tau)]_{kp} [U_4(\vec{x}, \tau)]_{lq} [U_4^*(\vec{x}, \tau)]_{mr} T_{ijklm}^\alpha T_{nopqr}^\beta
\end{aligned} \tag{8.3}$$

Each step of the propagator has four U_4 links corresponding to the four colour indices and one U_4^* anti-colour link. In terms of colour flow, the propagator has four forward lines and one backwards one. It is not symmetric, but this is not a surprise since it has already been discussed that the 35-plet does not have definite charge conjugation. Colour flow is maintained from source to sink as long as the operators “point” in the right direction. The definitions above ensure that the proper flow is achieved.

8.3 Correlator

The 35-plet correlator for a bound state created at time τ_i and destroyed at time τ_f is

$$C(\tau_f - \tau_i) = H^{(35)\alpha\dagger}(\tau_i) G^{(35)\alpha\beta}(\tau_i, \tau_f) H^{(35)\beta}(\tau_f). \tag{8.4}$$

Summation over α and β (which each run from 1 to 35 in the 35-plet) is implied. 35-plet states are not eigenstates of charge conjugation, so the only states that can be studied are the ten Λ^P states which can be created using the methods described here.

Chapter 9

Simulations

The framework for lattice calculations has been presented in the previous chapters. There is sufficient detail presented there so that someone familiar with lattice QCD could replicate the tests that were carried out. This chapter describes some of the technical aspects of the calculations that were run. It begins with a discussion of the smearing technique used to enhance the signal, then goes on to give details about how the final signal was extracted from the results of the calculations.

9.1 Smearing

In order to increase sensitivity to the ground states and reduce coupling to high-frequency modes in the theory (such as excited states), stout link smearing is applied to the spatial links in the lattice [52]. Smearing the gauge fields is a method that can remove high-energy modes from the final spectrum, suppressing short-range UV fluctuations. This can optimize and enhance the ground-state signal. Smearing involves “thermalizing” each link on the lattice. This is accomplished by adding a weighted sum of neighbouring spatial links to each link, then projecting the result back onto

SU(3). Every link is updated in this way, and several iterations over the full lattice can be performed. The weighting parameter, ρ , and the number of smearing iterations, n_ρ , are parameters that can be optimized. Smearing also acts to effectively increase the size of the operators on the lattice since the links involved become extended from their original positions by including contributions from neighbouring links. Smearing makes the operators effectively larger and as such is a method for building an operator of the appropriate physical size. The stout link smearing algorithm of Morningstar and Peardon is unique in that the projection onto SU(3) is done in an analytic way [52]. For a full explanation of this smearing technique, as well as how to implement it, see Ref. [52], including their Section III where the computational implementation of the technique is explained.

Since correlators have energy dependence $e^{-E\tau}$, where $\tau = it$ is the Euclidean time coordinate on the lattice, states at small times are more sensitive to contamination from excited states. Smearing helps reduce this, and it also helps to extend the signal to later time-steps, since noisy signals often degrade at later times. It is important to extend the signal as much as possible not just because it allows for a better fit to the data, but also because the first few time-steps are often excluded from the fit. This is because some excited state contamination often persists even after smearing, and its influence is greatest at early time-steps. It is the ground state however that is of most interest.

Every iteration of smearing involves multiplying spatial links by factors $e^{i\rho Q_\mu(x)}$, where ρ is the smearing parameter related to weightings, and $Q_\mu(x)$ is a carefully constructed traceless Hermitian matrix.¹ There is a different $Q_\mu(x)$ for every point x on the lattice and pointing in each of the three spatial directions μ . In SU(3) it is

¹See Ref. [52] for more details, where they include ρ inside the definition of $Q_\mu(x)$ in their equations (1) through (3).

constructed from the neighbouring gauge links at each lattice site by

$$Q_\mu(x) = \frac{i}{2} (\Omega_\mu^\dagger(x) - \Omega_\mu(x)) - \frac{iI}{6} \text{Tr} (\Omega_\mu^\dagger(x) - \Omega_\mu(x)) , \quad (9.1)$$

where I is the 3×3 identity matrix and

$$\Omega_\mu(x) = C_\mu(x) U_\mu^\dagger(x) , \quad (9.2)$$

and

$$C_\mu(x) = \sum_{\nu \neq \mu} (U_\nu(x) U_\mu(x + \hat{\nu}) U_\nu^\dagger(x + \hat{\mu}) + U_\nu^\dagger(x - \hat{\nu}) U_\mu(x - \hat{\nu}) U_\nu(x - \hat{\nu} + \hat{\mu})) . \quad (9.3)$$

Smearing is performed in the spatial directions only, $\mu, \nu \in (1, 2, 3)$. Since $Q_\mu(x)$ was constructed to be traceless and Hermitian, $e^{i\rho Q_\mu(x)}$ is an element of $SU(3)$, as is the product of $e^{i\rho Q_\mu(x)}$ with any gauge link on the lattice. The first smearing parameter, ρ , is the weighting given to the sums C of neighbouring links. The second smearing parameter, n_ρ , is the number of times the smearing algorithm is applied to the whole lattice configuration. In the $(n+1)^{th}$ smearing iteration, the gauge link $U_\mu(x)$ on the lattice is updated from the version in the previous iteration as follows:

$$U_\mu^{(n+1)}(x) = e^{i\rho Q_\mu^{(n)}(x)} U_\mu^{(n)}(x) \quad (9.4)$$

so that

$$U_\mu(x) \rightarrow U_\mu^{(1)}(x) \rightarrow U_\mu^{(2)}(x) \rightarrow \dots \rightarrow U_\mu^{(n_\rho)}(x) \quad (9.5)$$

In Figure 9.1, one can see how smearing improves the signal. The natural logarithm of the correlator is plotted for all the Λ^{PC} states as a function of the number of time steps separating the source and the sink. The slope of these lines gives the

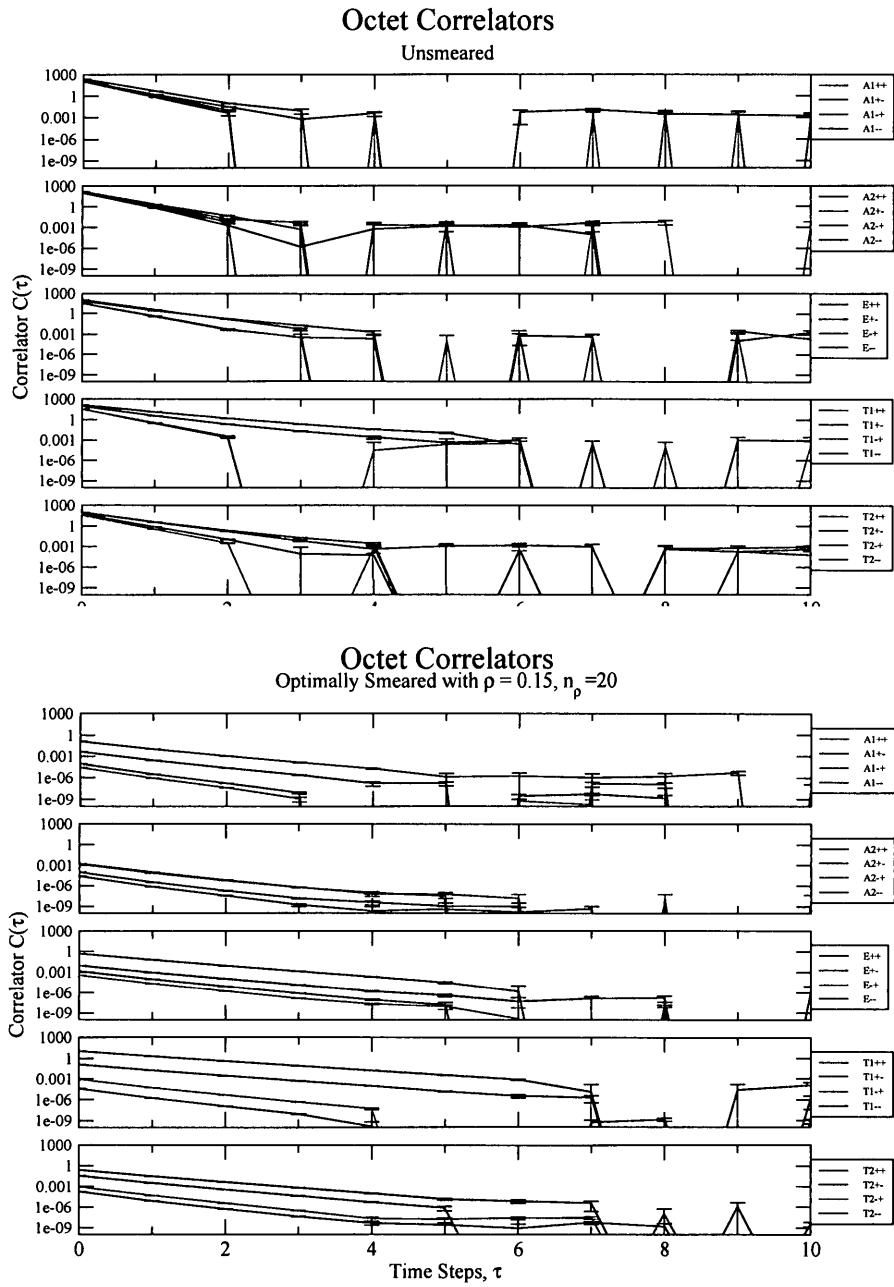


Figure 9.1: The effects of smearing on the octet gluelump states. The upper diagram is the unsmearred case, and the lower diagram shows the same calculation, but optimally smeared. Notice how much cleaner the signal is, and how smearing helps to extend the signal to later time steps. Smearing also suppresses excited states, and slopes are shallower emphasizing the ground state contribution.

particles' masses, since the correlator has energy dependence $C(\tau) \sim e^{-E\tau}$ for Euclidean time $\tau = it$. In the unsmearred case, the signal decays rapidly into noise. Smearing cleans up the signal, extending it to much later time steps. Smearing also suppresses excited states. The slopes on the smeared graph are shallower than in the unsmearred case, emphasizing the ground state contribution and allowing it to be read more clearly from the smeared graph.

Two smearing parameters were discussed, and they can be tuned in a systematic way. Although there are two free parameters, they need not be treated completely independently. Applying the smearing algorithm repeatedly, links get multiplied by factors $e^{i\rho Q}$ repeatedly. Since $(e^{i\rho Q})^{n\rho} = e^{i\rho n\rho Q}$, one can see that it is the product ρn_ρ of the two smearing parameters that determines the total amount of smearing. Of course, this is not entirely rigorous as $Q_\mu^{(n)}(x)$ is slightly different from the next iteration, $Q_\mu^{(n+1)}(x)$ which is based on links that were updated in iteration n . It serves as a guideline however.

Smearing can be optimized by examining space-temporal Wilson loops, which are closed rectangles on the lattice with one dimension having a set length along a spatial direction, and the other dimension having varying length in the time direction. This observable involves only gauge links, and it couples to the static quark-antiquark potential. A more direct route to optimizing smearing, however, is to examine the behaviour of gluelump states themselves as smearing is adjusted.

Since the correlators depend exponentially on energy, $C(\tau) \sim e^{-E\tau}$, the energy of a state is extracted from the slope of the natural logarithm of the correlator. An approximation to this is the “slope” between subsequent time steps. An “effective” energy can be defined as

$$E_{eff}(\tau) \sim -(\ln(C(\tau+a)) - \ln(C(\tau))) = \ln \frac{C(\tau)}{C(\tau+a)} \quad (9.6)$$

In particular, since early time steps are most contaminated by excited states, the effective energy at the source (between time step zero and time step one) is a good measure of the effectiveness of smearing.

$$E_{eff}(0) = \ln \left[\frac{C(0)}{C(a)} \right] \quad (9.7)$$

The correlator at the source point should never be used to try to extract any actual physics from lattice calculations due to the danger of possible contact terms, however it provides the most dramatic scenario for possible excited state contamination and thus is able to provide a good measure of smearing effectiveness.

One would expect the effective energy to decrease as smearing removes excited states. Applying too much smearing, however, can blur the signal away altogether. To optimize the smearing parameters, $E_{eff}(0)$ was examined for various Λ^{PC} reps as a function of the amount of smearing. With the number of smearing iterations, n_ρ , held constant, the weighting, ρ , was varied and the effective energy $E_{eff}(0)$ plotted as a function of the product ρn_ρ of the two smearing parameters. An example is shown in Figure 9.2 for the A_1^{++} gluelump in the octet representation which happens to be strongly affected by smearing and thus a good example.

Regardless of the smearing parameters, if too much smearing is applied, the signal disappears altogether. This can be seen in Figure 9.2 as the final points in each data series deviate upwards. Apart from these points, the general trend is for the effective energy to decrease as smearing increases, as one would expect. The effective energy decreases to a plateau. Any combination of smearing parameters in this plateau results in “optimal” smearing. Computationally, one would like to keep n_ρ as small as possible because more smearing iterations take more computing time.² With too

²In practice, though, smearing was only a small fraction of the running time regardless of the value of n_ρ chosen.

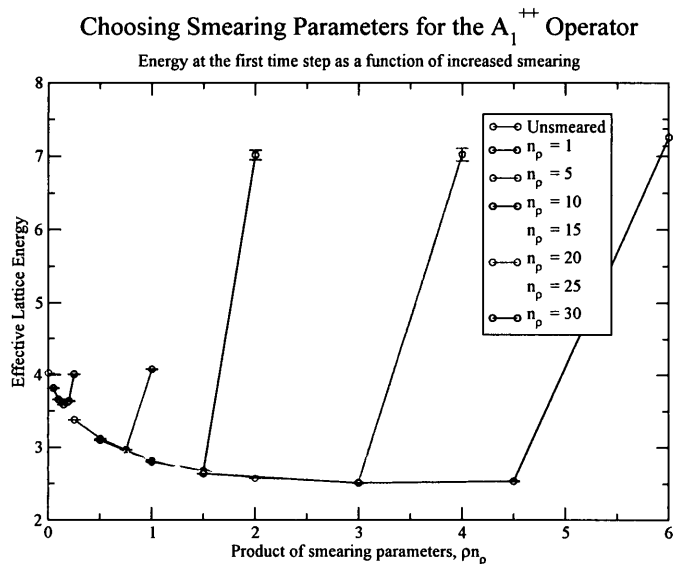


Figure 9.2: Choosing smearing parameters. The effective energy is plotted as a function of the amount of smearing.

small an n_ρ , however, the optimal plateau cannot be reached because increasing ρ past a certain amount causes the signal to disappear.

Plots of effective energies were examined for various Λ^{PC} states in each of the five different SU(3) representations (the octet, decuplet, 27-plet, 28-plet and 35-plet). The smearing parameters were optimized with $(\rho, n_\rho) = (0.20, 15)$ for the octet and decuplet, and $(\rho, n_\rho) = (0.15, 15)$ for the 27-plet and the 35-plet as well as for the octet and the decuplet running on the second (larger) ensemble of configurations. Smearing parameters were similar for the 28-plet, although this representation was not run to completion as it turned out to be prohibitively slow to run, as well as being very noisy.

9.2 Overview of Lattice Calculations

A lattice calculation involves first reading in a lattice configuration, then performing the required smearing on it. Then, for every possible “source” site on the lattice (every spatial position and every starting time) creation operators are generated. Annihilation operators are calculated first directly at the source site, then one step away in the time direction, then two steps away and so on. Periodic boundaries on the lattice mean that neighbouring times (and spatial locations) sometimes loop around from the end of the configuration back to the beginning. As the number of time steps separating the source and sink ($\Delta\tau$) increases, links are added on to the propagator. A correlator is calculated. Finally, for each value of $\Delta\tau$, the correlator is averaged over all spatial locations and all possible starting times. This is performed for all twenty Λ^{PC} states (or all ten Λ^P states when charge conjugation is not a good quantum number). The whole process is then repeated for another configuration until the calculations have been performed on all the configurations in the ensemble.

The configurations in the first ensemble have forty lattice sites in the time direction. This means that it is possible to calculate the correlator up to values of $\Delta\tau = 40$. As is seen in Figure 9.1, however, even with smearing the signal decays long before this. To save computing time, $\Delta\tau$ was often restricted to less than 40 in the calculations, although all possible starting time coordinates were still included in the average.

Calculations were run on the Compute Canada SHARCNET network of supercomputers (specifically the cluster “saw”). The octet and decuplet representations ran fairly quickly, but the bigger n-plet representations required more and more computing time. This is not surprising. The octet tensor basis consists of just eight rank-2 tensors whereas the 35-plet consists of 35 rank-5 tensors. As the rank of the tensors increases, the number of calculations in the lattice calculations increases drastically.

Table 9.1 lists the approximate running time for the various calculations. Except for the octet and decuplet which were run on both the first ensemble ($790\ 20^3 \times 40$ configurations) and the second ensemble ($650\ 28^3 \times 56$ configurations), all calculations were run only on the first ensemble. The maximum $\Delta\tau$ value is also shown for each calculation. This is important to note because while two runs may appear to have similar run times (for example the octet runs on the two different sized lattices), one may have calculated significantly fewer correlator steps.

Table 9.1: Lattice calculation run-times.

SU(3) Rep.	Ensemble	Max. $\Delta\tau$	No. of Configs.	Time per Config.
Octet	First ($20^3 \times 40$)	40	790	20 min
Octet	Second ($28^3 \times 56$)	20	650	35 min
Decuplet	First ($20^3 \times 40$)	40	790	2 hours
Decuplet	Second ($28^3 \times 56$)	10	650	3 hours
27-plet	First ($20^3 \times 40$)	20	790	12 hours
28-plet	First ($20^3 \times 40$)	10	790	600 hours
35-plet	First ($20^3 \times 40$)	10	790	100 hours

Table 9.1 shows the impact of larger and larger representations on the calculation run-time. In fact, it was decided that the 28-plet was prohibitively expensive computationally to run full-scale. Running the whole ensemble would have taken more than 50 core-years of computing time, even just for a maximum $\Delta\tau$ of 10 time steps. If the 28-plet had been particularly interesting to a phenomenological model, or if there was a good chance of obtaining a clear meaningful signal, then there might be a case for spending this amount of computer time on the calculation, but this was not the case. In fact, based on the Casimir colour factors discussed in Section 3.2, the 28-plet is predicted to be the heaviest of all the representations listed in Table 9.1, even heavier than the 35-plet. As states get heavier, the signal becomes harder and harder to extract. It is noisier and degenerates into noise faster. All the theoretical framework

has been laid out for the 28-plet (and the other representations) in previous chapters, however, so if there comes a time when computing is substantially faster, or if there is particular interest in the 28-plet, calculations could be performed on the lattice.

9.3 Signal Extraction

In principle, extracting the mass of a state is just a matter of measuring the slope of the decaying exponential correlation function. In practice, however, there are many subtleties. The biggest factor is in deciding which data points of the correlator to use. This will be referred to as the fitting window. Signals can also be composites of more than one state, so a correlator may be fit with one decaying exponential, or the sum of two or more decaying exponential functions. For example, the form of the fits might be

$$a_1 e^{-a_2 \tau} \quad \text{or} \quad a_1 e^{-a_2 \tau} + a_3 e^{-a_4 \tau} \quad \text{etc.} \quad (9.8)$$

In the above, the parameters a_2 and a_4 are mass parameters.

To begin with, a one-exponential functional form was fit to the correlators using fitting algorithms that originated from Numerical Recipes codes [53]. This was done first by starting at the origin (time-step zero) and extending the fit past the point where the signal appeared to decay away into noise. Including later (noisy) time steps does not affect the fit parameters much because the larger error bars on those points do not weight them heavily. On the other hand, it was found that the fit was sensitive to the choice of starting point. The origin point (and sometimes the first one or two steps thereafter) can be highly contaminated with excited states even after smearing. As one would expect, including these points in the fit causes a higher estimate of the ground state mass. It also results in a poor “goodness of fit,” as measured by the χ^2

(chi-square) per degree of freedom ($\chi^2/\text{d.o.f.}$),

$$\chi^2/\text{d.o.f.} = \frac{1}{\nu} \sum_{i=1}^N \frac{(C(\tau_i) - y(\tau_i))^2}{\sigma_i^2}, \quad (9.9)$$

where the number of degrees of freedom, $\nu = N - n$, is the number of points, N , in the fit minus the number of fit parameters, n . For a one-exponential fit, $n = 2$. The $C(\tau_i)$ are the measured correlator points included in the fit, σ_i are the statistical errors on these data points, and $y(\tau_i)$ are the expected values of the correlator at each time step assuming the correlator follows the prescribed exponential fit. For example, for a one-exponential fit,

$$y(\tau_i) = a_1 e^{-a_2 \tau_i}. \quad (9.10)$$

In general, if the theoretical model for the data (the $y(\tau_i)$ values) is a good fit to the actual data (the $C(\tau_i)$), then one would expect the variations of $C(\tau_i)$ from $y(\tau_i)$ to be on the order of the errors in the measured points. If $|C(\tau_i) - y(\tau_i)| \sim \sigma$, then each term in Equation 9.9 would be of order 1 and similarly the $\chi^2/\text{d.o.f.}$ value would be close to unity. A large $\chi^2/\text{d.o.f.}$ value (one that is significantly greater than unity) indicates that there is a large difference between the data points and the theoretical model it is being fit to. In that case, the fit is not good and the model does not describe the data. A $\chi^2/\text{d.o.f.}$ that is significantly less than one does *not* imply that the model is a bad fit to the data, but rather it might imply that the data seems “too good”, since the fit is better than the inherent errors in the data. The $\chi^2/\text{d.o.f.}$ may also be less than one if the proposed fit model is too elaborate. For example, this may occur if trying to fit more exponential functions to a lattice signal than the data can resolve. It may also be less than one if the data are correlated. Since the neighbouring time steps of a correlator on any individual ensemble are correlated, the average over all the configurations in the ensemble might be expected to have

correlation effects resulting in a $\chi^2/\text{d.o.f.}$ that is less than one.

Fits starting at time-step zero tended to have a very large $\chi^2/\text{d.o.f.}$ value. Because of the exponential form of the correlator, any excited states that are mixed in to the signal affect earlier time steps more dramatically (recall that the correlator is proportional to $e^{-E\tau}$, so at small times, higher energies dominate the signal). Removing the first time-step from the fit improved the $\chi^2/\text{d.o.f.}$ of the fit, and it also reduced the mass fit parameter, confirming that the first time step influenced the fit to a higher mass. Removing more and more early time steps from the fit keeps driving the mass fit down until it stabilizes. From then on, removing more early time-steps does not significantly affect the fit parameters, provided the overall number of degrees of freedom of the fit remains above 1. Fits are successful and stable when discounting at least the source time-step.

Table 9.2: A one-exponential fit to the T_1^{+-} octet correlator using chair-type operators on the ensemble with $a = 0.0982$.

time-steps in fit		degrees of freedom	quality of fit	exponential fit parameter
first	last	ν	$\chi^2/\text{d.o.f}$	(energy in lattice units)
0	10	9	675	1.6825 ± 0.0005
1	10	8	33	1.6181 ± 0.0009
2	10	7	1.3	1.580 ± 0.003
3	10	6	0.31	1.56 ± 0.01
4	10	5	0.37	1.55 ± 0.04
5	10	4	0.34	1.59 ± 0.19
3	15	11	0.38	1.56 ± 0.01
3	10	6	0.31	1.56 ± 0.01
3	9	5	0.24	1.56 ± 0.01
3	8	4	0.29	1.56 ± 0.01
3	7	3	0.37	1.56 ± 0.01
3	6	2	0.05	1.555 ± 0.009
3	5	1	0.02	1.556 ± 0.009
3	4	0	-	1.556 ± 0.009

The first half of Table 9.2 shows a one-exponential fit to the octet T_1^{+-} correlator (based on the calculation on the $20^3 \times 40$ ensemble) where all fits end at time step 10, which is beyond the point where the signal decays in that channel. In Figure 9.1, one can see that the smeared T_1^{+-} signal extends all the way to time step 6 or 7, and points after that are noisy. The fits in the first half of Table 9.2 progressively leave out more and more of the early time steps. The mass fit parameter correspondingly reduces, as does the $\chi^2/\text{d.o.f.}$ value of the fit, however even just excluding the origin time-step results in consistent mass results to two significant figures. Starting the fit at time-step 5 or later results in a large error on the fitted mass since that is approaching the end of the non-noisy correlator signal. This effect is shown graphically in Figure 9.3. The simulation mass (in lattice units) reduces to a plateau as more and more early time steps are excluded from the fit until finally there are not enough good data points left and the fit parameters (especially the mass) become less certain.

Based on these trials, a “starting point” could be selected as the first point to include in the fit. In the case of the T_1^{+-} example, time-step 3 might be determined to be the optimal starting point since it is the earliest fit that is statistically equal to all the later fits.

Although the first half of Table 9.2 suggests that the fit from time step 3 to 10 is the best choice, one might wonder about the effect of removing the later (noisy) time-steps from the fit. Earlier it was stated that these noisy time-steps do not significantly affect the fit since they are not heavily weighted due to their larger error bars. To prove that this is indeed the case, various fits were performed for the octet T_1^{+-} using time-step 3 as the starting point, but with different ending points. The results of these fits are listed in the second half of Table 9.2. It is clear that even extending the fit to time-step 15 (which is *well* past the point where any discernible exponential function can be seen) results in a fit that yields the same mass as one that only extends to time-step 10, or for that matter 9, or 8, all the way down to

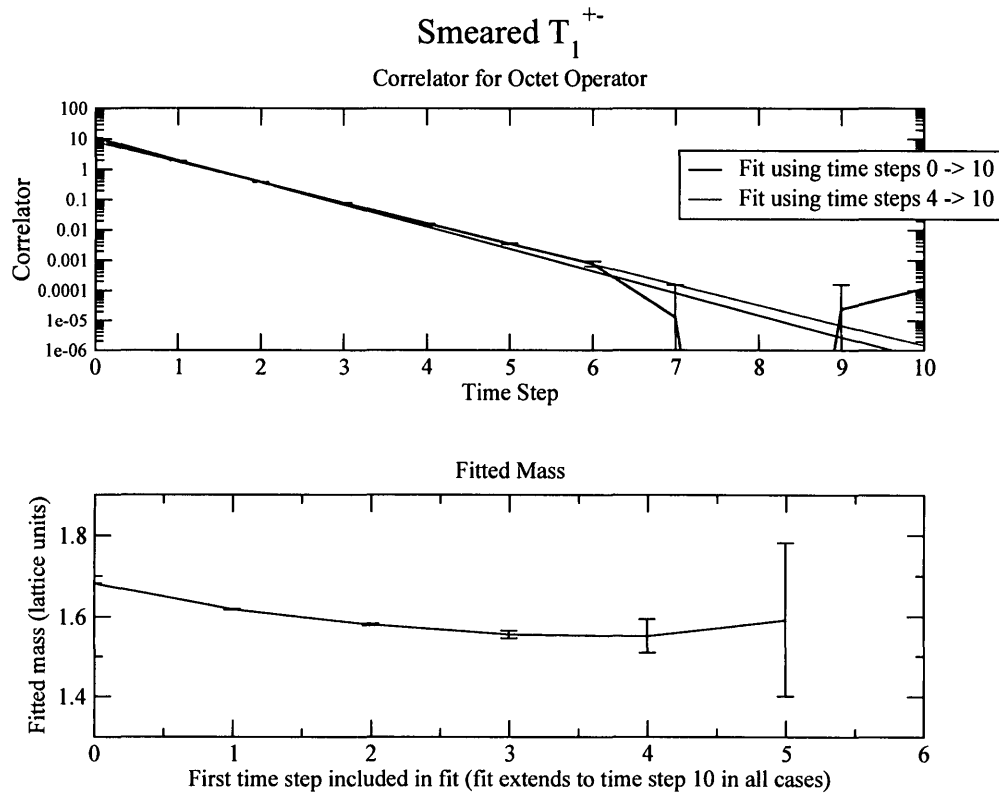


Figure 9.3: Choosing the region to fit.

time-step 4. The mass fit parameter (and even the error on this parameter) stays very stable. Even the $\chi^2/\text{d.o.f.}$ of the fit remains fairly constant, as one might expect. The last three entries in Table 9.2 show what happens to the $\chi^2/\text{d.o.f.}$ as the number of data points in the fit approaches the number of fit parameters and the overall number of degrees of freedom goes to zero. In general, for most of the fits for various Λ^{PC} states, there is some variation of the $\chi^2/\text{d.o.f.}$ depending on the final time-step that is included in the fit. The fits in the Appendix show the optimal ending point for the lowest $\chi^2/\text{d.o.f.}$ value.

The results shown in Table 9.2 are very encouraging - not only are fits possible, but they are very stable. Removing time-steps 0, 1 and 2 from the fit, the $\chi^2/\text{d.o.f.}$

value remained relatively constant at a value of approximately 0.4, indicating that the remaining fits are all of similarly good quality.

In addition to one-exponential fits, two-exponential fits were attempted for all the correlators in each representation. It is possible that some of the signals were actually composed of three or more states (requiring three or more exponentials to fit), but each additional exponential in the fit introduces two more fit parameters, the exponent itself and the overall weighting. A two-exponential fit therefore involves four fit parameters and a three-exponential fit has six. Most of the correlators decay away to noise in fewer than ten time steps. So a three-exponential fit (with six fit parameters) would require at least seven or eight good usable data points in the correlator, and this was not the case for most of the states. In the few cases where there were sufficient time-steps in the correlator (such as the octet T_1^{+-}), a three-exponential fit was attempted, but these fits did not resolve any new states or enhance the ground-state.

For the majority of the correlators in all the different colour n-plet representations, a two-exponential fit returned a result that involved a sum of two weightings of the *same* exponential function. In these cases two states clearly could not be resolved. There were several states however (the octet T_1^{+-} being one) that were easily fit to a two-exponential function. With a relatively small number of time steps included in the fit, every additional data point matters, and sometimes including just one more time-step is the difference between resolving an excited state or not. Including time-steps 0 or 1 superimposes an excited state on top of the ground state signal. For most of the correlators studied, this meant that a one-exponential fit that included those early time steps had a big $\chi^2/\text{d.o.f.}$ value. This just shows that there was indeed more than only the ground state present. Sometimes there were simply not enough degrees of freedom left to introduce the two additional parameters necessary to attempt to isolate that excited state through a two-exponential fit. A two-exponential fit is

nice in that it confirms the ground state by separating out excited states explicitly, but in most cases simply excluding one or two early correlator points and using a one-exponential fit also led a very good fit to the ground state.

In general, the calculations that were performed led to excellent fits to the ground states of all the different representations. There was evidence (from the large $\chi^2/\text{d.o.f.}$ value of fits that included the origin time step) that most of the representations also had excited states, and in some cases a two-exponential fit was possible which nicely confirms the ground state. The excited states that resulted from these fits are likely superpositions of several excited states, and not independent states. It is clear from the tabulated results in Appendix B that wherever a two-exponential fit was possible, the resulting ground state agreed with the ground state of the corresponding one-exponential fit. Next-generation calculations of these same representations with more computing power or finer lattice configurations may be able to map out more excited states and be even more confident of the ground states presented here.

Table 9.2 seems to indicate that a simulation energy value of about 1.56 ± 0.01 in lattice units might be well-motivated for the octet T_1^{+-} ground state, where the quoted error is strictly statistical. A more rigorous determination is necessary, however, and this leads finally to a discussion of errors.

9.4 Errors

The Numerical Recipes fitting algorithms [53] were used to generate the fit parameters for each data set, but they do not immediately give the errors on those fit parameters. The errors that appear in Table 9.2 and indeed the individual error bars on each time-step of the correlator were generated using the “bootstrapping” method [36, 54]. The correlator at any time-step is the average over calculations on a whole ensemble of hundreds of configurations. The system does not necessarily follow Gaussian statistics

however, so the standard deviation of the set may not be a good measure of the error. The bootstrapping method provides a good measure of the error.

For an ensemble of N_{ens} configurations, one begins by picking N_{ens} random configurations from the ensemble (with replacement so the same configuration may be picked more than once) to create a bootstrap ensemble. One then performs the same analysis on this new bootstrap ensemble as the original true ensemble, finding the correlator for each time step. This result is saved and the process is repeated about $3 \times N_{ens}$ times. This results in $3N_{ens}$ calculations of the correlator.

A $1\text{-}\sigma$ error bar encompasses about 68% of the data in a sample, so 68% of the bootstrap samples should fall within this range. One therefore orders the results of the $3N_{ens}$ correlators for any particular time step from lowest to highest and then eliminates the top and bottom 15.9%. The remaining range (from highest to lowest) represents a $\pm 1\sigma$ spread, so the error bar on the true mean is half of the difference between the highest and lowest remaining bootstrap results.

This same principle can be used to find the errors on the fit parameters. A set of $3N_{ens}$ bootstrap ensembles is created, and the fit is calculated on each. The middle 68% of the results gives a $\pm 1\sigma$ spread that is interpreted as the error on the true fit.

All of the above are just statistical errors, but there are certainly also systematic errors affecting the data. Table 9.2 shows that the choice of which data points to include in the fit varies the mass parameter slightly. The choice of the final time step to include in the fit does not alter the fit parameters, since later time-steps have very large error bars. In some cases (though not necessarily apparent for the octet T_1^{+-} in Table 9.2), the choice of the final time step affects the $\chi^2/\text{d.o.f.}$ value of the fit, and so it is accordingly selected to minimize this quantity. The initial time-step included in the fitting window does however affect the simulation energy. For the central value, one chooses the earliest fit that is statistically equal to all later fits. For the octet T_1^{+-} , time-step 3 yields a simulation energy of 1.56 ± 0.01 . If any later time is chosen

as the first point in the fitting window, the resulting simulation energy is statistically equivalent to this choice. If, however, the neighbouring *earlier* time step is included in the fit (time-step 2 in this case), the resulting simulation energy is 1.580, or 0.02 larger than the central value. This is a reasonable indication of the systematic error involved in choosing the fitting window. To be explicit, a one-sigma systematic error was assigned to be half this difference, or

$$\left| \frac{E(\tau_i) - E(\tau_i - 1)}{2} \right|. \quad (9.11)$$

Here $E(\tau)$ is the measured simulation energy for a fitting window starting at time τ , and fits starting at τ_i or later are statistically equivalent. Table 9.2 therefore gives a simulation energy for the octet T_1^{+-} of $1.56 \pm 0.01 \pm 0.01$ in lattice units, where the first error is statistical and the second is systematic.

There are other possible systematic effects to consider. Instead of just using a one-exponential fit to the correlator, for some gluelump states it is also possible to fit a two-exponential model to the data. The ground state energy from the two-exponential fit should agree with the result of the one-exponential fit. Any discrepancy might be another systematic error. For the octet T_1^{+-} in the calculation using chair-type operators on the ensemble with $a = 0.0982$, (fits tabulated in the Appendix in Table B.3) the ground state of a two-exponential fit is $1.549 \pm 0.007 \pm 0.020$ with statistical and systematic errors as defined above. This result is consistent with the established simulation energy of $1.56 \pm 0.01 \pm 0.01$ even within just statistical errors, so no additional systematic error is needed. In general, the ground states in all possible two-exponential fits in the various calculations agreed within error with the corresponding one-exponential fit.

The case of the octet gluelump is unique in that even more comparisons are possible. Different types of operators that couple to the same states can be compared.

In order to reproduce the results of Foster and Michael, a set of plaquette-based operators was created, both using a 1×1 building block and a 2×2 one. Calculations were carried out with these operators on the original (coarser) ensemble. Using the 1×1 building block, the T_1^{+-} simulation energy was $1.56 \pm 0.01 \pm 0.01$ in lattice units. Using the 2×2 building blocks, it was $1.50 \pm 0.05 \pm 0.06$ from a one-exponential fit and 1.54 ± 0.01 from a two-exponential fit (no systematic error because all fits even including the origin time-step 0 agreed). These are again consistent with the chair-shaped operator result of $1.56 \pm 0.01 \pm 0.01$. There was similarly good agreement for all the octet gluelump states that could be accessed with plaquette-based operators.³ This again indicates that this possible source of systematic error is smaller than the dominant source (the choice of fitting window), and since results are consistent, a separate systematic error is not needed.

Another possible systematic error may be due to the lattice ensemble itself. The octet gluelump system was measured on a second ensemble of configurations with a finer lattice spacing. The results are tabulated in the Appendix in Table B.4, where simulation energies are measured in units of the lattice spacing, which is $a = 0.0685$ as opposed to $a = 0.0982$ in the original ensemble. To directly compare the results on the finer ensemble to those on the coarser ensemble, one must first account for this factor. Converting from lattice units where masses are actually Ma (where a is the lattice spacing) to physical units, the octet T_1^{+-} simulation energy on the coarser lattice is $3.13 \pm 0.02 \pm 0.02$ GeV and on the finer lattice it is $3.87 \pm 0.03 \pm 0.04$, but this still cannot be directly compared to the coarser results above. Since the inherent unphysical lattice self-energy may be different on the two ensembles, only mass differences between states can be compared across the two ensembles. To achieve this, the energy of the lowest lying state (the T_1^{+-} in both cases) is subtracted from

³Recall that only 10 of the 20 possible Λ^{PC} states on the lattice can be created with plaquette-based operators.

the remaining gluelump states. The mass splitting between the octet T_1^{+-} and the next lightest octet gluelump, the T_1^{--} , is $0.33 \pm 0.02 \pm 0.07$ GeV on the coarser lattice and $0.25 \pm 0.06 \pm 0.07$ GeV on the finer lattice. In both cases the first error is statistical and the second is systematic. Since these are energy differences between the T_1^{+-} and the T_1^{--} , errors for the two states were added in quadrature to get the results quoted for the mass differences.

It is clear that the mass splittings in this example agree within error (even just the statistical error in this case). In fact, all the octet mass splittings from the finer ensemble agree with those from the coarser ensemble if both the statistical error and the systematic error already established (based on the choice of fitting window) are taken into consideration. A separate systematic error for this effect is therefore not needed. Lattice spacings of less than 0.1 fm were used as is conventional for SU(3) lattice calculations. Since no lattice spacing effect was resolvable between the two ensembles used, and since the lattice spacings were fine compared to an SU(3) scale of $\Lambda_{QCD} \sim \mathcal{O}(100 \text{ MeV})$, this adds reassurance to the assumption that neither ensemble was unsuitably coarse for the gluelump system. It is worth mentioning, however, that mass splittings tend to be larger on the finer ensemble than the coarser ensemble. They do still agree within error, but the reason for this difference could be fundamental. A finer lattice spacing is closer to the continuum limit, and lattice calculations are often extrapolated to a lattice spacing of $a = 0$ to recover continuum behaviour as lattice energies (and possibly splittings) can depend on this parameter.

If the $\chi^2/\text{d.o.f.}$ had been systematically larger than unity in the majority of fits, this might also introduce systematic error since it indicates that the fit was not very good, but this was not a problem for any of the states examined, in any of the colour representations.

Overall, a well-motivated ground-state simulation energy for the octet T_1^{+-} is thus $3.13 \pm 0.02 \pm 0.02$ GeV, where the first error is statistical and the second is

systematic. This is remarkably precise for such an inherently noisy system. One should not, however, make the mistake of interpreting this as evidence for a gluelump bound state at a mass of 3.13 GeV. Recall (see Section 2.4) that by approximating the heavy colour-octet particle as a stationary source of infinite mass on the lattice, an inherent unphysical lattice self-energy is introduced to the system. Only mass *differences* within a colour representation are physical. These are tabulated in the following chapter.

It should be noted that not all of the systematic errors discussed in this section can be examined so thoroughly for all the Λ^{PC} gluelump states in the different colour representations. Two-exponential fits were only possible in a few situations. The octet was the only representation for which different shapes of operators were used. Only the octet was studied thoroughly on the finer ensemble. A preliminary exploration of the decuplet on the finer ensemble was performed, but further refinements and optimizations would be needed to extract analyzable results from that representation, as is discussed in the next chapter. The only systematic effect that was measurable for all cases was the variation due to the choice of fitting window. In the octet sector, this was seen to be the largest source of systematic error.

9.5 Simultaneous Fits

As has been reiterated many times, only mass differences are physical in the gluelump spectrum; the absolute scale is obscured by an unphysical lattice offset amount. Rather than fitting each irrep Λ^{PC} separately and subtracting off the lattice energy of the lowest lying state, it is therefore preferable to fit the lowest lying state simultaneously with each heavier Λ^{PC} state. Two correlators are measured simultaneously,

$$C_1 = f_1 e^{-M_1 \tau} \quad \text{and} \quad C_2 = f_2 e^{-(M_1 + \delta M_{12}) \tau}, \quad (9.12)$$

where C_1 is the correlator of the lowest lying gluelump state in a particular colour representation (for example, the T_1^{+-} in the octet), and C_2 is the correlator for one of the other Λ^{PC} states in that representation. The fit parameters f_1 , f_2 and M_1 are not of physical importance. The mass difference δM_{12} is the physics to be extracted. In this simultaneous fit, the statistical error on δM_{12} can be determined directly using bootstrapping instead of adding two statistical errors together in quadrature as was discussed above. This may result in a lower statistical error than was predicted in the previous method because it should remove any correlation between the errors.

The systematic error due to the choice of fitting window can also be found more directly instead of examining the contributions from two states separately. A one-sigma systematic error is assigned to be

$$\left| \frac{\delta M_{12}(\tau_i) - \delta M_{12}(\tau_i - 1)}{2} \right|, \quad (9.13)$$

where $\delta M_{12}(\tau)$ is the mass difference between gluelump Λ^{PC} (with fitting window starting at time τ) and the lowest lying gluelump state in the colour representation. The fitting window for the lowest lying state is always optimized, and the fitting window for Λ^{PC} is optimized with $\tau = \tau_i$.

The results of the simultaneous fits agree with the results obtained by taking the difference of two individual fits.

Chapter 10

Results

In this chapter, the results from the calculations of gluelumps in various $SU(3)$ colour representations are presented. The spectrum of states is given, and a final comparison between these octet results and the original results of Foster and Michael is presented.

10.1 Spectrum

In order to replicate the earlier work on gluelumps containing octet-rep coloured particles (Ref. [18]), calculations were first performed using lattice operators based on square building blocks of size 1×1 or 2×2 . Correlator results are presented in Figures 10.1 and 10.2. Using square-based operators, only half of the possible lattice quantum states are accessible, so a new set of chair-shaped operators (along with a new set of generating tensors) was developed. The correlation function for the full octet spectrum is shown in Figure 10.3, and again in Figure 10.4 which was on a different ensemble of finer-spaced lattices. The fits are tabulated in the Appendix in Tables B.1 to B.4. The results on the different sized lattice ensembles as well as results using different shaped operators agreed within error.

Correlators for gluelumps containing a decuplet-coloured particle are shown in Figures 10.5 and 10.6. The second plot is of an exploratory calculation of the decuplet on a finer lattice spacing. Although smearing was “optimized” for this calculation,¹ it drove the signal down to the level of noise in many channels, so in fact it may have been over-smearred. Further fine-tuning and refining of smearing is left for future work. At this time, results from the octet did not motivate the need to re-run the other colour representations on the finer ensemble. In the octet case, mass splittings on the finer ensemble (which was significantly slower to run than the coarser ensemble) agreed within error with those on the coarser lattice.

Gluelumps containing 27-plet and 35-plet coloured particles are shown in Figures 10.7 and 10.8. Although all the theoretical underpinning was laid out for gluelumps containing 28-plet coloured particles, calculations of that representation were not practical. Based on Casimir colour factors (see Section 3.2), the 28-plet representation is expected to be heavier than any of the other representations studied here. One can already see that the 35-plet signal is significantly less clear than the smaller colour representations, and the 28-plet is predicted to be worse. It was also prohibitively slow to run on the computer cluster, and since it is not specifically called for in any particular current phenomenological model, the motivation to spend the computing time was not there. A cursory run of the 28-plet was performed in order to ensure that results were gauge invariant and sensible.

Instead of plotting the correlation function directly, one could have also plotted the effective energy to see the effects of excited states more easily. This is the naive exponential “fit” between adjacent correlator points, and it was defined in Eq. 9.6 as $E_{eff}(\tau) = \ln \left(\frac{C(\tau)}{C(\tau+1)} \right)$. It still includes an unphysical lattice off-set. Effective energy plots are shown for the octet on the coarse and fine ensembles in Figs. 10.9 and 10.10.

¹As described in Section 9.1, smearing is considered to be optimized when the effective lattice energy from the 0th and 1st time steps is minimized.

1x1 Plaquette-based Octet Correlators Optimally Smeared with $\rho = 0.15, n_p = 20$

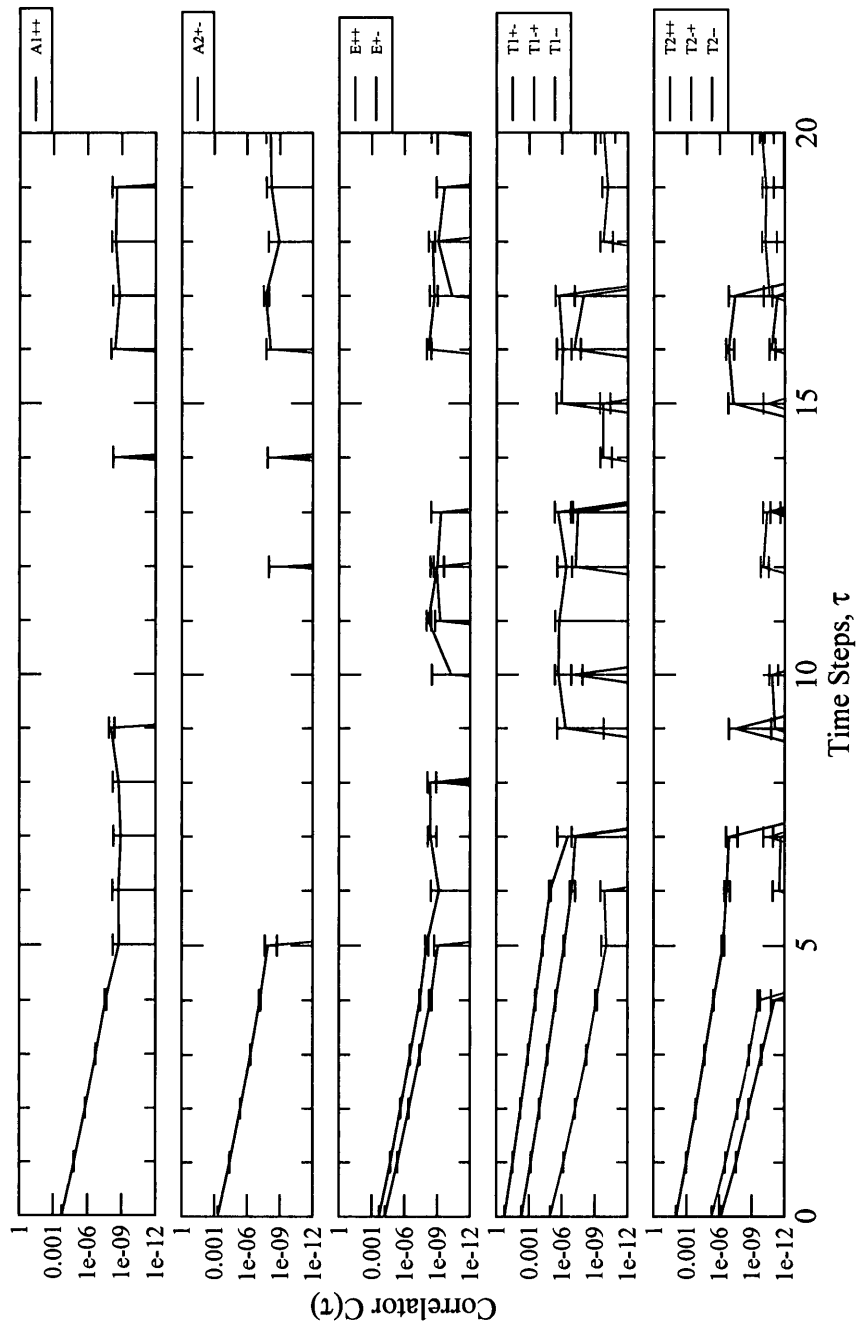


Figure 10.1: The octet correlators based on 1×1 plaquettes, calculated on an ensemble of $790 \cdot 20^3 \times 40$ lattice configurations at lattice spacing $a = 0.0982(19)$ fm (simulation energies include an unphysical lattice self-energy off-set value).

2x2 Plaquette-based Octet Correlators

Optimally Smeared with $\rho = 0.15, n_p = 15$

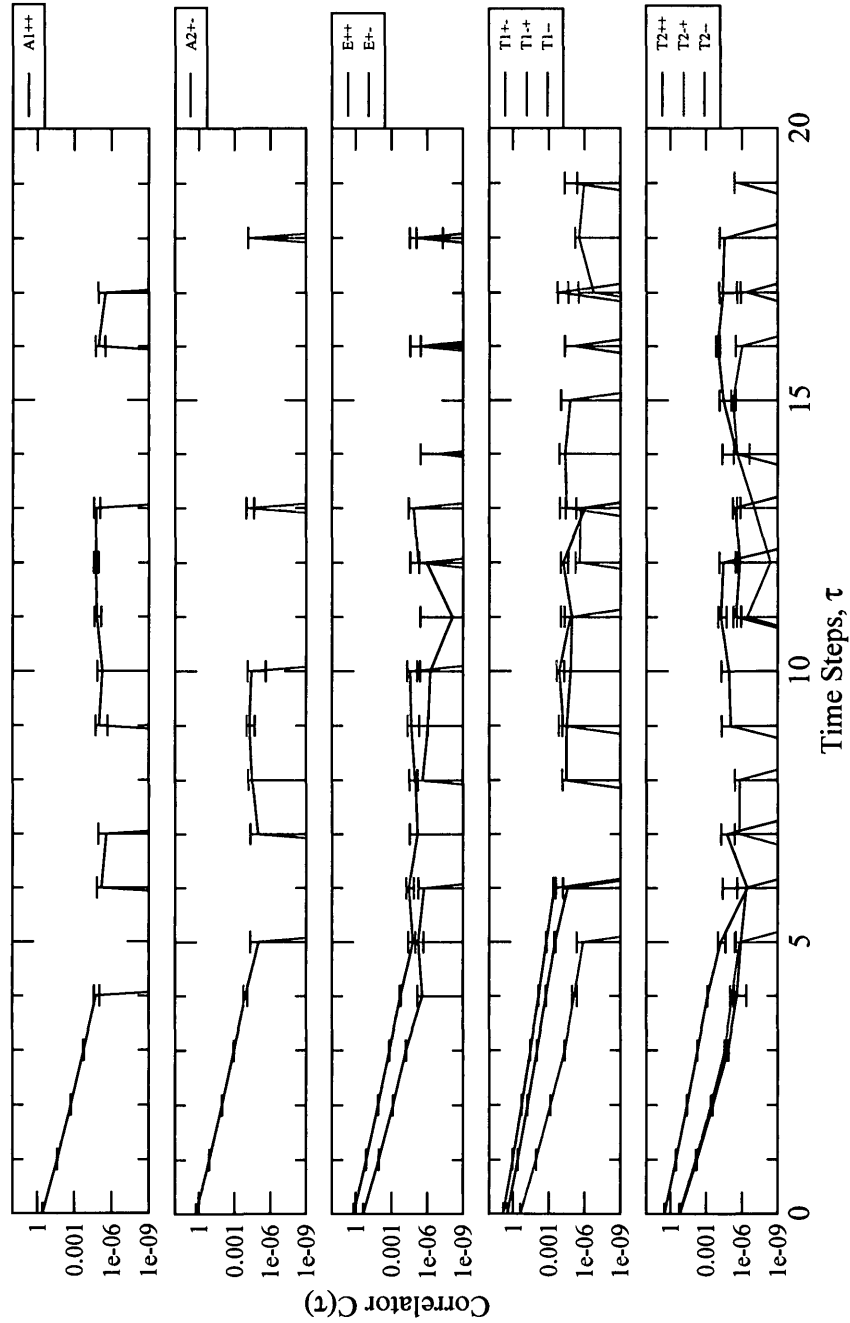


Figure 10.2: The octet correlators based on 2×2 plaquettes, calculated on an ensemble of $790 \cdot 20^3 \times 40$ lattice configurations at lattice spacing $a = 0.0982(19)$ fm (simulation energies include an unphysical lattice self-energy off-set value).

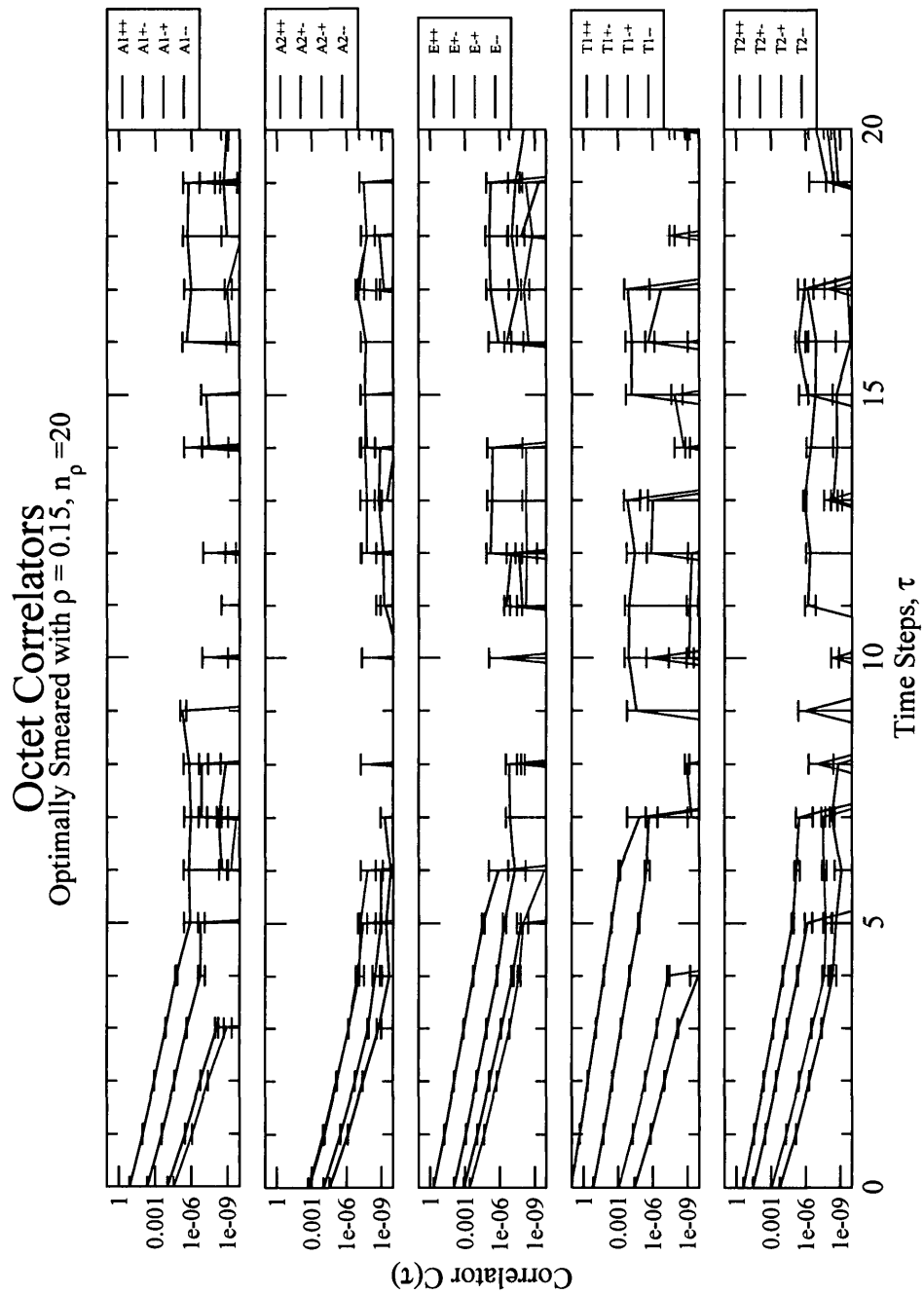


Figure 10.3: The octet correlators on an ensemble of 790 $20^3 \times 40$ lattice configurations at lattice spacing $a = 0.0982(19)$ fm (simulation energies include an unphysical lattice self-energy off-set value).

Octet Correlators on $28^3 \times 56$ Lattice
 Optimally Smeared with $\rho = 0.15, n_p = 15$

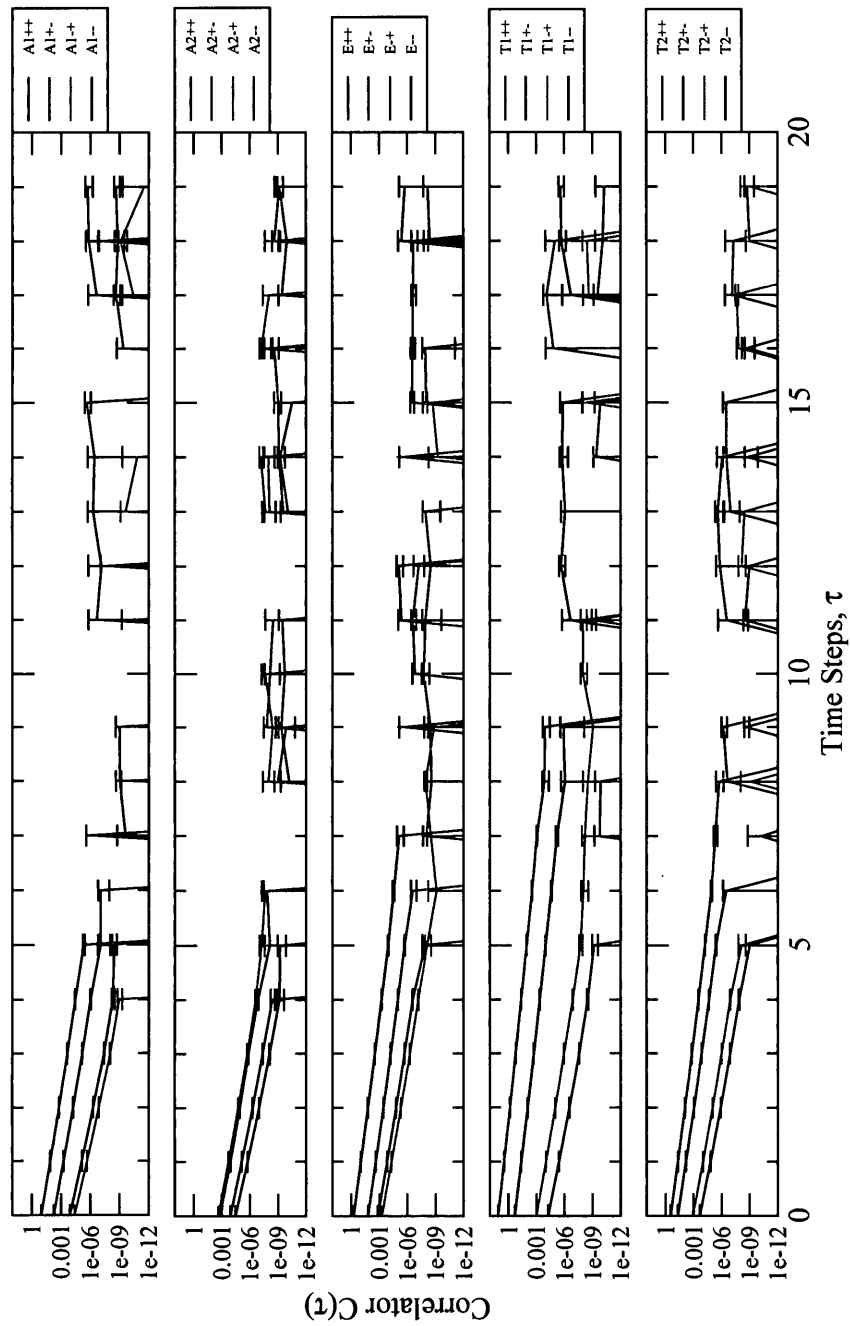


Figure 10.4: The octet correlators on an ensemble of 650 $28^3 \times 56$ lattice configurations at lattice spacing $a = 0.0685(26)$ fm (simulation energies include an unphysical lattice self-energy off-set value).

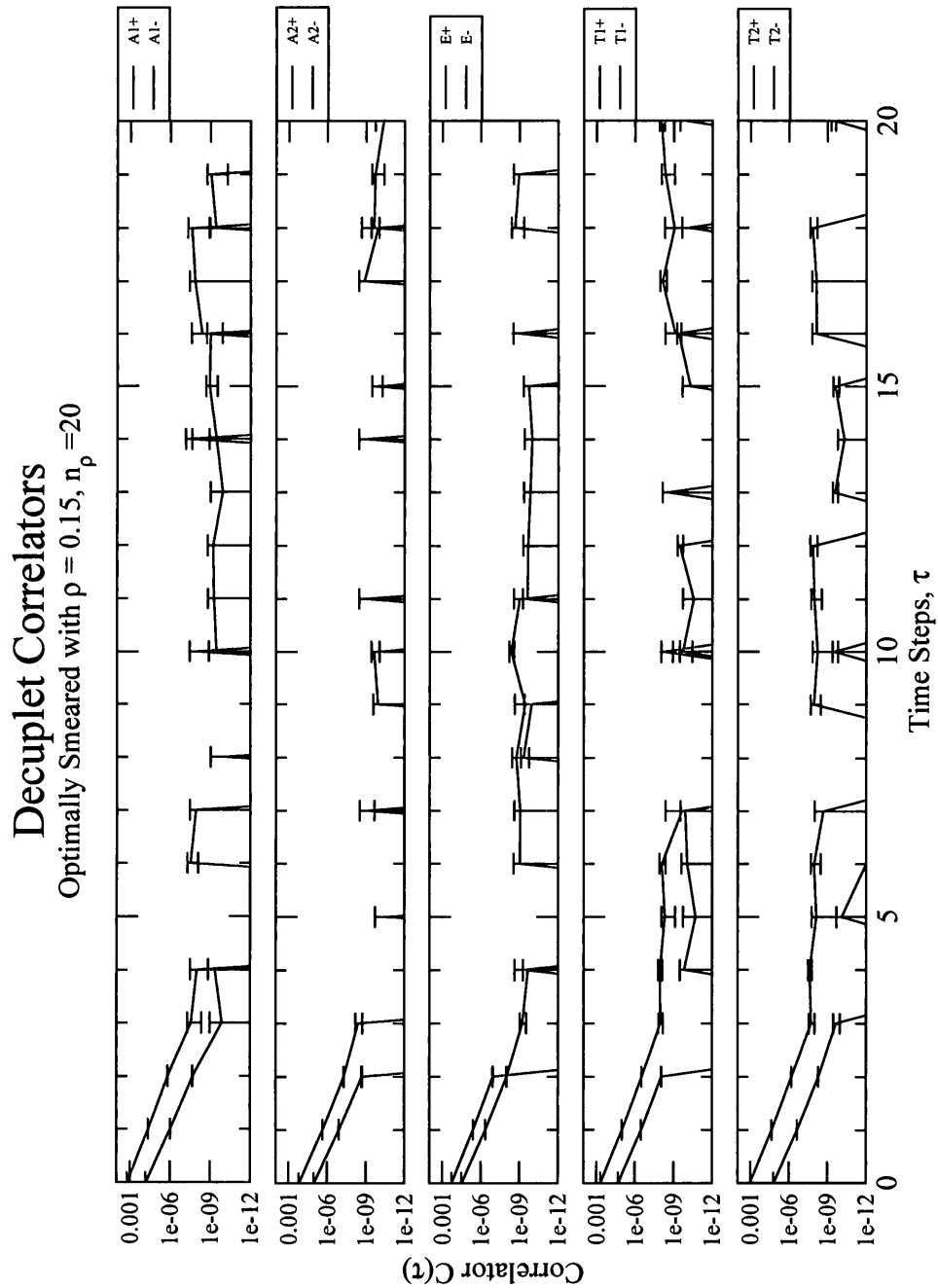


Figure 10.5: The decuplet correlators on an ensemble of 790 $20^3 \times 40$ lattice configurations at lattice spacing $a = 0.0982(19)$ fm (simulation energies include an unphysical lattice self-energy off-set value).

Decuplet Correlators on $28^3 \times 56$ Lattice
 Optimally Smeared with $\rho = 0.15, n_p = 15$

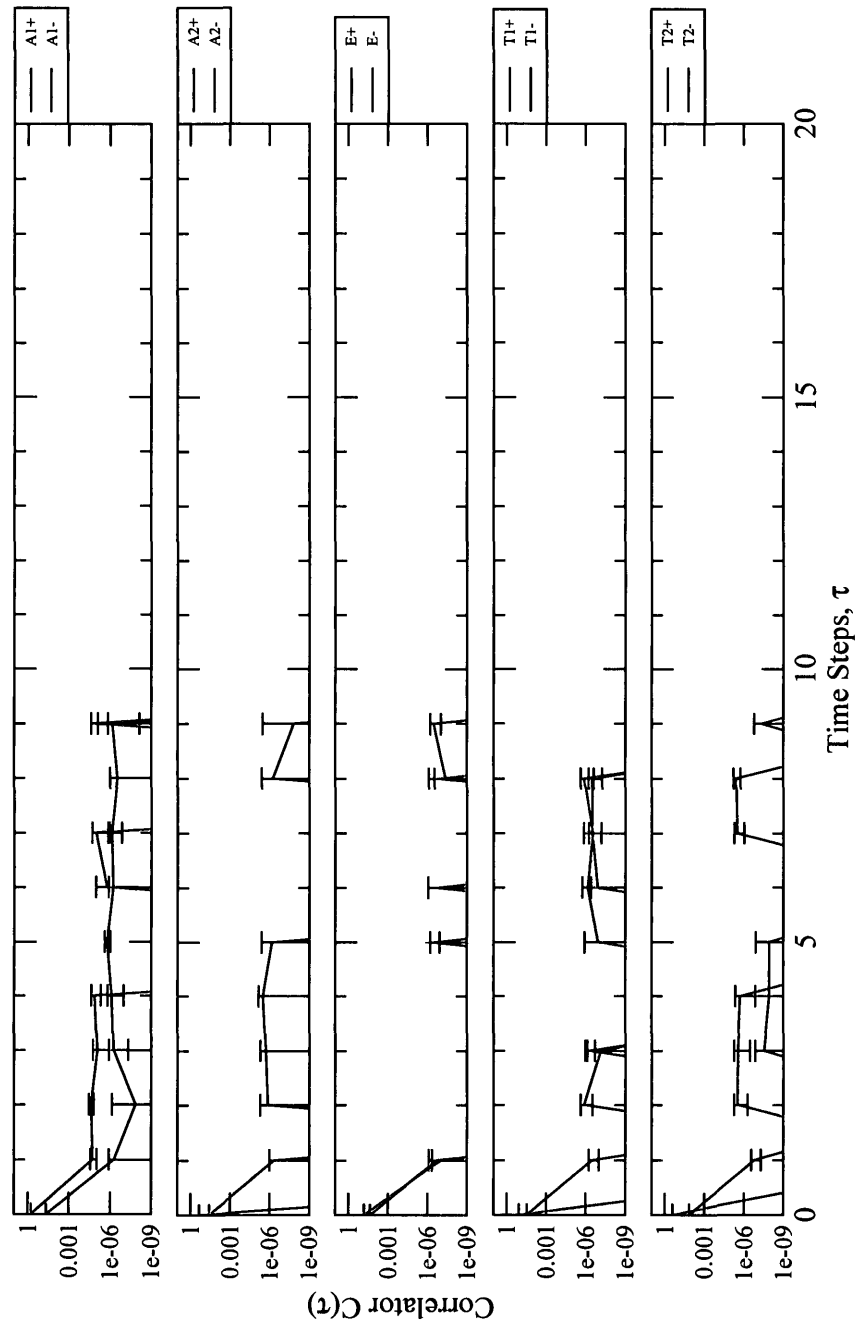


Figure 10.6: The decuplet correlators on an ensemble of 650 $28^3 \times 56$ lattice configurations at lattice spacing $a = 0.0685(26)$ fm (simulation energies include an unphysical lattice self-energy off-set value).

27-Plet Correlators
 Optimally Smeared with $\rho = 0.15$, $n_p = 15$

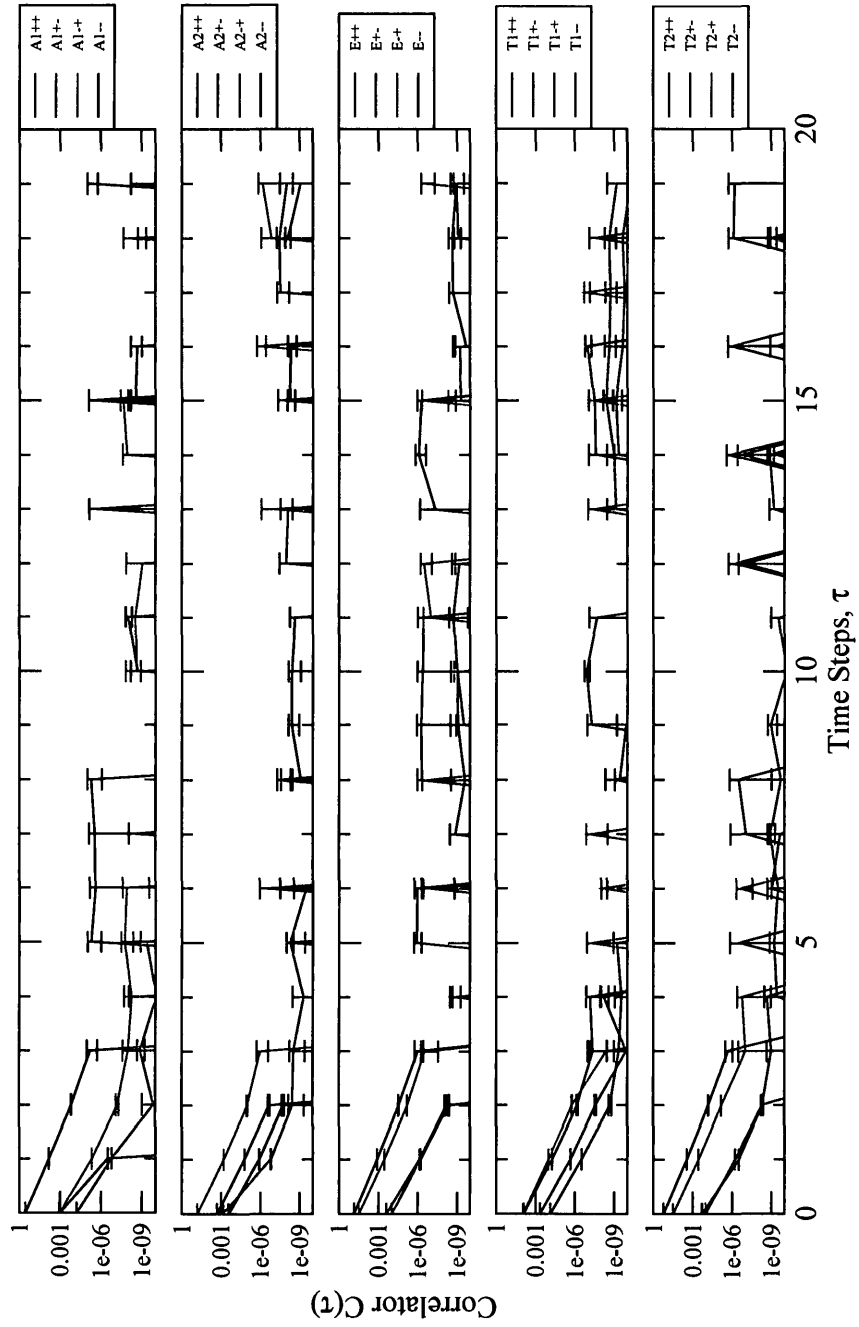


Figure 10.7: The 27-plet correlators on an ensemble of $790 \times 20^3 \times 40$ lattice configurations at lattice spacing $a = 0.0982(19)$ fm (simulation energies include an unphysical lattice self-energy off-set value).

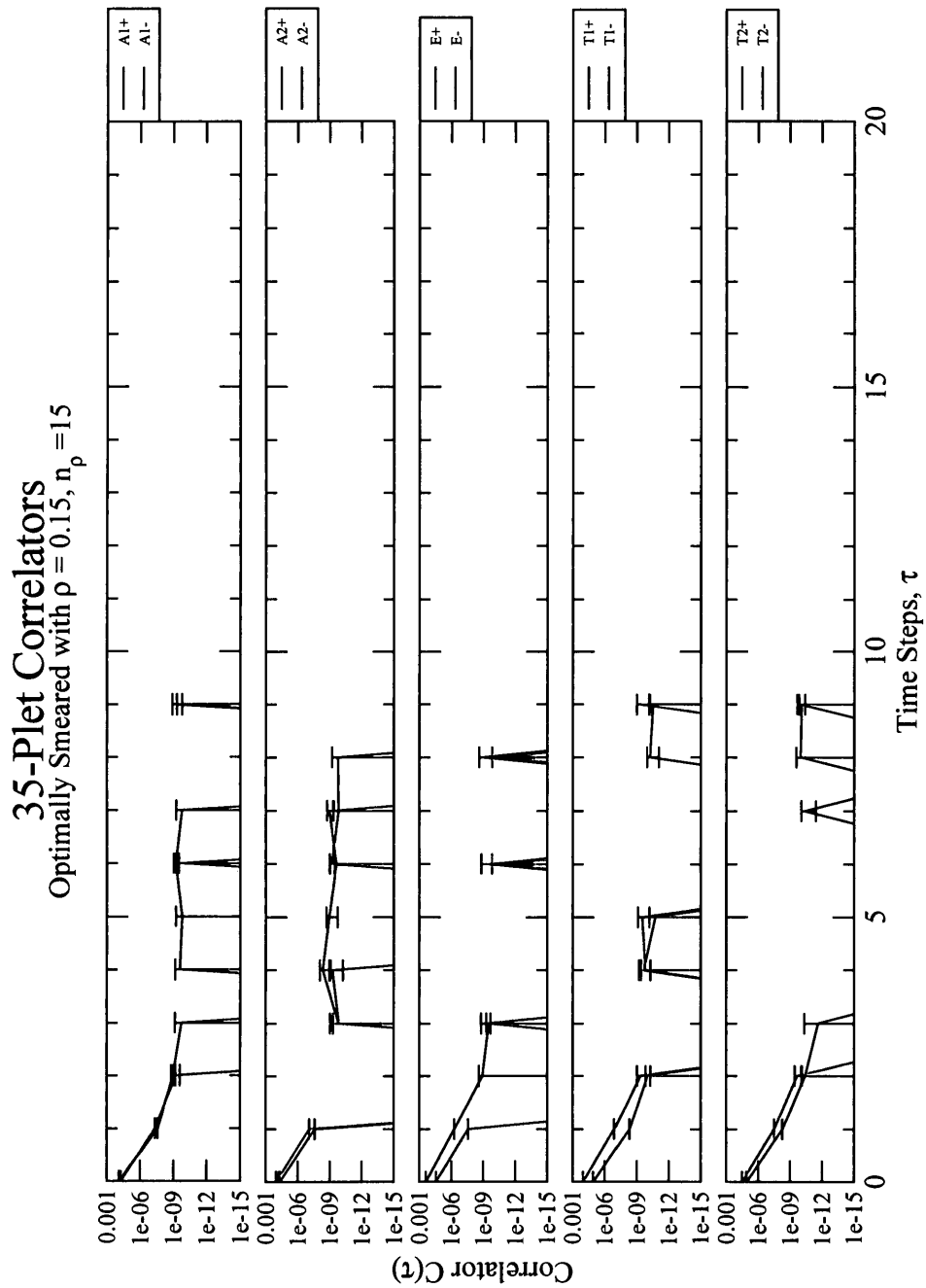


Figure 10.8: The 35-Plet correlators on an ensemble of 790 $20^3 \times 40$ lattice configurations at lattice spacing $a = 0.0982(19)$ fm (simulation energies include an unphysical lattice self-energy off-set value).

Octet Operators on $20^3 \times 40$ Lattice
 Optimally Smeared with $\rho=0.15, n_p=20$

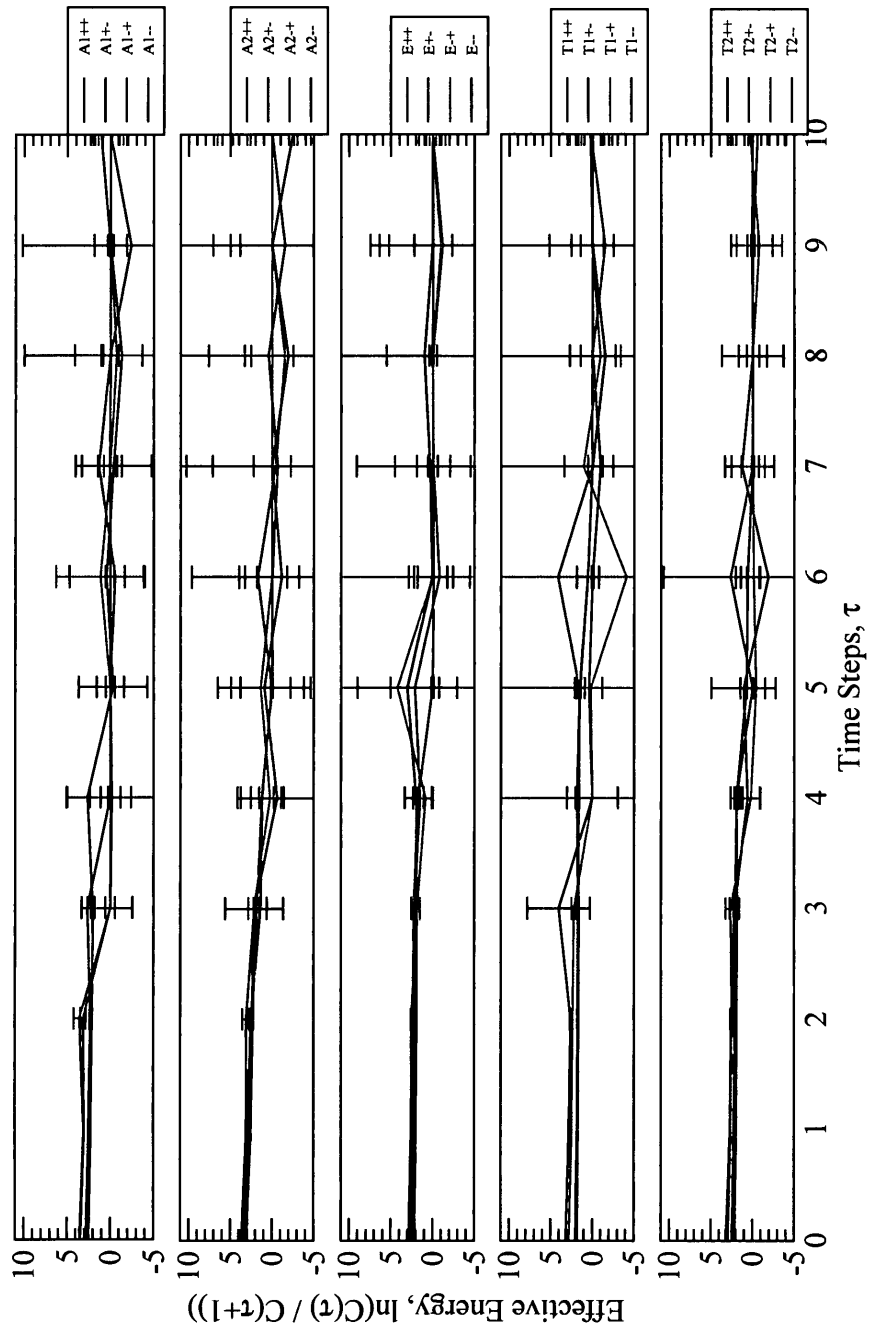


Figure 10.9: The octet effective energies on an ensemble of 790 $20^3 \times 40$ lattice configurations at lattice spacing $a = 0.0982(19)$ fm (simulation energies include an unphysical lattice self-energy off-set value).

Octet Operators on $28^3 \times 56$ Lattice
 Optimally Smeared with $\rho=0.15, n_p=15$

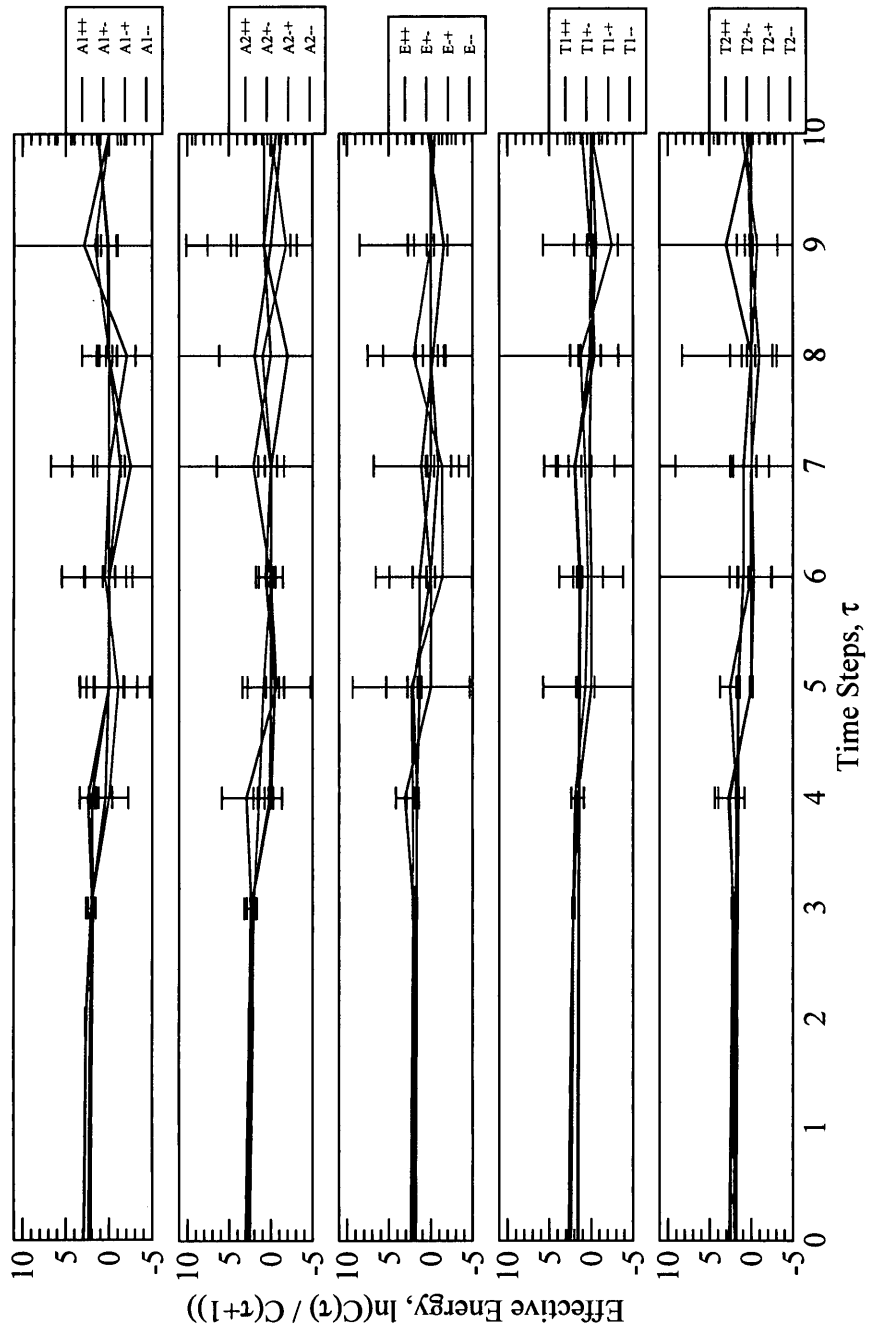


Figure 10.10: The octet effective energies on an ensemble of 650 $28^3 \times 56$ lattice configurations at lattice spacing $a = 0.0685(26)$ fm (simulation energies include an unphysical lattice self-energy off-set value).

10.2 Masses

The data shown in Figures 10.1 through 10.8 can be analyzed to extract mass splittings for gluelump systems in various states. The techniques used for analysis were described in the previous chapter. The raw results of these fits are presented in Appendix B with tables corresponding to each of Figures 10.1 through 10.5 and Figures 10.7 to 10.8. There was simply not enough clean signal in the case of the decuplet gluelumps on the $28^3 \times 56$ ensemble to perform meaningful fits, so there is no result table corresponding to Figure 10.6. In all the other cases, all the possible fits with various starting time-steps are shown. All simulation masses (energies) are given in lattice units where mass is measured in inverse units of the lattice spacing, a , which varies depending on which ensemble of lattices was used. Statistical errors are shown for each fit. Also shown is τ_i , the first time-step of the correlator that is included in the fit, and τ_f , the final time-step included in the fit. This was chosen so as to minimize the overall $\chi^2/\text{d.o.f.}$ (also shown in the tables) while still giving the same fit values.

In some cases, it was possible to fit a two-exponential function, and in those cases the second mass parameter is listed as an excited state, although it should not be interpreted as an individual excited state but rather a superposition of contaminations from all higher-order states. The numbers in those tables are *simulation* energies - they include an unphysical lattice self-energy off-set value that is characteristic of the ensemble of lattice configurations itself and so are not physical masses. Mass splittings between states are physical, however, and are sufficient to establish a characteristic spectrum for each colour representation.

It is clear even at first glance that many of the expected behaviours are seen. The lattice energies of the octet states are generally the smallest, the decuplet states are the next smallest, then the 27-plet states, and finally the 35-plet states have

the highest lattice energies. Preliminary tests of the 28-plet indicated even higher lattice energies still. Although this is in the order predicted by the Casimir colour factors in Section 3.2, the lattice energies themselves are not physical. Without knowing the actual masses of the exotic colour representation particles (*all* the colour representation particles are approximated as infinitely heavy), it is impossible to compare absolute bound particle masses. The mass splittings might also be expected to scale with the Casimir factors, but the resolution of the results here cannot confirm this. The calculations can confirm that gluelumps from colour representations with large Casimir factors are more noisy and the signals are damped more quickly as a function of Euclidean time, all indications of heavier systems.

The raw results in Appendix B have a lot of information in them that is consolidated and refined in this section.

Ideally, one wants simulation energies to be less than about 1 in lattice units so that the systems being studied “fit” well on the lattice spacings used. This is discussed in detail in Section 2.2. Like the results of Foster and Michael,² all the octet lattice energies found here are greater than one as can be seen in the tables in Appendix B, although many of the mass splittings are less than one. This shows how an improvement could be made in future studies. Using finer lattices or larger operators, one might be able to further optimize the gluelump study. With octet simulation energies ranging from about 1.5 to 3 (in lattice units), lattices with spacings up to three times finer might be required for optimal calculation. Table B.4, which is at a lattice spacing about 30% finer than the other calculations, seems to show a reduction in lattice energy in most cases, although the overall lattice self-energy does not necessarily scale with a , so the off-set may partially counteract this. The decuplet energies are on the order of about 3.5 in lattice units, while energies of more

²The lightest state in Foster and Michael’s study was the T_1^{+-} which had a mass of about 1.33 in their lattice units.

than 5 are seen in the 27-plet and 35-plet cases. It may be worth re-visiting the gluelump spectrum with finer lattices and more computing power, however the fact that the octet mass splittings on the two different lattice ensembles agree with each other within error indicates that these ensembles are still suitable for the gluelump studies. If they did not agree, it would be an indication that at least the coarser lattice was not fine enough to fit the gluelump states, but this is not what was seen. It is also worth noting that many of the mass splittings (which are physical while the simulation energies are not) are indeed less than 1 in lattice units.

Foster and Michael used a clever technique to make the gluelump operators effectively larger and thus make the lattice spacing seem finer. They had two versions of their operators with the same shapes but based on different sized building blocks. One used 1×1 plaquettes, the other used 2×2 plaquettes. The same operators were recreated here and the results for the octet calculations are shown in Tables B.1 and B.2. It seems that the operators based on the larger 2×2 plaquettes were easier to fit, and more excited states could be resolved. There may therefore be motivation to build larger chair-based operators and re-run not only the octet, but also the decuplet and larger colour n -plet representation calculations. This may be a way to extend the operators spatially without needing finer lattices that require much more computing power to employ. The smearing techniques used also work to extend the spatial extent of the operators, so perhaps the improvement by building larger chairs might not be too dramatic. It is left for future work. All further discussion relates to calculations run with the chair-shaped operators derived here.

Table 10.1 shows the results for the octet gluelump spectrum on the two different lattice ensembles. Although the central values on the finer ensemble tend to be slightly higher than those on the coarser lattice, these differences are not large compared to the quoted errors, and the two ensembles agree within error. The results shown are mass differences in real energy units (GeV), since absolute lattice energies include

an unphysical lattice offset amount. The states are ordered from lightest to heaviest, and show the statistical errors (listed first) as well as the systematic errors separately. All mass differences are with respect to the lightest octet gluelump state, the T_1^{+-} , and they were calculated via simultaneous fits as described in Section 9.5.

As discussed in Section 9.4, choosing a fitting window with too many early correlator points caused some variation in the mass fit parameter. The central value for each simulation energy was therefore chosen as the result of the fit that included the earliest possible time-step while still being statistically equal to all fits starting at later time steps. The statistical error is the bootstrapping error on that fit. The systematic error was taken as half the difference between this central value and the result of a fit that included one additional earlier time-step, as defined in Equation 9.13. All other systematic errors (caused by effects such as fitting to a two-exponential function or using different shaped operators) were smaller than this. The other effects could not be resolved within the established statistical and systematic errors already assigned. For the octet, typical statistical errors on the mass differences were about 5%, and most systematic errors were around 10%.

In Table 10.1, J denotes the continuum angular momentum of the light (gauge) degrees of freedom and does not include the spin of the octet particle. It is the lowest spin assignment for each possible irrep Λ^{PC} , although other spin assignments are possible (see Table 2.2).

Some of the larger colour representations also had good data that extended several time-steps. In these cases, the central value for each mass difference in the spectrum along its statistical and systematic errors were chosen in the same way as for the octet. Unlike for the octet, in the case of the larger colour multiplets, the only systematic error that could be examined was due to the choice of fitting window. In the octet, this was seen to be the largest effect anyways, so it likely stands as a good estimate of systematics in the other systems as well.

Table 10.1: The mass spectrum of gluelumps containing a static octet particle at two different lattice spacings. The first error is statistical and the second is systematic. J denotes the lowest continuum angular momentum assignment for the light (gauge) degrees of freedom and does not include the spin of the octet particle.

Λ^{PC}	J	$M(\Lambda^{PC}) - M(T_1^{+-})$ [GeV]	
		$a = 0.0982$ fm	$a = 0.0685$ fm
T_1^{--}	1	$0.33 \pm 0.02 \pm 0.07$	$0.24 \pm 0.05 \pm 0.06$
E^{--}	2	$0.66 \pm 0.02 \pm 0.07$	$0.87 \pm 0.04 \pm 0.05$
T_2^{--}	2	$0.67 \pm 0.02 \pm 0.06$	$0.64 \pm 0.11 \pm 0.09$
E^{+-}	2	$0.94 \pm 0.03 \pm 0.08$	$1.18 \pm 0.05 \pm 0.06$
T_2^{+-}	2	$1.12 \pm 0.03 \pm 0.08$	$1.39 \pm 0.06 \pm 0.06$
A_1^{++}	0	$1.14 \pm 0.05 \pm 0.11$	$1.55 \pm 0.12 \pm 0.09$
A_2^{+-}	3	$1.39 \pm 0.12 \pm 0.22$	$2.27 \pm 0.05 \pm 0.25$
A_1^{--}	0	$1.44 \pm 0.09 \pm 0.19$	$1.73 \pm 0.23 \pm 0.26$
E^{++}	2	$1.51 \pm 0.07 \pm 0.11$	$2.07 \pm 0.03 \pm 0.15$
T_1^{-+}	1	$1.59 \pm 0.06 \pm 0.12$	$2.31 \pm 0.04 \pm 0.16$
A_2^{-+}	3	$1.71 \pm 0.14 \pm 0.24$	$2.54 \pm 0.06 \pm 0.23$
T_2^{-+}	2	$1.86 \pm 0.09 \pm 0.11$	$2.52 \pm 0.04 \pm 0.19$
E^{-+}	2	$1.89 \pm 0.10 \pm 0.06$	$2.45 \pm 0.04 \pm 0.16$
A_2^{++}	3	$1.91 \pm 0.33 \pm 0.42$	$3.20 \pm 0.12 \pm 0.29$
T_2^{++}	2	$2.00 \pm 0.13 \pm 0.13$	$2.88 \pm 0.05 \pm 0.18$
T_1^{++}	1	$2.14 \pm 0.15 \pm 0.19$	$2.14 \pm 0.38 \pm 0.45$
A_1^{+-}	0	$2.82 \pm 0.04 \pm 0.41$	$3.44 \pm 0.13 \pm 0.19$
A_2^{--}	3	$2.97 \pm 0.05 \pm 0.59$	$3.58 \pm 0.19 \pm 0.32$
A_1^{-+}	0	$3.02 \pm 0.05 \pm 0.48$	$3.82 \pm 0.18 \pm 0.17$

For gluelumps containing a decuplet-coloured particle, statistical errors on the mass differences were around 10%, but systematic errors were larger than in the octet, typically around 50%. The final spectrum for the decuplet gluelumps is tabulated in Table 10.2. Recall that since the decuplet is not an eigenstate of charge conjugation, the only possible states are the ten Λ^P irreps. The lightest state in the decuplet spectrum appears to be the A_1^- , corresponding to continuum $J^P = 0^-$. All mass splittings are relative to this state.

For gluelumps containing a 27-plet coloured particle, statistical errors were around

Table 10.2: The mass spectrum of gluelumps containing a static decuplet particle. The first error is statistical and the second is systematic. J denotes the lowest continuum angular momentum assignment for the light (gauge) degrees of freedom and does not include the spin of the decuplet particle.

Λ^P	J	$M(\Lambda^P) - M(A_1^-)$ [GeV]
T_1^-	1	$0.39 \pm 0.05 \pm 0.33$
E^-	2	$0.40 \pm 0.05 \pm 0.33$
T_2^-	2	$0.41 \pm 0.04 \pm 0.32$
T_1^+	1	$0.57 \pm 0.05 \pm 0.48$
A_2^+	3	$0.89 \pm 0.10 \pm 0.47$
E^+	2	$0.90 \pm 0.07 \pm 0.45$
T_2^+	2	$0.96 \pm 0.06 \pm 0.37$
A_1^+	0	$1.05 \pm 0.10 \pm 0.38$
A_2^-	3	$1.48 \pm 0.17 \pm 0.44$

20% (except in the cases of very small mass splittings with larger relative error), and systematic errors again averaged about 50%. This is a first examination of this system, and results are exploratory and should be refined with future work. Not all of the states could be well-resolved with the simultaneous fit method explained in Section 9.5, and Table 10.3 is a partial spectrum. The difficulty in obtaining simultaneous fits may be in part due to the fact that several states appear with very small mass splittings right at the lightest end of the spectrum. It is not even clear within errors which state is the lowest lying, although the T_2^{++} (corresponding to $J^{PC} = 2^{++}$) was used for the results in Table 10.3. Table B.6 in the Appendix shows individual fits of all lattice irreps in the 27-plet sector.

For gluelumps containing a 35-plet coloured particle, simultaneous fits were even more challenging. The lattice energies were large, and the errors correspondingly large as well. Statistical errors on mass differences were around 50%, and systematic errors were much more than this. The lattice energies of gluelumps in this colour representation were so large that the signal (a decaying exponential with the mass

Table 10.3: The resolvable mass spectrum of gluelumps containing a static 27-plet particle. The first error is statistical and the second is systematic. J denotes the lowest continuum angular momentum assignment for the light (gauge) degrees of freedom and does not include the spin of the 27-plet particle.

Λ^{PC}	J	$M(\Lambda^{PC}) - M(T_2^{++})$ [GeV]
E^{++}	2	$0.04 \pm 0.06 \pm 0.24$
A_1^{++}	0	$0.05 \pm 0.07 \pm 0.19$
T_2^{-+}	2	$0.50 \pm 0.08 \pm 0.45$
E^{-+}	2	$0.53 \pm 0.09 \pm 0.43$
T_1^{-+}	1	$0.66 \pm 0.09 \pm 0.38$
A_2^{-+}	3	$0.74 \pm 0.17 \pm 0.50$
A_2^{++}	3	$1.12 \pm 0.23 \pm 0.45$
T_1^{+-}	1	$1.29 \pm 0.26 \pm 0.93$
T_1^{++}	1	$1.34 \pm 0.20 \pm 0.57$
T_2^{+-}	2	$1.91 \pm 0.32 \pm 0.45$
E^{+-}	2	$2.13 \pm 0.41 \pm 0.30$
T_1^{--}	1	$2.49 \pm 0.55 \pm 0.44$

parameter in the exponent) damps down to the level of noise quickly. There were not many points in the correlators to use, and the fitting window for the central value of any state had to start at time-step 1 in all cases. Fits starting at time-step 2 or later yielded results consistent with zero, as can be seen in Table B.7. Because of this limitation, even the usable fits were probably still contaminated by excited states. There simply were not enough good points in the correlators to reach a plateau where the contamination was absent. Systematic errors were very large (they involve fits starting at the origin time-step) and energies not reliable. In half of the states in the 35-plet spectrum, systematic errors on the mass differences were more than 100%. This really means that a spectrum or even hierarchy of states cannot be reliably presented. So although fits are presented in the Appendix (see Table B.7), one should use caution in trying to interpret mass differences in this representation as accurate physics. It is presented here more as proof-of-concept. All the framework

is ready for someone with more computing power to revisit this sector if the interest arises.

There are a few things to notice about the results. Table 10.1 in particular is state-of-the-art lattice analysis. Results are presented to three significant figures with statistical errors less than about 5% and a detailed understanding of systematic errors which, even conservatively estimated, remain under about 15%. The contents of Table 10.1 are displayed visually in Figure 10.11 with statistical and systematic errors added linearly. The results of the larger colour representations are ground-breaking in that these systems have not been studied before, but they are still somewhat preliminary. Especially the 27-plet and 35-plet results should be treated with caution. Since many of the states overlap within the larger errors in those representations, the spectrum cannot be well-resolved.

Tables 10.1 to 10.3 list the lowest continuum spin J that each state may couple to.³ For a more complete list of the possible spin assignments, see Table 2.2. It is worth noting that both the E^{PC} and the T_2^{PC} irreps couple to spin-2 to lowest order. For the same P and C values, the E and T_2 states in all the presented colour representations are indeed degenerate (beautifully so in most cases), suggesting that they are both coupling to the same physical spin-2 state.

Where two-exponential fits were possible (only in the octet), excited states for certain Λ^{PC} representations could be found and they are shown in the raw result tables in the Appendix. They are not included in Table 10.1, as they are likely not distinct states, but rather a combination of all contaminating excited states. These excited states may be spin excitations in higher spin states, or radial excitations of the ground-state in which case they would have the same (lower) spin assignment as

³The spin J technically corresponds to the spin quantum number of the light (gauge) degrees of freedom in the bound state. If the heavy colour-multiplet particle is non-scalar, its spin can be added to this J as discussed in Section 2.3 to get the spin assignment for the complete bound state.

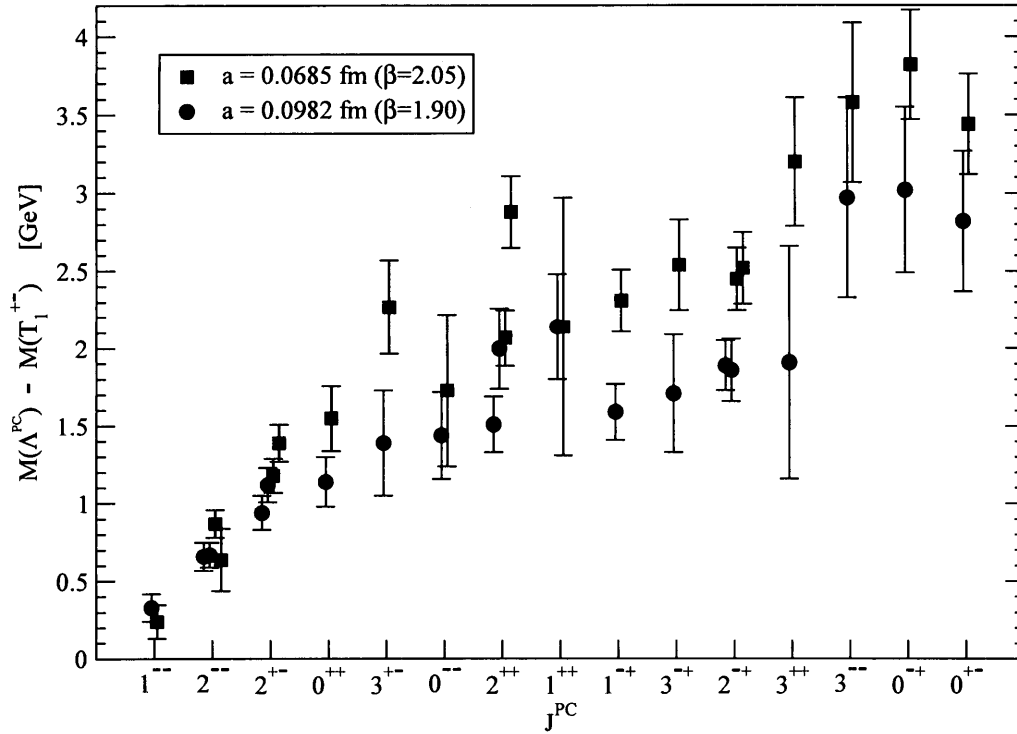


Figure 10.11: The content of Table 10.1 (mass spectrum of glueballs containing a static octet particle) is displayed visually. Statistical and systematic errors were added linearly.

the ground state.

It is interesting that the lightest particles in the octet colour representation are not scalar. The two lightest states are both spin 1. Spin-2 (and possibly even spin-3) states occur at lighter masses than the lightest spin-0 particle. In the decuplet, a scalar particle is the lightest. Although it seems that a spin-2 glueball and a spin-0 glueball are the lowest lying states in the 27-plet and 35-plet respectively, the errors in those colour multiplets are so large and the mass splittings are so small that many states including the lowest lying ones overlap within error.

The ordering of the octet mass hierarchy found here agrees with the analytic estimates discussed in Section 1.4 as well as with the previous lattice results of Foster

and Michael in Ref. [18]. In Table 10.1 some states (such as the E^{--} and the T_2^{+-}) are seen that could not be calculated by Foster and Michael due to the types of operators they used. These two do not represent new physical states that they missed, however. The E^{--} couples to the same physical 2^{--} state as the T_2^{--} that they do see, and similarly the T_2^{+-} with the E^{+-} 2^{+-} state. Since the E -reps and T_2 -reps both couple to spin $J = 2$ to lowest order, these reps can offer independent testing of the same continuum state. The first previously unobserved state is the 0^{--} (A_1^{--}), which is found to be as light or lighter than some of the states studied previously in Ref. [18].

The final table of lattice results in Ref. [18] reports only five mass splittings. These are summarized here in Table 10.4 along with the model estimates that were discussed in Section 1.4. These model results have now been converted to mass splittings for comparison purposes.

Table 10.4: Summary of published octet mass splittings ($\Lambda^{PC} - T_1^{+-}$) by various model estimates as well as from the previous lattice study of Foster and Michael [18]. The ordering in the table is dictated by the lattice results, which include the published statistical errors. See text and Table 10.5 for suggested revisions to the lattice mass splittings, as well as an explanation as to why the errors may be an underestimate.

J^{PC}	Mass Splitting (GeV)				
	lattice calculations	model estimates			
	previous work [18]	bag model [28]	Coulomb gauge [29]	string model [30]	transverse gluons [31]
1^{--}	0.368 ± 0.007	0.55	0.39	0.47	0.37
2^{--}	$0.567^a \pm 0.010$	0.54	0.59	0.49	0.57
3^{+-}	0.972 ± 0.024	1.01	1.12	0.84	0.97
2^{+-}	0.973 ± 0.036	1.21	0.71	0.83	0.94
0^{++}	1.092 ± 0.028	1.2		0.91	
4^{--}			1.61		1.29
3^{--}					1.34

^a This entry repairs a simple typo in column 4 of Table III in Ref. [18], as can be seen by comparing with column 3 of that same table and with Fig. 3 in Ref. [18].

These results are compared to the current mass splittings for all 20 Λ^{PC} states in the octet sector graphically in Figure 10.12.

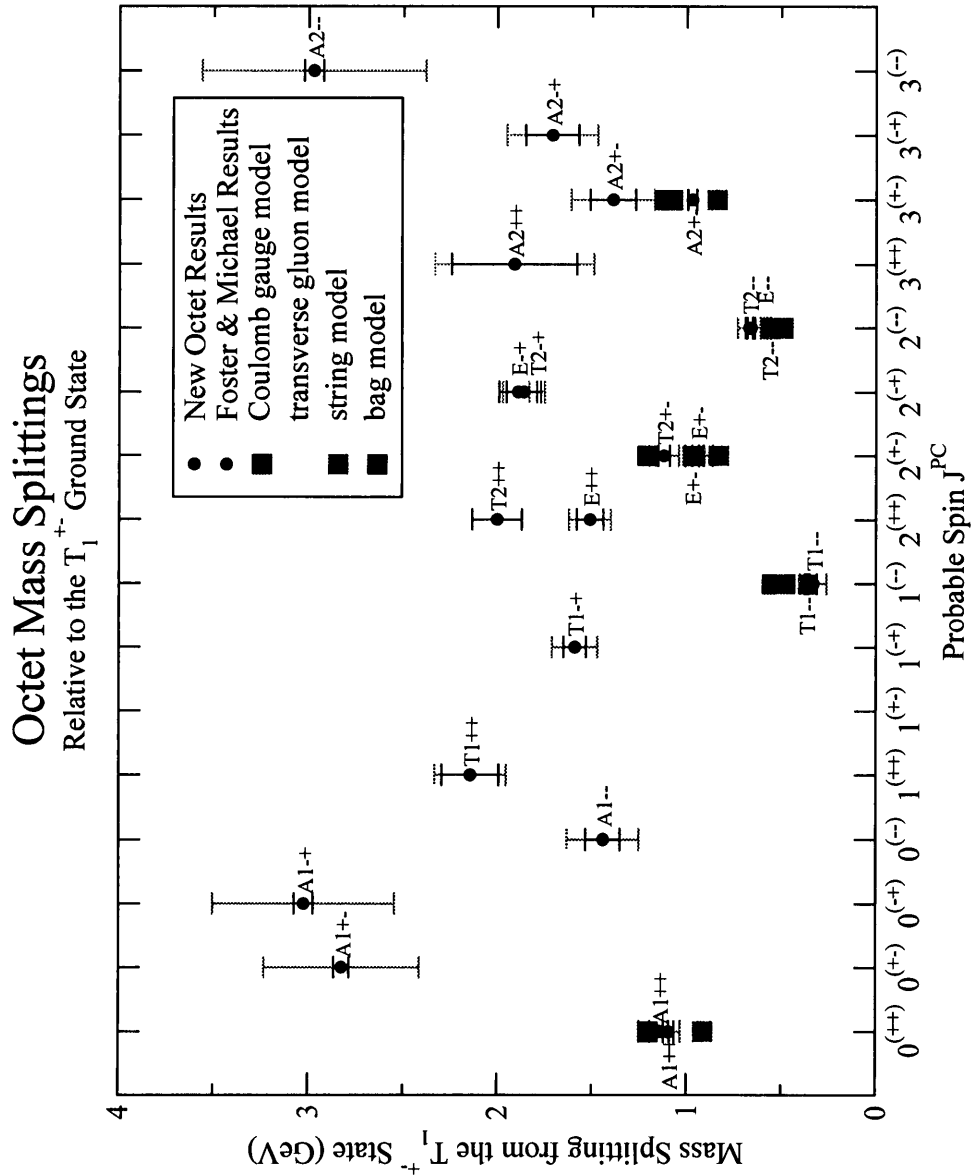


Figure 10.12: Comparison of octet mass splittings ($\Lambda^{PC} - T_1^{+-}$) between the current work and the previous results of Foster and Michael [18]. For the current results, statistical errors are shown in solid red and systematic errors in dashed red. For Foster and Michael's results (in blue), only statistical errors are shown, and even these may be underestimated as is discussed in the text. Various model estimates are also shown, without errors.

Figure 10.12 shows the octet mass splittings relative to the T_1^{+-} ground state for all the possible Λ^{PC} representations based on the results of Table 10.1 with the lowest possible J spin number assigned to each ground state. The continuum estimates of Foster and Michael are also included for their lightest five states as reported in their Table III. These are the *only* states that Foster and Michael applied their full analysis to, and the only mass splittings that appear in their final summary table. Results in Figure 10.12 are separated into probable J^{PC} quantum numbers. In all the cases where more than one Λ^{PC} irrep couples to the same continuum J^{PC} quantum number, the states are degenerate within error. All of the current results agree with the previous results of Foster and Michael.

Although Foster and Michael develop operators to couple to ten Λ^{PC} states and do in fact perform fits for all ten representations on various sized lattices, their final analysis (which includes extrapolation of the mass splittings as measured on several lattice sizes to the continuum limit of $a = 0$) only includes the five mass splittings listed in Table 10.4. Their mass splittings agree with the current findings within error. In the results presented by Foster and Michael, only statistical errors were given. They acknowledge the inherent minimum 10% systematic error due to using quenched lattices, but do not include it in the results of their Table III. No other systematic effects were discussed or included in their 1999 study, which is part of the reason why their results appear to be so much more precise than the current measurements. Current findings indicate that systematic errors cannot be neglected. In fact, more so than statistical errors, current results show that they are the limiting factor in precise lattice measurements of the glueball spectrum.

Even the statistical errors on the results of Foster and Michael are somewhat dubious. Although they did use some very sophisticated analysis techniques (they combined results from their 1×1 plaquette operators with their 2×2 results each with different smearing parameters into a 4×4 matrix of correlations and used the

variational technique to maximize ground-state contributions), their fitting methods were somewhat unconventional for a lattice calculation. Instead of fitting an exponential function to a whole series of points of the correlator, they “fit” pair-wise combinations of adjacent points from the correlator. This is equivalent to the effective energies defined in Eq. 9.6. These were used here to visually display the correlation functions, but they are not suitable for extracting masses. For this, a whole series of points should be fit. Fitting two points with an exponential function (which has two parameters) is of course always an exact fit. Table II of Ref. [18] lists the results of these “fits”, and since they are always perfect, the errors are only due to the statistical error on the correlator points, not a statistical fitting error. A “mass” was generated in each pairwise fit, first using time-steps 1 and 2. In some cases this was the only fit possible. In most cases however another mass was found by “fitting” timesteps 2 and 3, then if possible this was repeated for steps 3 and 4, then 4 and 5. In the text of the paper, they said that they chose the earliest fit that was statistically equal to all following fits as their central value. This is similar to what was done in the current work, and it is the right thing to do. Unfortunately, the analysis that follows Table II in Ref. [18] is *not* based on those central values. All of the analysis is completely based on just the earliest fits, the ones from timesteps 1 and 2. These are universally higher than the following fits (as they are contaminated with excited states) and not statistically equal to later fits. They also have much smaller statistical errors than later fits, which again adds to the artificial precision of their final results.

Foster and Michael repeated their analysis at several different lattice spacings a , then the results were extrapolated to the continuum limit of $a = 0$ for the five lightest states. The mass splittings of these five continuum estimates above the lightest gluelump (the T_1^{+-}) are what was reported in their Table III, repeated above in Table 10.4. They claim a moderate dependence of the mass splittings on the lattice spacing, a , especially for heavier states. Current results did find that the central values on

the finer lattice ensemble were slightly larger than on the coarser lattice (and this effect was perhaps stronger for the heavier states), but the discrepancy was not large compared to the size of the errors. In fact, it seems that a mis-plotted point in a critical figure in Ref. [18] led to an artificially large estimate of the lattice spacing dependence. The A_1^{++} point from the $\beta = 5.7$ ensemble has a very large influence on the continuum extrapolation, but it is not consistent with the data given in Table II of Ref. [18].

Table 10.5: Re-analysis of previous lattice results from Ref. [18] of the spectrum of glueballs containing a static octet particle at two different lattice spacings. The first error is statistical, the second represents the systematic error in choosing the fitting window, and the third error is a 10% systematic error to account for the use of quenched lattices. J denotes the continuum angular momentum of the light (gauge) degrees of freedom and does not include the spin of the octet particle. These results should be compared to the current findings in Table 10.1.

Λ^{PC}	J	$M(\Lambda^{PC}) - M(T_1^{+-})$ [GeV]	
		$a = 0.0948$ fm ($\beta = 6.0$)	$a = 0.0683$ fm ($\beta = 6.2$)
T_1^{--}	1	$0.33 \pm 0.01 \pm 0.02 \pm 0.03$	$0.30 \pm 0.02 \pm 0.02 \pm 0.03$
T_2^{--}	2	$0.52 \pm 0.01 \pm 0.01 \pm 0.05$	$0.55 \pm 0.02 \pm 0.02 \pm 0.05$
E^{+-}	2	$0.85 \pm 0.02 \pm 0.02 \pm 0.08$	$0.90 \pm 0.03 \pm 0.02 \pm 0.09$
A_2^{+-}	3	$0.74 \pm 0.07 \pm 0.10 \pm 0.07$	$0.97 \pm 0.03 \pm 0.03 \pm 0.10$
A_1^{++}	0	$0.90 \pm 0.03 \pm 0.02 \pm 0.09$	$0.91 \pm 0.04 \pm 0.07 \pm 0.09$
E^{++}	2	$1.15 \pm 0.03 \pm 0.06 \pm 0.12$	$1.25 \pm 0.04 \pm 0.04 \pm 0.13$
T_1^{-+}	1	$1.23 \pm 0.03 \pm 0.05 \pm 0.12$	$1.36 \pm 0.03 \pm 0.04 \pm 0.14$
T_2^{-+}	2	$1.51 \pm 0.04 \pm 0.03 \pm 0.15$	$1.61 \pm 0.05 \pm 0.04 \pm 0.16$
T_2^{++}	2	$1.70 \pm 0.10 \pm 0.02 \pm 0.17$	$1.61 \pm 0.06 \pm 0.13 \pm 0.16$

The concerns with some of the analysis that led to the final published mass splittings from Ref. [18] do not detract from the value of their raw results. The fits presented in their Table II have been re-analysed here for all ten Λ^{PC} states accessible to Foster and Michael. Although the correlators could not be re-fit so as to include more than two data points in each exponential fit, central values were chosen in a way

consistent with how they were intended. The earliest fit that was statistically equal to later fits was chosen as the central value. Statistical errors still do not really reflect fitting errors, but they are taken as quoted. Systematic errors were estimated in the same way that they were estimated here, by examining the difference between the central value and a fit that started at one earlier time-step, then using Equation 9.13. A second systematic error of 10% is also shown, indicative of the error expected when using a quenched lattice. Mass splittings were converted into units of GeV and the results are compiled in Table 10.5 for the two finest lattice spacings. These are the numbers that should be compared to the current octet results in Table 10.1. Foster and Michael also claimed to find several excited states, but these are not included on this list.

The re-analysed results of Foster and Michael no longer show a strong dependence on the lattice spacing, and continuum extrapolation is not necessary. These results agree with the current findings.

Chapter 11

Conclusion

Techniques from lattice QCD have been used to generate the gluelump spectrum. Gluelumps are bound states of Standard Model particles (gluons and virtual quarks) with a heavy coloured particle. They have been studied previously only containing a colour-octet particle, inspired by the possibility of a supersymmetric gluino. As this sector may gain phenomenological interest as collider physics is able to create these states, a more thorough examination was needed. Since supersymmetry is not the only possible beyond-the-Standard-Model scheme (perhaps not even the favourite one anymore either), the gluelump spectrum also needed to be expanded to include states with coloured particles from different $SU(3)$ colour representations.

In this work, considerable group theory foundations were laid in order to fully calculate not only gluelumps containing octet-rep particles, but also decuplet, 27-plet, 28-plet and 35-plet particles on the lattice. Previous lattice gluelump studies were not able to access the whole octet spectrum, and did not address the possibility of larger colour-multiplet inclusions. This is novel work, and may find application beyond the gluelump sector.

The full spectrum of gluelumps containing colour-octet particles was presented,

and compared to previous studies. A detailed error analysis was carried out, and the system was carefully examined in four unique independent lattice calculations which all yielded consistent results. The hierarchy of states agrees well with previous studies, but is much more complete and precise. The spectrum was extended to colour-decuplet particles, as well as particles from the 27-plet and 35-plet representations of $SU(3)$. Some of these results are preliminary and could be improved upon with future studies, but this work provides an exciting first look at those systems.

The results found here predict clear experimental signatures and can be easily adapted to numerous different theoretic models of Beyond-the-Standard-Model physics. They are also published in Reference [1].

Bibliography

- [1] K. Marsh and R. Lewis. A lattice QCD study of generalized gluelumps. *arXiv:1309.1627 [hep-lat]*, 2013.
- [2] G. Aad et al. [ATLAS Collaboration]. Search for squarks and gluinos with the ATLAS detector in final states with jets and missing transverse momentum using 4.7 fb^{-1} of $\sqrt{s}=7$ TeV proton-proton collision data. *Phys. Rev. D*, 87:012008, Jan 2013.
- [3] A. Atre, R.S. Chivukula, P. Ittisamai, E.H. Simmons, and J-H. Yu. Probing color octet couplings at the Large Hadron Collider. *Phys. Rev. D*, 86(054003), 2012.
- [4] R.S. Chivukula, E.H. Simmons, and N. Vignaroli. A flavorful top-coloron model. *Phys. Rev. D*, 87(075002), 2013.
- [5] Eugenio Del Nobile, Roberto Franceschini, Duccio Pappadopulo, and Alessandro Strumia. Minimal matter at the large hadron collider. *Nuclear Physics B*, 826(12):217 – 234, 2010.
- [6] F. Aguila, J. Blas, and M. Prez-Victoria. Electroweak limits on general new vector bosons. *Journal of High Energy Physics*, 2010(9):1–47, 2010.
- [7] Tao Han, Ian Lewis, and Zhen Liu. Colored resonant signals at the LHC: largest rate and simplest topology. *Journal of High Energy Physics*, 2010(12):1–26, 2010.
- [8] Jason Kumar, Arvind Rajaraman, and Brooks Thomas. Higher representations and multijet resonances at the LHC. *Phys. Rev. D*, 84:115005, Dec 2011.
- [9] Victor Ilisie and Antonio Pich. QCD exotics versus a standard model Higgs boson. *Phys. Rev. D*, 86:033001, Aug 2012.
- [10] Yevgeny Kats and Matthew J. Strassler. Probing colored particles with photons, leptons, and jets. *Journal of High Energy Physics*, 2012(11):1–39, 2012.

- [11] E. Bertuzzo, P.A.N. Machado, and R.Zukanovich Funchal. Can new colored particles illuminate the Higgs? *Journal of High Energy Physics*, 2013(2):1–20, 2013.
- [12] L. Del Debbio. The conformal window on the lattice. *Proceedings of Science, Lattice 2010*:004.
- [13] D.D. Dietrich and F. Sannino. Conformal window of SU(N) gauge theories with fermions in higher dimensional representations. *Phys. Rev. D*, 75(085018), 2007.
- [14] T.A. Ryttov and F. Sannino. Conformal windows of SU(N) gauge theories higher dimensional representations and the size of the unparticle world. *Phys. Rev. D*, 76(105004), 2007.
- [15] L. Del Debbio, M.T. Frandsen, H. Panagopoulos, and F. Sannino. Higher representations on the lattice: perturbative studies. *Journal of High Energy Physics*, 2008(06):007, 2008.
- [16] Shu-Qin Xie and Qi-Ren Zhang. A possible 27-plet of dibaryons. *Physics Letters*, 143B(4,5,6):441–444, 1984.
- [17] S.P. Rosen. Finite transformations in various representations of SU(3). *J. Math. Phys.*, 12(4):673–681, 1971.
- [18] M. Foster and C. Michael. Hadrons with a heavy color-adjoint particle. *Phys. Rev. D*, 59(094509), 1999.
- [19] I.H. Jorjusz and C. Michael. The field configurations of a static adjoint source in SU(2) lattice gauge theory. *Nuclear Physics B*, 302:448–470, 1987.
- [20] N.A. Campbell, I.H. Jorjusz, and C. Michael. The adjoint source potential in SU(3) lattice gauge theory. *Physics Letters*, 167B(1):91–93, 1986.
- [21] C. Michael. Hadronic forces from the lattice. *Nuclear Physics B (Proc. Suppl.)*, 26:417–419, 1992.
- [22] Particle Data Group. Review of Particle Physics. *J. Phys. G: Nucl. Part. Phys*, 33:1120–1147, 2006. Supersymmetry Searches Review.
- [23] D.N. Spergel et al. [WMAP Collaboration]. Wilkinson Microwave Anisotropy Probe (WMAP) Three Year Observations: Implications for Cosmology. *The Astrophysical Journal Supplement Series*, 170(2):377, 2007.

- [24] G.R. Farrar and P. Fayet. Phenomenology of the production, decay and detection of new hadronic states associated with supersymmetry. *Phys. Lett. B*, 76(5):575–579, 1978.
- [25] M. Chanowitz and S. Sharpe. Spectrum of gluino bound states. *Phys. Lett. B*, 126(3-4):225–230, 1983.
- [26] A.W. Thomas and W. Weise. *The Structure of the Nucleon*. Wiley-VCH, 2001.
- [27] K. Johnson. The MIT bag model. *ACT A Physica Polonica*, B6(6), 1975.
- [28] G. Karl and J. Paton. Gluelump spectrum in the bag model. *Phys. Rev. D*, 60(034015), 1999.
- [29] P. Guo, A.P. Szczepaniak, G. Galata, A. Vassallo, and E. Santopinto. Gluelump spectrum from Coulomb gauge QCD. *Phys. Rev. D*, 77(056005), 2008.
- [30] Yu.A. Simonov. Gluelump spectrum in the QCD string model. *Nucl. Phys. B*, 592:350–368, 2001.
- [31] F. Buisseret. Gluelump model with transverse constituent gluons. *Eur.Phys.J.*, A38:233–238, 2008.
- [32] V. Bornyakov, G. Schierholz, and T. Streuer. Glueball and gluelump spectrum in abelian projected QCD. *Nucl. Phys. Proc. Suppl.*, 106:676–678, 2002.
- [33] M. Creutz. *Quarks, gluons and Lattices*. Cambridge University Press, 1983.
- [34] I. Montvay and G. Munster. *Quantum Fields on a Lattice*. Cambridge University Press, 1994.
- [35] H.J. Rothe. *Lattice Gauge Theories: An Introduction*. World Scientific, 2005.
- [36] T. DeGrand and C. DeTar. *Quarks, gluons and Lattices*. World Scientific Publishing Company, 2006.
- [37] C. Gattringer and C. Lang. *Quantum Chromodynamics on the Lattice*. Springer, 2009.
- [38] CP-PACS/JLQCD Collaborations: T. Ishikawa et al. *Phys. Rev. D*, 78(011502), 2008.
- [39] Mark G. Beckett, Paul Coddington, Balint Joo, Chris M. Maynard, Dirk Pleiter, Osamu Tatebe, and Tomoteru Yoshie. Building the international lattice data grid. *Computer Physics Communications*, 182:1208–1214, 2011.

- [40] Japan Lattice Data Grid. <http://www.jldg.org>.
- [41] C. Michael. The glueball spectrum from lattice gauge theory. *Acta Physica Polonica*, B21(2):119–127, 1989.
- [42] R.G. Petry, D. Harnett, R. Lewis, and R.M. Woloshyn. Exploring the meson spectrum with twisted mass lattice QCD. *Phys. Rev. D*, 78(074502), 2008.
- [43] J.B. Bronzan. Parametrization of SU(3). *Phys. Rev. D*, 38(6), 1988.
- [44] J. Ambjorn, P. Olesen, and C. Peterson. Stochastic confinement and dimensional reduction. 1. Four-dimensional SU(2) lattice gauge theory. *Nucl. Phys. B*, 240(189), 1984.
- [45] L. Del Debbio, M. Faber, J. Greensite, and S. Olejnik. Casimir scaling versus Abelian dominance in QCD string formation. *Phys. Rev. D*, 53(5891), 1996.
- [46] G.S. Bali. QCD forces and heavy quark bound states. *Phys. Rept.*, 343(1), 2001.
- [47] A. Mykkanen, M. Panero, and K. Rummukainen. Casimir scaling and renormalization of Polyakov loops in large-N gauge theories. *JHEP*, 1205(69), 2012.
- [48] D.B Lichtenberg. *The Standard Model of Elementary Particles (Monographs and Textbooks in Physical Science Lecture Notes)*. Bibliopolis, 1991.
- [49] H. Georgi. *Lie Algebras in Particle Physics*. Westview Press, 1999.
- [50] B. Berg and A. Billoire. Glueball spectroscopy in 4d SU(3) lattice gauge theory I. *Nuclear Physics B*, 221:109–140, 1983.
- [51] L. Del Debbio, A. Patella, and C. Pica. Higher representations on the lattice: Numerical simulations. SU(2) with adjoint fermions. *Phys. Rev. D*, 81(094503), 2010.
- [52] Colin Morningstar and Mike Peardon. Analytic smearing of SU(3) link variables in lattice QCD. *Phys. Rev. D*, 69(054501), 2004.
- [53] W.H. Press, S.A. Teukolsky, W.T. Vetterling, and B.P Flannery. *Numerical Recipes in Fortran 90, Second Edition Volume 2 of Fortran Numerical Recipes*. Cambridge University Press, 1996.
- [54] B. Efron and R.J. Tibshirani. *An Introduction to the Bootstrap*. Chapman and Hall, CRC Press, 1993.

Appendix A

Abbreviations and Symbols

Table A.1: List of abbreviations and symbols

Abbreviation	Full Form
BSM	beyond the Standard Model
$G^{\alpha\beta}(\tau_0, \tau_1)$	propagator
$H^{\alpha\dagger}(\tau_0)$	creation operator
$H^\beta(\tau_1)$	destruction operator
LHC	Large Hadron Collider
LSP	lightest supersymmetric particle
O^{PC}	octahedral group irreducible representation (with parity P and charge conjugation C)
QCD	quantum chromodynamics
SM	Standard Model
SU(3)	special unitary group (dim. 3)
SUSY	Supersymmetry
T^μ	tensor
τ	Euclidean time, $\tau = it$
τ_0	creation time
τ_1	annihilation time
Λ	one of the octahedral group irreps.

Appendix B

Results of Fitting

Results of fitting exponential functions to the various simulations. Tables show fits with various starting times listed as the initial time-step, τ_i . The final time-step is of little consequence to the fit value (including noisy data points does not significantly affect the fit) but it is indicated in the tables as τ_f and it was chosen to be the fit with the lowest $\chi^2/\text{d.o.f.}$ value. All values are in lattice units. To convert to conventional units of MeV, one can divide the numbers in lattice units by the lattice spacing, a , in fm and then apply the conversion factor 197.327 MeV fm , which restores factors of \hbar and c which were previously set to unity. Errors shown are statistical only. Fits starting at time-steps later than those shown in the tables are consistent with zero, meaning that no signal can be resolved from noise past that point.

Table B.1: 1×1 plaquette-based octet on lattice spacing $a = 0.0982(19)$ fm.

gluelump Λ^{PC}	τ_i	τ_f	$\chi^2/\text{d.o.f.}$	ground state energy
A_1^{++}	0	39	55	2.473 ± 0.002
	1	36	1.4	2.239 ± 0.005
	2	7	0.2	2.13 ± 0.03
	3	7	0.1	2.0 ± 0.2
A_2^{+-}	0	39	92	2.460 ± 0.001
	1	39	1.3	2.232 ± 0.003
	2	15	0.4	2.11 ± 0.02
	3	15	0.3	2.0 ± 0.2
E^{++}	0	39	51	2.600 ± 0.001
	1	33	1.0	2.397 ± 0.004
	2	5	0.1	2.30 ± 0.03
	3	6	0.3	2.2 ± 0.3
E^{+-}	0	39	226	2.3231 ± 0.0008
	1	39	2.1	2.107 ± 0.002
	2	6	0.7	2.03 ± 0.01
	3	6	0.9	2.00 ± 0.09
	4	10	0.7	1.4 ± 0.4
T_1^{+-}	0	39	150	1.6785 ± 0.0005
	1	39	7.7	1.6175 ± 0.0009
	2	19	0.8	1.580 ± 0.002
	3	9	0.2	1.56 ± 0.01
	4	9	0.3	1.55 ± 0.04
	5	9	0.4	1.6 ± 0.2
T_1^{-+}	0	39	86	2.712 ± 0.003
	1	39	1.1	2.465 ± 0.004
	2	9	0.6	2.38 ± 0.03
	3	7	0.2	2.0 ± 0.2
T_1^{--}	0	39	401	1.9299 ± 0.0006
	1	39	7.9	1.784 ± 0.001
	2	15	0.5	1.720 ± 0.004
	3	9	0.3	1.70 ± 0.02
	4	9	0.2	1.8 ± 0.1

Continued on next page

Table B.1 – concluded from previous page

gluelump Λ^{PC}	τ_i	τ_f	$\chi^2/\text{d.o.f.}$	ground state energy
T_2^{++}	0	39	18	2.771 ± 0.007
	1	7	0.1	2.714 ± 0.006
	2	7	0.2	2.71 ± 0.08
	3	8	0.2	2.8 ± 0.6
T_2^{-+}	0	39	64	2.844 ± 0.001
	1	9	0.9	2.574 ± 0.005
	2	8	0.7	2.51 ± 0.04
	3	8	0.5	2.1 ± 0.3
T_2^{--}	0	39	160	2.0722 ± 0.0007
	1	39	3.5	1.952 ± 0.001
	2	5	0.3	1.889 ± 0.006
	3	5	0.2	1.86 ± 0.03
	4	24	0.8	1.9 ± 0.3

Table B.2: 2×2 plaquette-based octet on lattice spacing $a = 0.0982(19)$ fm.

gluelump Λ^{PC}	τ_i	τ_f	$\chi^2/\text{d.o.f.}$	ground state energy	excited state energy
A_1^{++}	0	19	63	2.7393 ± 0.0009	
	1	10	1.3	2.516 ± 0.006	
	2	7	0.2	2.36 ± 0.05	
	3	8	0.3	2.3 ± 0.5	
A_2^{+-}	0	19	51	2.5652 ± 0.0005	
	1	19	2.1	2.435 ± 0.004	
	2	7	0.2	2.27 ± 0.03	
	3	7	0.3	2.2 ± 0.3	
	0	7	0.3	1.9 ± 0.1	2.71 ± 0.03
	1	7	0.4	2.25 ± 0.04	5.00 ± 0.09
E^{++}	0	19	65	2.9796 ± 0.0008	
	1	19	1.3	2.734 ± 0.006	
	2	4	0.4	2.50 ± 0.06	
	3	19	0.7	2.8 ± 0.6	
E^{+-}	0	19	182	2.3813 ± 0.0003	
	1	19	2.8	2.264 ± 0.002	
	2	8	0.5	2.17 ± 0.02	
	3	8	0.7	2.1 ± 0.1	
T_1^{+-}	0	19	586	1.7794 ± 0.0003	
	1	19	34	1.7085 ± 0.0007	
	2	19	1.5	1.648 ± 0.003	
	3	15	1.1	1.62 ± 0.01	
	4	7	0.5	1.50 ± 0.05	
	5	15	0.7	1.6 ± 0.2	
	0	15	0.9	1.54 ± 0.01	2.15 ± 0.03
	1	15	0.9	1.57 ± 0.04	2.3 ± 0.2
	2	15	0.9	1.21 ± 0.2	1.72 ± 0.04
T_1^{-+}	0	19	70	3.0058 ± 0.0006	
	1	3	0.2	2.786 ± 0.006	
	2	19	0.6	2.74 ± 0.07	
	3	10	0.4	1.9 ± 0.4	
T_1^{--}	0	19	746	1.9793 ± 0.0003	

Continued on next page

Table B.2 – concluded from previous page

gluelump Λ^{PC}	τ_i	τ_f	$\chi^2/\text{d.o.f.}$	ground state energy	excited state energy
	1	19	22	1.8787 ± 0.0009	
	2	19	0.8	1.797 ± 0.004	
	3	6	0.2	1.76 ± 0.02	
	4	11	0.6	1.8 ± 0.1	
	0	4	0.2	1.68 ± 0.02	2.37 ± 0.03
	1	19	0.7	1.73 ± 0.05	2.6 ± 0.2
	2	19	0.7	1.73 ± 0.03	2.7 ± 0.4
T_2^{++}	0	19	42	3.2904 ± 0.0007	
	1	6	0.5	3.053 ± 0.008	
	2	6	0.3	2.9 ± 0.1	
T_2^{-+}	0	19	57	3.1769 ± 0.0006	
	1	19	1.7	2.939 ± 0.007	
	2	14	1.3	2.64 ± 0.09	
T_2^{--}	0	19	254	2.1979 ± 0.0003	
	1	19	7.0	2.104 ± 0.001	
	2	10	0.3	2.023 ± 0.008	
	3	10	0.3	1.99 ± 0.05	
	4	7	0.1	2.3 ± 0.3	
	0	10	0.3	1.89 ± 0.04	2.55 ± 0.05
	1	10	0.4	1.92 ± 0.07	2.6 ± 0.1

Table B.3: Chair-based octet on lattice spacing $a = 0.0982(19)$ fm.

gluelump Λ^{PC}	τ_i	τ_f	$\chi^2/\text{d.o.f.}$	ground state energy	excited state energy
A_1^{++}	0	39	52	2.465 ± 0.002	
	1	38	1.4	2.232 ± 0.005	
	2	7	0.2	2.12 ± 0.03	
	3	7	0.2	2.0 ± 0.2	
A_1^{+-}	0	39	12	3.370 ± 0.002	
	1	3	0.2	2.96 ± 0.02	
	2	5	0.2	3.1 ± 0.3	
A_1^{-+}	0	39	10	3.536 ± 0.002	
	1	10	0.5	3.06 ± 0.02	
	2	10	0.4	3.5 ± 0.2	
A_1^{--}	0	39	45	2.698 ± 0.005	
	1	38	1.4	2.457 ± 0.006	
	2	4	0.6	2.27 ± 0.04	
	3	17	0.9	2.5 ± 0.4	
A_2^{++}	0	39	13	3.341 ± 0.002	
	1	14	0.7	2.92 ± 0.02	
	2	9	0.3	2.5 ± 0.2	
A_2^{+-}	0	39	52	2.662 ± 0.009	
	1	39	1.0	2.464 ± 0.007	
	2	16	0.5	2.25 ± 0.06	
	3	8	0.3	1.8 ± 0.3	
A_2^{-+}	0	39	24	2.910 ± 0.004	
	1	39	0.8	2.641 ± 0.008	
	2	4	0.2	2.40 ± 0.07	
	3	16	0.5	2.0 ± 0.6	
A_2^{--}	0	39	11	3.617 ± 0.003	
	1	6	0.1	3.03 ± 0.02	
	2	6	0.2	3.1 ± 0.4	
E^{++}	0	39	63	2.640 ± 0.001	
	1	39	0.9	2.416 ± 0.004	
	2	6	0.3	2.31 ± 0.03	
	3	6	0.4	2.2 ± 0.3	

Continued on next page

Table B.3 – continued from previous page

gluelump Λ^{PC}	τ_i	τ_f	$\chi^2/\text{d.o.f.}$	ground state energy	excited state energy
E^{+-}	0	39	211	2.3297 ± 0.0004	
	1	39	2.2	2.108 ± 0.002	
	2	4	0.4	2.02 ± 0.01	
	3	10	0.7	2.05 ± 0.09	
	4	10	0.9	1.4 ± 0.4	
E^{-+}	0	39	51	2.816 ± 0.001	
	1	26	0.8	2.555 ± 0.005	
	2	26	0.8	2.49 ± 0.05	
	3	26	0.6	1.8 ± 0.3	
E^{--}	0	39	142	2.0877 ± 0.0008	
	1	39	3.3	1.956 ± 0.002	
	2	8	0.1	1.885 ± 0.007	
	3	8	0.1	1.87 ± 0.04	
	4	7	0.1	2.0 ± 0.3	
T_1^{++}	0	39	52	3.144 ± 0.002	
	1	38	2.0	2.802 ± 0.007	
	2	4	0.7	2.62 ± 0.07	
	3	7	1.6	3.1 ± 0.3	
T_1^{+-}	0	39	161	1.6825 ± 0.0005	
	1	39	7.8	1.6181 ± 0.0009	
	2	19	0.8	1.580 ± 0.003	
	3	9	0.2	1.56 ± 0.01	
	4	9	0.3	1.55 ± 0.04	
	5	9	0.4	1.6 ± 0.2	
	0	6	0.2	1.549 ± 0.007	2.49 ± 0.05
	1	9	0.3	1.51 ± 0.04	2.1 ± 0.2
T_1^{-+}	0	39	95	2.713 ± 0.002	
	1	39	1.7	2.461 ± 0.004	
	2	6	0.2	2.35 ± 0.03	
	3	6	0.1	2.2 ± 0.2	
T_1^{--}	0	39	26	1.9333 ± 0.0006	
	1	39	8.3	1.789 ± 0.001	
	2	15	0.5	1.722 ± 0.004	
	3	15	0.4	1.70 ± 0.02	
	4	9	0.3	1.8 ± 0.1	

Continued on next page

Table B.3 – concluded from previous page

gluelump Λ^{PC}	τ_i	τ_f	$\chi^2/\text{d.o.f.}$	ground state energy	excited state energy
	5	15	0.3	1.4 ± 0.5	
T_2^{++}	0	39	26	2.765 ± 0.007	
	1	34	1.1	2.683 ± 0.006	
	2	4	0.4	2.55 ± 0.06	
	3	34	1.0	2.1 ± 0.5	
T_2^{+-}	0	39	175	2.3875 ± 0.0009	
	1	39	1.8	2.196 ± 0.002	
	2	39	0.8	2.11 ± 0.01	
	3	39	0.8	2.1 ± 0.1	
	4	39	0.8	2.2 ± 0.5	
T_2^{+}	0	39	70	2.869 ± 0.001	
	1	31	1.4	2.590 ± 0.005	
	2	4	0.1	2.48 ± 0.04	
	3	31	1.3	2.5 ± 0.4	
T_2^{-}	0	39	158	2.070 ± 0.0007	
	1	39	3.6	1.950 ± 0.001	
	2	5	0.3	1.888 ± 0.006	
	3	10	0.7	1.86 ± 0.03	
	4	24	0.8	1.8 ± 0.2	

Table B.4: Chair-based octet on lattice spacing $a = 0.0685(26)$ fm.

gluelump Λ^{PC}	τ_i	τ_f	$\chi^2/\text{d.o.f.}$	ground state energy	excited state energy
A_1^{++}	0	19	84	2.1205 ± 0.0008	
	1	19	9.5	2.046 ± 0.002	
	2	8	0.8	1.948 ± 0.008	
	3	5	0.1	1.89 ± 0.04	
	4	8	0.5	2.0 ± 0.3	
A_1^{+-}	0	19	54	2.8100 ± 0.0007	
	1	16	1.3	2.665 ± 0.004	
	2	16	0.8	2.54 ± 0.04	
	3	16	0.7	1.9 ± 0.3	
A_1^{-+}	0	19	56	2.9598 ± 0.0006	
	1	17	0.5	2.788 ± 0.005	
	2	17	0.3	2.67 ± 0.06	
	3	17	0.2	2.2 ± 0.5	
A_1^{--}	0	19	102	2.326 ± 0.001	
	1	19	7.7	2.255 ± 0.002	
	2	7	1.4	2.13 ± 0.01	
	3	7	0.4	1.95 ± 0.08	
	4	18	1.3	2.2 ± 0.5	
A_2^{++}	0	19	46	2.7848 ± 0.0007	
	1	19	2.8	2.656 ± 0.004	
	2	5	1.4	2.46 ± 0.04	
	3	19	1.8	2.6 ± 0.3	
A_2^{+-}	0	19	142	2.373 ± 0.003	
	1	19	7.2	2.309 ± 0.002	
	2	14	0.4	2.13 ± 0.02	
	3	13	0.2	2.3 ± 0.1	
A_2^{-+}	0	19	77	2.471 ± 0.001	
	1	18	5.3	2.386 ± 0.002	
	2	12	0.5	2.23 ± 0.02	
	3	12	0.4	2.1 ± 0.1	
A_2^{--}	0	19	66	3.016 ± 0.001	
	1	18	1.4	2.805 ± 0.005	

Continued on next page

Table B.4 – continued from previous page

gluelump Λ^{PC}	τ_i	τ_f	$\chi^2/\text{d.o.f.}$	ground state energy	excited state energy
	2	5	0.8	2.59 ± 0.06	
	3	13	0.8	2.3 ± 0.5	
E^{++}	0	19	113	2.2422 ± 0.0006	
	1	19	12	2.170 ± 0.002	
	2	4	0.4	2.065 ± 0.008	
	3	9	0.8	2.06 ± 0.05	
	4	9	0.3	2.6 ± 0.3	
E^{+-}	0	19	349	1.9100 ± 0.0002	
	1	19	37	1.8608 ± 0.0007	
	2	14	2.5	1.792 ± 0.003	
	3	6	1.0	1.76 ± 0.02	
	4	7	1.3	1.69 ± 0.07	
	5	14	2.3	2.2 ± 0.4	
E^{-+}	0	19	106	2.3814 ± 0.0005	
	1	19	6.4	2.307 ± 0.002	
	2	7	0.4	2.19 ± 0.01	
	3	7	0.1	2.11 ± 0.07	
	4	16	0.8	2.1 ± 0.5	
E^{--}	0	19	170	1.7722 ± 0.0003	
	1	19	45	1.7394 ± 0.0007	
	2	19	1.4	1.680 ± 0.002	
	3	19	0.6	1.648 ± 0.009	
	4	19	0.6	1.63 ± 0.05	
	5	10	0.4	1.4 ± 0.2	
T_1^{++}	0	19	137	2.6574 ± 0.0006	
	1	19	5.0	2.556 ± 0.002	
	2	19	0.9	2.40 ± 0.02	
	3	8	0.2	2.1 ± 0.1	
	4	8	0.2	1.7 ± 0.6	
T_1^{+-}	0	19	181	1.4423 ± 0.0002	
	1	19	114	1.4294 ± 0.0004	
	2	19	10	1.395 ± 0.001	
	3	19	1.7	1.367 ± 0.003	
	4	6	0.7	1.342 ± 0.009	
	5	9	0.9	1.30 ± 0.03	

Continued on next page

Table B.4 – continued from previous page

gluelump Λ^{PC}	τ_i	τ_f	$\chi^2/\text{d.o.f.}$	ground state energy	excited state energy
	6	19	1.2	1.3 ± 0.1	
	0	19	17	0.88 ± 0.02	1.474 ± 0.001
	1	6	0.2	1.31 ± 0.02	1.82 ± 0.07
	2	19	1.1	1.24 ± 0.07	1.59 ± 0.05
	3	19	1.2	1.27 ± 0.04	1.68 ± 0.06
T_1^{-+}	0	19	165	2.3355 ± 0.0009	
	1	19	11	2.258 ± 0.001	
	2	5	0.1	2.146 ± 0.008	
	3	5	0.3	2.15 ± 0.06	
	4	9	0.5	1.8 ± 0.4	
T_1^{--}	0	19	511	1.5855 ± 0.0002	
	1	19	147	1.5580 ± 0.0004	
	2	19	8.2	1.508 ± 0.001	
	3	17	1.3	1.469 ± 0.004	
	4	8	0.1	1.43 ± 0.02	
	5	9	0.2	1.40 ± 0.06	
	6	11	0.7	1.4 ± 0.2	
	0	19	6.0	1.09 ± 0.02	1.648 ± 0.003
T_2^{++}	0	19	65	2.497 ± 0.002	
	1	19	5.4	2.469 ± 0.002	
	2	8	0.3	2.34 ± 0.01	
	3	8	0.2	2.2 ± 0.1	
	4	8	0.2	2.4 ± 0.6	
T_2^{+-}	0	19	292	1.9978 ± 0.0003	
	1	19	40	1.9470 ± 0.0007	
	2	19	1.1	1.870 ± 0.003	
	3	8	0.6	1.83 ± 0.02	
	4	8	0.6	1.75 ± 0.09	
	5	7	0.2	2.3 ± 0.4	
T_2^{-+}	0	19	139	2.4263 ± 0.0005	
	1	19	11	2.349 ± 0.001	
	2	14	0.7	2.22 ± 0.01	
	3	5	0.6	2.14 ± 0.07	
	4	14	0.7	2.5 ± 0.4	
T_2^{--}	0	19	207	1.7716 ± 0.0003	

Continued on next page

Table B.4 – concluded from previous page

gluelump Λ^{PC}	τ_i	τ_f	$\chi^2/\text{d.o.f.}$	ground state energy	excited state energy
	1	19	60	1.7400 ± 0.0007	
	2	19	3.9	1.683 ± 0.002	
	3	14	1.0	1.631 ± 0.008	
	4	8	0.5	1.57 ± 0.04	
	5	12	0.8	1.5 ± 0.2	

Table B.5: Chair-based decuplet on lattice spacing $a = 0.0982(19)$ fm.

gluelump Λ^P	τ_i	τ_f	$\chi^2/\text{d.o.f.}$	ground state energy
A_1^+	0	39	1.7	4.235 ± 0.002
	1	5	0.1	3.86 ± 0.05
	2	5	0.3	3.4 ± 0.5
A_1^-	0	39	8.3	3.649 ± 0.002
	1	5	0.6	3.33 ± 0.02
	2	27	0.9	3.3 ± 0.1
A_2^+	0	39	2.9	4.248 ± 0.007
	1	7	0.9	3.78 ± 0.05
	2	7	0.8	2.6 ± 0.6
A_2^-	0	39	1.8	4.510 ± 0.003
	1	9	1.1	4.07 ± 0.08
	2	9	1.3	4.4 ± 0.2
E^+	0	39	5.4	4.235 ± 0.002
	1	4	1.0	3.78 ± 0.03
	2	9	1.5	2.8 ± 0.5
E^-	0	39	8.6	3.862 ± 0.001
	1	9	1.2	3.53 ± 0.02
	2	9	1.2	3.6 ± 0.2
T_1^+	0	39	10	4.092 ± 0.007
	1	11	0.8	3.62 ± 0.02
	2	11	0.9	3.6 ± 0.2
T_1^-	0	38	13	3.856 ± 0.001
	1	3	0.2	3.53 ± 0.01
	2	38	1.6	3.3 ± 0.2
T_2^+	0	39	6.2	4.179 ± 0.002
	1	6	0.3	3.81 ± 0.03
	2	6	0.1	3.2 ± 0.4
T_2^-	0	39	12	3.860 ± 0.001
	1	17	1.5	3.54 ± 0.01
	2	39	1.6	3.3 ± 0.2

Table B.6: Chair-based 27-plet on lattice spacing $a = 0.0982(19)$ fm.

gluelump Λ^{PC}	τ_i	τ_f	$\chi^2/\text{d.o.f.}$	ground state energy
A_1^{++}	0	19	2.4	3.988 ± 0.001
	1	4	0.2	3.80 ± 0.03
	2	4	0.1	3.2 ± 0.4
A_1^{+-}	0	2	0.2	5.886 ± 0.007
	1	16	1.1	5.0 ± 0.1
A_1^{-+}	0	19	1.0	5.491 ± 0.004
	1	4	0.3	4.3 ± 0.2
A_1^{--}	0	4	0.2	8.14 ± 0.07
	1	10	0.6	5.2 ± 0.3
A_2^{++}	0	15	1.4	4.777 ± 0.002
	1	3	0.1	4.3 ± 0.1
A_2^{+-}	0	7	0.7	8.4 ± 1.6
	1	7	0.5	3.7 ± 0.9
A_2^{-+}	0	19	2.3	4.631 ± 0.003
	1	9	0.3	4.14 ± 0.08
	2	9	0.2	2.3 ± 0.8
A_2^{--}	0	19	2.3	5.353 ± 0.004
	1	4	0.4	4.2 ± 0.2
E^{++}	0	19	6.3	4.026 ± 0.001
	1	4	0.3	3.79 ± 0.02
	2	4	0.2	3.3 ± 0.3
E^{+-}	0	17	0.7	5.130 ± 0.004
	1	17	0.7	4.8 ± 0.2
E^{-+}	0	19	4.7	4.465 ± 0.001
	1	6	0.4	4.03 ± 0.04
	2	6	0.4	3.1 ± 0.5
E^{--}	0	12	0.7	5.79 ± 0.01
	1	10	0.3	4.7 ± 0.3
T_1^{++}	0	18	2.4	5.008 ± 0.002
	1	3	0.4	4.4 ± 0.1
	2	6	1.3	2.5 ± 1.0
T_1^{+-}	0	19	2.1	5.34 ± 0.02

Continued on next page

Table B.6 – concluded from previous page

gluelump Λ^{PC}	τ_i	τ_f	$\chi^2/\text{d.o.f.}$	ground state energy
	1	19	1.0	4.4 ± 0.1
T_1^{-+}	0	19	5.0	4.478 ± 1.727
	1	4	0.1	4.10 ± 0.04
	2	4	0.6	3.5 ± 0.3
T_1^{--}	0	10	0.5	5.451 ± 0.005
	1	10	0.4	5.0 ± 0.2
T_2^{++}	0	19	10.6	4.061 ± 0.001
	1	3	0.3	3.77 ± 0.02
	2	9	0.9	3.5 ± 0.2
T_2^{+-}	0	17	1.1	5.173 ± 0.004
	1	4	0.4	4.7 ± 0.2
T_2^{-+}	0	19	6.2	4.471 ± 0.001
	1	4	0.2	4.02 ± 0.04
	2	14	0.6	3.3 ± 0.4
T_2^{--}	0	19	1.9	6.41 ± 0.04
	1	3	0.8	4.1 ± 0.2

Table B.7: Chair-based 35-plet on lattice spacing $a = 0.0982(19)$ fm.

gluelump Λ^P	τ_i	τ_f	$\chi^2/\text{d.o.f.}$	ground state energy
A_1^+	0	8	1.4	8.04 ± 0.08
	1	4	0.4	3.1 ± 0.4
	2	8	1.9	3 ± 5
A_1^-	0	5	0.8	7.08 ± 0.04
	1	5	0.2	4.3 ± 0.5
	2	9	0.9	0.000 ± 0.007
A_2^+	0	3	0.4	7.56 ± 0.04
	1	9	1.4	4.8 ± 0.2
A_2^-	0	4	0.5	7.14 ± 0.03
	1	3	0.7	5.2 ± 0.2
	2	9	1.0	4 ± 5
E^+	0	8	1.3	6.083 ± 0.004
	1	3	1.2	5.3 ± 0.2
	2	8	2.0	2 ± 3
E^-	0	2	0.3	6.90 ± 0.01
	1	8	2.3	5.2 ± 0.2
T_1^+	0	9	1.5	7.78 ± 0.03
	1	9	1.1	4.0 ± 0.5
T_1^-	0	8	0.2	6.705 ± 0.007
	1	8	0.3	5.0 ± 0.2
	2	8	0.4	0 ± 1
T_2^+	0	3	0.4	7.72 ± 0.03
	1	6	0.7	4.8 ± 0.5
T_2^-	0	9	1.0	6.91 ± 0.01
	1	9	0.9	4.9 ± 0.3
	2	9	1.4	1 ± 1